UC Irvine

UC Irvine Electronic Theses and Dissertations

Title

Adaptations to glutamine deprivation in cancer and its use as a dietary supplement in cancer therapeutics

Permalink

https://escholarship.org/uc/item/63491163

Author

Ishak Gabra, Mari Boules

Publication Date

2019

Peer reviewed|Thesis/dissertation

eScholarship.org Powered by the California Digital Library
University of California

UNIVERSITY OF CALIFORNIA,
IRVINE

Adaptations to glutamine deprivation in cancer and its use as a dietary supplement in cancer therapeutics

DISSERTATION

submitted in partial satisfaction of the requirements
for the degree of

DOCTOR OF PHILOSOPHY

in Biological Sciences

by

Mari B. Ishak Gabra

Dissertation Committee:
Associate Professor Mei Kong, Chair
Professor David Fruman
Associate Professor Olga Razorenova

2019

Chapter 2 © 2018 Nature Oncogenesis
Chapter 3 © 2019 Nature Communications
All other materials © 2019 Mari Ishak Gabra

DEDICATION

To

my parents and friends

in recognition of their endless support

"The three great essentials to achieve anything worth while are: Hard work, Stick-to-itiveness, and Common sense."

-- Thomas A. Edison

TABLE OF CONTENTS

LIST OF FIGURES

LIST OF TABLES

ACKNOWLEDGMENTS

I would like to express the deepest appreciation to my thesis advisor, Dr. Mei Kong, who is a remarkable scientist and a supportive mentor. I am grateful for her patience, and encouragement during my research endeavor. Her guidance and enthusiasm towards my project are instrumental in making this dissertation possible. I could not have imagined having a better advisor and mentor for my PhD study.

I would also like to thank my committee members, Dr. David Fruman and Dr. Olga Razorenova for the constant encouragement and extreme support for my thesis studies and career as a scientist. I am especially grateful for their insightful comments and suggestions that helped improve upon my thesis project. I also want to thank the University of Irvine and the T32 committee for financial support that was provided by the University of California, Irvine, by the National Cancer Institute of the National Institutes of Health under Award Number T32CA009054.

I would also like to thank members of the Kong laboratory, who provided their support and help during the last years. Last but not least, I would like to thank my family and friends for their emotional and spiritual support during my studies and in helping me focus on achieving my goals and beyond.

CURRICULUM VITAE

Mari B. Ishak Gabra

RESEARCH INTEREST

My current research interest focuses on understanding the aberrant metabolism in cancer, and the mechanisms of metabolic adaptation in response to the tumor microenvironment to promote cancer survival.

EDUCATION

Bachelor of Science in Biochemistry **2010**
University of California, Los Angeles Los Angeles, CA
Minor: Classic Civilizations

Master of Science in Chemistry **2015**
San Diego State University San Diego, CA
Advisor: Jeffery Gustafson
Thesis Title: Bcl-2 inhibitor scaffolds that are preorganized along an axis of chirality; the effect of atropisomerism on protein binding.

Ph.D. in Molecular Biology and Biochemistry **2019**
University of California, Irvine Irvine, CA
Advisor: Mei Kong
Thesis Title: Adaptations to glutamine deprivation in cancer and its use as a dietary supplement in cancer therapeutics

RESEARCH EXPERIENCE

Graduate Researcher **Aug 2015 – Dec 2019**
University of California, Irvine Irvine, CA

R&D Assay Development Intern **Jun 2019 – Oct 2019**
DiaSorin Molecular LLC Irvine, CA

Bioanalytical Consultant **June 2015 - Present**
Contracted Greater Los Angles

Research Assistant **Jan 2011 – Jul 2013**
Inter Science Institute Inglewood, CA

Lab Assistant **May 2009 – Dec 2010**
UCLA School of Medicine – Cardiology Los Angeles, CA

TEACHING/ADMINSTRATIVE EXPERIENCE

Teaching Assistant **Jan 2019 – Jun 2019**
University of California, Irvine Irvine, CA

Teaching Assistant **Aug 2013 – Jun 2014**
San Diego State University San Diego, CA

Administrative Assistant **Jun 2009 – Dec 2010**
UCLA Hospital – Cardiology Division Los Angeles, CA

MENTOR EXPERIENCE

Jacqueline Nguyen **Jan 2019 – Jun 2019**
Undergraduate

Alicia Davis **Jan 2017 – Mar 2017**
Rotational graduate student

Arianna Ayonon **Jan 2015 – Jun 2015**
Undergraduate

PUBLICATIONS

1. Reid MA, Lowman XH, Pan M, Tran TQ, Warmoes MO, **Ishak Gabra MB**, et al. IKKbeta promotes metabolic adaptation to glutamine deprivation via phosphorylation and inhibition of PFKFB3. Genes & development. 2016;30(16):1837-51. PubMed PMID: 27585591; PubMed Central PMCID: PMC5024682

2. Tran TQ, **Ishak Gabra MB**, Lowman XH, et al. Glutamine deficiency induces DNA alkylation damage and sensitizes cancer cells to alkylating agents through inhibition of ALKBH enzymes. PLoS Biology. 2017;15(11):e2002810. PubMed PMID: 29107960; PubMed Central PMCID: PMC5673162.

3. **Ishak Gabra MB**, Yang Y, Lowman XH et al. IKKβ activates p53 to promote cancer cell adaptation to glutamine deprivation. Oncogenesis. 2018;7(11):93. PubMed PMID: 30478303; PubMed Central PMCID: PMC6255781.

4. Yang Y, **Ishak Gabra MB**, Hanse EA, et al. MiR-135 suppresses glycolysis and promotes pancreatic cancer cell adaptation to metabolic stress by targeting phosphofructokinase-1. Nature Communications. 2019;10(1):809. PubMed PMID: 30778058; PubMed Central PMCID: PMC6379428.

5. Lowman XH, Hanse EA, Yang Y, **Ishak Gabra MB** et al. p53 promotes cancer cell adaptation to glutamine deprivation by upregulating slc7a3 to increase arginine uptake. Cell Reports. 2019. PubMed PMID: 30865893; PubMed Central PMCID: PMC6510239.

6.Yang Y, **Ishak Gabra MB** and Mei Kong. Metabolic adaptations to glutamine deprivation in pancreatic cancer. Journal of Life Sciences, Vol. 1, No. 2, September 2019:26-32 doi.org/10.36069/JoLS/20190903

7. Tran TQ, Hanse EA, Habowski AN, Li H, **Ishak Gabra MB** et al. Metabolic control of Wnt and cellular differentiation in colorectal cancer. Nature Cancer. Under revision

8. Davis RT , Blake K , Ma D, **Ishak Gabra MB** et al. Transcriptional diversity and bioenergetic shift in human breast cancer metastasis revealed by single-cell RNA sequencing. Nature Cell Biology. Under revision

9. **Ishak Gabra MB**, Yang Y, Li H, et al. Dietary glutamine supplementation suppresses epigenetically-activated oncogenic pathways to inhibit melanoma tumour growth. Nature Communications. Under revision.

LEADERSHIP EXPERINCE

American Red Cross Student Group	2008 - 2010
Habitat for Humanity	2006 – 2007

HONORS AND AWARDS

Cancer Biology & Therapeutics T32 Training Grant	2019
Francis Berger Foundation Scholarship	2015
Harry Hamber Memorial Scholarship	2015
AWIS Scholarship	2014
Alpha Gamma Sigma Honors Humanitarian Award	2007
Dean's Honor List	2006 – 2008

ASSOCIATION MEMBERSHIP

American Association for Cancer Research	2018-present
American Red Cross Chapter, UCLA	2009-present
Honors Society Program, UCLA	2008-2009
Alpha Gamma Sigma Honors Society	2005-2008

POSTER SESSIONS

Annual MB&B Departmental Retreat	2018
City of Hope Research Symposium	2015
CSUPURB Biotechnology Symposium	2012-2013

ABSTRACT OF THE DISSERTATION

Adaptations to glutamine deprivation in cancer and its use as a dietary supplement in cancer therapeutics

By

Mari B. Ishak Gabra

Doctor of Philosophy in Biological Sciences

University of California, Irvine, 2019

Assistant Professor Mei Kong, Chair

Tumors reprogram pathways of nutrient acquisition and metabolism to meet their bioenergetic needs and fast proliferation. Glutamine, a non-essential amino acid, was shown to contribute to several core metabolic pathways, as well as epigenetic modifications, in proliferating tumor cells. However, neovasculature development in growing tumors fail to deliver oxygen and key nutrients, such as glutamine, to regions of solid tumors. Concurrently, increased glutamine utilization in cancer cells often lead to its depletion. Similar to hypoxia, cancer cells initiate remodeling of metabolism and gene expression to adapt to these periods of glutamine deprivation.

This dissertation will present recent understanding of nutrient stress in the microenvironment, with special focus on glutamine metabolism, and the role of glutamine metabolism in supporting deregulated epigenetics in cancer. Specifically, we demonstrate a potential survival mechanism mediated by an IKKβ-p53 signaling axis in cancer upon glutamine deprivation. We found that, upon glutamine depletion, IKKβ can directly phosphorylate p53 on Serine 392, which activates

it, independent of the NF-κB pathway. The newly identified IKKβ-p53 signaling axis is necessary in mediating survival through the upregulation of p53 downstream genes.

Finally, we investigate the therapeutic potential of using dietary glutamine supplementation to inhibit tumor growth by exploiting the protean role of glutamine in cancer metabolism and epigenetics. Our results indicate glutamine supplementation in melanoma tumors downregulates the expression of oncogenes via epigenetic reprogramming and cooperates with targeted therapies. These results further solidify the connection between metabolites and epigenetic changes that can be detrimental to cancer cells that adapted to glutamine deprivation in their microenvironment.

INTRODUCTION

CHAPTER 1: Reprogramming of glutamine metabolism in cancer

Background

Before the discovery of oncogenes and tumor suppressors, the first observations on metabolic reprogramming in cancer was characterized over a century ago when Otto Warburg observed an increase in glucose utilization by tumor cells. Since then, the field of cancer metabolism has gained interest in order to understand the principles of how metabolic pathways are altered in cancer cells compared to normal cells, and how these alterations can support the acquisition and maintenance of tumorigenesis. Of interest, glutamine plays a major role in supporting cancer progression despite its depletion from the cancer environment. How glutamine metabolism is reprogrammed to drive tumor progression, how does its metabolism drive epigenetic changes, and how to exploit these metabolic adaptations for therapeutic benefits are still key questions driving the field of cancer metabolism. In this chapter, I highlight recent understanding in glutamine metabolism in cancer, its effect on epigenetics, and potential therapeutic opportunities.

Cancer and its microenvironment

Solid tumors are highly disorganized and interact with various cell types including endothelial cells, stromal fibroblast, other cancer cells, and immune cells (1). These interactions can directly inflict changes in signal transduction, gene expression, metabolic rewiring, as well as, proliferation within regions of the tumor (2). Thus, the collective properties compromising the tumor microenvironment (TME) leads to a heterogenous population in cancer cells, with varying metabolic requirement and properties within the same tumor (3). This TME creates many challenges for cancer cells including oxidative stress, nutrient depletion, hypoxia, and immune surveillance (Figure 1). Additionally, the fast proliferative nature of cancer cells often leads to poor blood vessel development, which are characterized by leaky vessels that do not deliver sufficient nutrients or effectively remove metabolic waste products such as lactate (4).

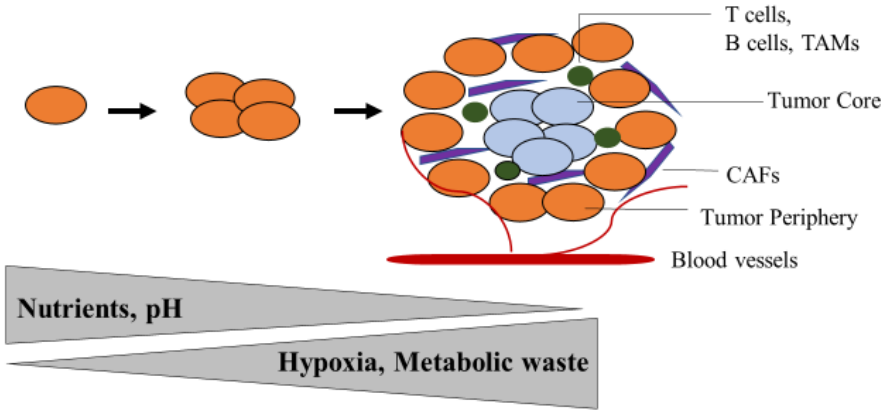

Figure 1: Tumors are metabolically heterogenous. Heterogeneity in the microenvironment with cancer progression. Cancer cells experience intrinsic (epigenetic, genetic, and metabolic programs) and extrinsic variables (nutrient and oxygen availability, waste and pH gradients). CAF, cancer associated fibroblast. TAM, tumor associated macrophage.

In addition to surviving metabolic stress due to insufficient nutrients and accumulated waste products, the dysregulated vasculature surrounding the tumor limit gas exchange and creates regions of hypoxia. Hypoxia has been extensively studied and has been shown to enhance the glycolytic pathway driven by the activation of the transcription factor, hypoxia-inducible factor

1α (HIF-1α), and consequently lead to additional lactate deposition (5). The buildup of lactate creates an acidic TME that directly influences immune cell response, as well as, provide a carbon source to neighboring cancer cells (6, 7). This complex TME can allow cancer cells to outcompete immune and stromal cells for nutrients necessary to carry out biosynthesis and bioenergetic activities.

Deregulated glucose and glutamine metabolism in cancer

Despite the harsh conditions in the TME, fast-growing cancer cells, driven by oncogenes, exhibit increased uptake of nutrients from the environment to support their fast proliferation (8, 9). For example, cancer cells have a higher demand for glucose, which is converted to lactate even in the presence of oxygen, a phenomenon known as the "Warburg effect" (10) (Figure 2). This feature was successfully exploited for diagnostic imaging in positron emission tomography (PET) scanning using ^{18}F-deoxyglucose (FDG), which is a radioactive glucose analog (11). Further studies supported the Warburg effect in showing that alterations in PI-3 kinase/Akt signaling act as a master regulator for glucose uptake and metabolism in cancer. For instance, PI3K/Akt increases the expression and translocation of GLUT1 for the uptake of extracellular glucose, while Akt enhances the activity of hexokinase to prevent the efflux of glucose back outside the cells (12, 13). This diversion of glucose in cultured cancer cells to produce more lactate serves to recycle the pool of NADH and allow glycolysis to persist. Additionally, as previously mentioned, higher lactate production allows for its secretion through monocarboxylate transporters such as MCT4 to acidify the extracellular space (14). Lactate can also be internalized as source of carbon to maintain tumor growth by directly contributing to tricarboxylic acid (TCA) cycle *in vivo* (15) and blocking lactate uptake reduced respiration and suppressed xenograft tumor growth in mice (16). Nonetheless, many studies have now

demonstrated that cancer cells are still capable of producing energy through glucose oxidation and mitochondrial function.

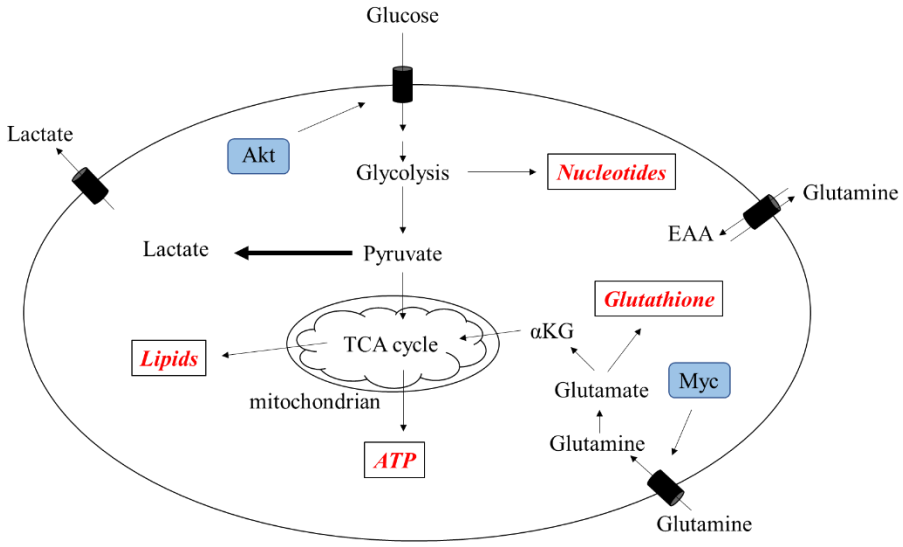

Figure 2: Anabolic pathways that promote tumor growth. Tumor cells depend on glucose to generate glycolytic intermediates to support biosynthetic pathways for nucleotide and lipid biosynthesis and energy production. Tumor cells also exhibit increased uptake of glutamine, which is converted to glutamate by glutaminase to support glutathione production and other biosynthetic processes. Glutamine derived α-ketoglutarate (αKG) can enter the tricarboxylic acid (TCA) cycle to generate energy for the cell.

Glutamine metabolism has been tightly connected to deregulation in glucose metabolism in cancer. As cancer cells divert glucose from the TCA cycle, these cells demonstrate a higher uptake of glutamine *in vitro* (17). The high demand for glutamine in proliferating cells was first observed in the 1950s by Harry Eagle, who demonstrated that *in vitro* cultured HeLa cells required excess glutamine in medium compared to other amino acids (18). The increased reliance on glutamine is critical for the proliferative nature of cancer cells as it is converted to α-ketoglutarate (αKG) and enters the TCA cycle (Figure 2) (19). Moreover, glutamine provides a nitrogen source for the biosynthesis of other amino acids and nucleotides needed for fast growth and replication (20). Finally, glutamine can combat cellular oxidative stress as it supports the synthesis of the antioxidant, glutathione (GSH) (21).

Glutamine is highly abundant in tissue and plasma and the conversion of glutamine to αKG catalyzed by glutaminase enzyme (GLS) often prevents the depletion of the TCA cycle intermediates in cultured cell lines and some tumors in mice (17). Glutamine can also play a role in the uptake of essential amino acids. For instance, the import of the essential amino acid leucine through the neutral antiporter LAT1 was shown to be coupled with the efflux of glutamine (22). This can also be extended to the broad substrates of LAT1 including isoleucine, valine, methionine, and several others (23). While the signaling pathways regulating glutamine uptake are still under investigation, several oncogenes that drive glutamine utilization have been identified. One major oncogenotype is enhanced MYC expression in certain cancer cells (24, 25). MYC is a transcription factor upregulated in proliferating cell and is a driver of glutamine utilization as it induces the expression of the glutamine transporters ASCT2 and SN2, as well as GLS1 among other enzymes that catalyze glutamine (26-28). Similarly, KRAS has been implicated in driving the upregulation of key metabolic enzymes such as GOT1, which would convert glutamine-derived aspartate into oxaloacetate to support growth in pancreatic cancer cells (29).

Tightly linked to metabolism, tumors show heterogeneity in how they experience hypoxia, which directly impacts the metabolism of glucose and glutamine. For instance, HIF-1α increases the expression of several glycolytic enzymes as well as glucose transporters to increase lactate production from glucose (30, 31). In comparison, the effect of HIF-1α on glutamine metabolism is still unclear. A recent study shows that glutamine is effectively shuttled to support lipid synthesis through reductive metabolism of αKG to synthesize acetyl coenzyme A, a central biosynthetic precursor in fatty acid synthesis (32). HIF1α activation also reprograms glutamine reductive metabolism in order to synthesize citrate to maintain cell growth in cells with defective

mitochondria (33). Further work still needed to understand the role glutamine plays in cancer survival and growth under hypoxic stress.

Tumors often persist under glutamine-deprived conditions

It has become more apparent that the paradox of nutrient-addicted cancer cells is that they deplete extracellular nutrients from their environment, and usually become nutrient poor compared to normal tissues (34). As solid tumors grow, increased uptake of glutamine and dysfunctional tumor vascularization often deplete extracellular glutamine from the environment. In fact, like hypoxia, multiple *in vivo* studies demonstrated that glutamine depletion is observed in several solid tumors, including melanomas (35), pancreatic adenocarcinoma (34), colorectal cancer (36), hepatoma and squamous cell carcinoma (37). Therefore, cancer cells develop several mechanisms to survive periods of nutrient starvation and several studies have already begun to delineate some of these alternate adaptations.

One mode of metabolic adaptation in cancer cells is through activating signaling pathways to reduce their glutamine dependency. For instance, recent studies demonstrated metabolic adaptation to glutamine deprivation through the activation of both wild type and mutant p53 in cancer cells to promote survival through the induction of downstream genes such as p21 (38, 39). The activation of p53 under low glutamine has also been shown to induce the expression of microRNA or the arginine transporter SLC7A3 to induce further metabolic adaptations and promote survival (40, 41). In a different study, glutamine deprivation was shown to activate IKKβ, which directly phosphorylates 6-phosphofructo-2-kinase/fructose-2,6-biphosphatase isoform 3 (PFKFB3) and drive aerobic glycolysis to reduce dependence on glutamine (42).

Alternatively, cancer cells can actively promote the uptake of other nutrients to supply their bioenergetic needs or sustain survival upon glutamine depletion. For example, asparagine was sufficient in suppressing apoptosis upon glutamine withdrawal by activating ATF4-dependent adaptive stress response and rescuing cell survival (43). While in KRAS-driven pancreatic cancer cells, they can escape the effects of glutamine withdrawal through activating micropinocytosis, which is a feeding mechanism that internalizes and degrades proteins from their microenvironment (44). This mechanism was also demonstrated in lung, sarcoma, and colon cancer cells expressing mutant KRAS (45). Thus, the activation of oncogenes or loss of tumor suppressors can poise cancer cells in a state of active nutrient scavenging to support their uncontrolled proliferation. The specific mechanisms of how cancer cells attain this metabolic reprogramming and promote survival are continuously being elucidated in order to advance targeted therapies.

Metabolites and deregulated epigenetics

It has become evident that metabolic reprogramming and changes in TME can drive changes in epigenetics that are necessary for cancer survival and progression (46, 47). Indeed, several interactions exist between metabolites and epigenetics modifications such as methylation and acetylation of DNA or histones. These epigenetics modifications are dynamic, reversible, and control gene transcription in response to the changing microenvironment to regulate tumor progression (48).

The epigenetic state is governed by the status of DNA methylation, histone modifications, and chromatin structure. DNA methylation involves the addition of a methyl group to the 5’cytosine in a cluster of CpG islands and is generally associated with repressed transcription. In

comparison, there are several identified histone modifications. Histone acetylation increases accessibility to the DNA and contribute to active transcription (49). In comparison, trimethylation of histone at lysine 9, 27, and 20 (H3K9, H3K27 and H3K20) are associated with repressed transcription and H3K4, H3K36 are often associated with active transcription. Specifically, histone methylations are controlled by the activity of various histone methyltransferases (HMTs) and histone demethylases (HDMs) that govern cellular processes such as transcription and replication (50). Defects in this epigenetic system is apparent in cancer. For example, mutations in the DNA methyltransferase 3-A (DNMT3A) and HMTs, such MLL2 and EZH2, are commonly observed in several human cancers (51-53).

Almost all chromatin modifications require specific metabolites as cofactors. Specifically, HMTs require S-adenosylmethionine (SAM), which is an intermediate metabolite in one-carbon metabolism (Figure 3) (54). In comparison, certain HDMs require αKG as a cofactor for the removal of methyl groups from histones (55). In such a way, the availability of metabolites can directly lead to genetic alterations in response to nutrient availability in the tumor cells or the microenvironment. Interestingly, several studies have begun to delineate this link between cancer metabolism and epigenetics. For instance, it has been previously shown that, under methionine restricted regimen, one-carbon metabolism regulation determines the availability of methionine and modulates levels of H3K4me3 to alter gene transcription (56). Moreover, glucose metabolism, specifically the pentose phosphate pathway, has also been shown to affect regions of chromatin with histone H3K9 modifications that contribute to metastasis in pancreatic cancer (57).

Of interest, JHDMs, Jumonji-domain containing HDMs, which require αKG as a cofactor to mediate histone demethylase activity, further link metabolism and epigenetics (Figure 3) (58).

For instance, JARID1B, a demethylase of H3K4me3 that requires αKG as a cofactor, has been associated with tumor suppressive activity in melanoma (59). Other studies show that cancer cells expressing isocitrate dehydrogenase 1 (IDH1) and IDH2 that catalyze the production of 2-hydroxyglutarate, an analogue of αKG, were able to inhibit H3K9 JHDM activity and increase histone methylation to induce dedifferentiation (60). Similarly, previous work in our lab show that low glutamine in the core regions of solid tumors led to histone hypermethylation due to decreased αKG levels and inhibition of JHDM demethylases (35).

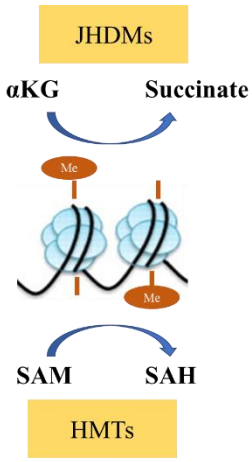

Figure 3: Mechanism of metabolite dependent histone methylation. JmjC-domain-containing histone demethylases (JHDMs) use α-ketoglutarate (αKG) to remove methylation from histones and forms succinate. Histone methylation transferases (HMTs) use S-Adenosyl methionine (SAM) as a cofactor to methylate histones and realse S-adenosyl-L-homocysteine (SAH)

Glutamine deprivation promotes dedifferentiation in cancer

In order to metastasize and induce resistance to targeted therapies, tumor cells can dedifferentiate and acquire mesenchymal traits such as motility, invasiveness and stem cell attributes. This reversible process where cells can undergo mesenchymal transitions during tumor progression is known as epithelial–mesenchymal transition (EMT) (61). It is becoming evident that the EMT state in cancer is controlled by reversible changes in epigenetics and extracellular conditions such hypoxia and nutrient availability (62, 63). For instance, changes in levels of H3K4 and

H3K27 methylation have been shown to control key developmental genes, and consequently affect tumor plasticity and biology (64, 65). Similarly, increase in H3K27 methylation by the activity of the methyltransferase, EZH2 and its analog EZH1, was sufficient to maintain embryonic stem pluripotency (66). Furthermore, activated PI3K/AKT pathway increased metastasis in breast cancer cells by inhibiting the activity of the H3K4 demethylase KDM5A (67).

Since key JHDMs depend on cofactors such as αKG, it is plausible that nutrient deprivation experienced by tumor cells would consequently elicit epigenetic changes and EMT-associated dedifferentiation (61). Indeed, low glutamine levels in the core region of melanoma tumors affect histone methylation and contribute to dedifferentiation and resistance to therapeutics (35). Variation in the intracellular levels of αKG and succinate can also contribute to the histone/DNA demethylation to govern pluripotency in mouse embryonic stem cells (68). This study and others indicate a possible therapeutic potential in exploiting the link between metabolism and epigenetics, which reversibly control the dedifferentiation state in cancer cells and affect tumor growth progression as well as therapeutic response. However, the mechanism of how *in vivo* levels of glutamine and its downstream metabolites in different regions of solid tumors affect growth and resistance remains unclear.

Summary and research direction

It is evident that metabolic heterogeneity rises from both environmental and genetic factors that influence cancer cell metabolism. Additionally, given the reversible nature of epigenetics modifications, it is imperative to understand the impact of metabolism, in particularly *in vivo* levels of glutamine, on cancer. Therefore, understanding the role of metabolic interactions and adaptive pathways in tumor development and progression can provide a strategy to improve

cancer therapies. Therefore, the work discussed in this thesis dissertation is divided between two goals. First, contribute to ongoing research on delineating the survival mechanisms that allow cancer cells to survive periods of glutamine deprivation. This stemmed from the observation that the knockdown of IKKβ, which is activated in the absence of glutamine to modulate glycolysis and survival, directly affected p53 activation, a major metabolic regulator in cancer. Thus, characterizing a novel IKKβ-p53 signaling axis would be beneficial in understanding adaptive mechanisms in cancer cells upon metabolic stress.

This thesis dissertation also focuses on understanding the role of glutamine metabolism *in vivo* and the potential for the use of glutamine supplementation in modulating melanoma epigenetics to inhibit tumor progression and increase the efficacy of targeted therapies. Despite being widely studied *in vitro*, glutamine metabolism *in vivo* was not directly assessed. With the recent reports using infusion of labeled glucose and glutamine, it has become apparent that certain tumors in mice and humans has higher preference for pyruvate carboxylation in supplying the TCA intermediates versus glutamine catabolism and led to accumulation of glucose-derived glutamine (69, 70). Furthermore, *in vitro* conditions that reproduce *in vivo* levels of nutrients demonstrate the increased glutamine uptake did not directly lead to increased growth (71). More importantly, breast cancer cells exhibit differences in glutamine metabolism with basal-type cells being highly dependent on glutamine while luminal-type cells are glutamine independent (72). Thus, an important note to consider is that not all cancer cells depend on exogenous glutamine and more studies are needed to understand the role of glutamine metabolism in cancer cells in the context of the complex microenvironment.

References

1. Egeblad M, Nakasone ES, Werb Z. Tumors as organs: complex tissues that interface with the entire organism. Dev Cell. 2010;18(6):884-901. Epub 2010/07/16. doi: 10.1016/j.devcel.2010.05.012. PubMed PMID: 20627072; PubMed Central PMCID: PMCPMC2905377.
2. Hanahan D, Weinberg Robert A. Hallmarks of Cancer: The Next Generation. Cell.144(5):646-74. doi: 10.1016/j.cell.2011.02.013.
3. Yuneva Mariia O, Fan Teresa WM, Allen Thaddeus D, Higashi Richard M, Ferraris Dana V, Tsukamoto T, et al. The Metabolic Profile of Tumors Depends on Both the Responsible Genetic Lesion and Tissue Type. Cell Metabolism. 2012;15(2):157-70. doi: https://doi.org/10.1016/j.cmet.2011.12.015.
4. Jain RK. Normalization of tumor vasculature: an emerging concept in antiangiogenic therapy. Science. 2005;307(5706):58-62. Epub 2005/01/08. doi: 10.1126/science.1104819. PubMed PMID: 15637262.
5. Xie H, Simon MC. Oxygen availability and metabolic reprogramming in cancer. J Biol Chem. 2017. Epub 2017/08/27. doi: 10.1074/jbc.R117.799973. PubMed PMID: 28842498.
6. Choi SY, Collins CC, Gout PW, Wang Y. Cancer-generated lactic acid: a regulatory, immunosuppressive metabolite? J Pathol. 2013;230(4):350-5. Epub 2013/06/05. doi: 10.1002/path.4218. PubMed PMID: 23729358; PubMed Central PMCID: PMCPMC3757307.
7. San-Millan I, Brooks GA. Reexamining cancer metabolism: lactate production for carcinogenesis could be the purpose and explanation of the Warburg Effect. Carcinogenesis. 2017;38(2):119-33. Epub 2016/12/21. doi: 10.1093/carcin/bgw127. PubMed PMID: 27993896; PubMed Central PMCID: PMCPMC5862360.
8. DeBerardinis RJ, Lum JJ, Hatzivassiliou G, Thompson CB. The Biology of Cancer: Metabolic Reprogramming Fuels Cell Growth and Proliferation. Cell Metabolism. 2008;7(1):11-20. doi: http://dx.doi.org/10.1016/j.cmet.2007.10.002.
9. Kroemer G, Pouyssegur J. Tumor Cell Metabolism: Cancer's Achilles' Heel. Cancer Cell. 2008;13(6):472-82. doi: https://doi.org/10.1016/j.ccr.2008.05.005.
10. Warburg O. On respiratory impairment in cancer cells. Science. 1956;124(3215):269-70.
11. Zhu A, Lee D, Shim H. Metabolic positron emission tomography imaging in cancer detection and therapy response. Semin Oncol. 2011;38(1):55-69. Epub 2011/03/03. doi: 10.1053/j.seminoncol.2010.11.012. PubMed PMID: 21362516; PubMed Central PMCID: PMCPMC3075495.
12. Barthel A, Okino ST, Liao J, Nakatani K, Li J, Whitlock JP, Jr., et al. Regulation of GLUT1 gene transcription by the serine/threonine kinase Akt1. J Biol Chem. 1999;274(29):20281-6. Epub 1999/07/10. doi: 10.1074/jbc.274.29.20281. PubMed PMID: 10400647.
13. Wieman HL, Wofford JA, Rathmell JC. Cytokine stimulation promotes glucose uptake via phosphatidylinositol-3 kinase/Akt regulation of Glut1 activity and trafficking. Mol Biol Cell. 2007;18(4):1437-46. Epub 2007/02/16. doi: 10.1091/mbc.e06-07-0593. PubMed PMID: 17301289; PubMed Central PMCID: PMCPMC1838986.
14. Guillaumond F, Leca J, Olivares O, Lavaut MN, Vidal N, Berthezene P, et al. Strengthened glycolysis under hypoxia supports tumor symbiosis and hexosamine biosynthesis in pancreatic adenocarcinoma. Proc Natl Acad Sci U S A. 2013;110(10):3919-24. Epub 2013/02/15. doi: 10.1073/pnas.1219555110. PubMed PMID: 23407165; PubMed Central PMCID: PMCPMC3593894.
15. Faubert B, Li KY, Cai L, Hensley CT, Kim J, Zacharias LG, et al. Lactate Metabolism in Human Lung Tumors. Cell. 2017;171(2):358-71 e9. Epub 2017/10/07. doi: 10.1016/j.cell.2017.09.019. PubMed PMID: 28985563; PubMed Central PMCID: PMCPMC5684706.
16. Sonveaux P, Vegran F, Schroeder T, Wergin MC, Verrax J, Rabbani ZN, et al. Targeting lactate-fueled respiration selectively kills hypoxic tumor cells in mice. J Clin Invest. 2008;118(12):3930-42. Epub 2008/11/27. doi: 10.1172/jci36843. PubMed PMID: 19033663; PubMed Central PMCID: PMCPMC2582933.
17. Boroughs LK, DeBerardinis RJ. Metabolic pathways promoting cancer cell survival and growth. Nat Cell Biol. 2015;17(4):351-9. doi: 10.1038/ncb3124.
18. Eagle H, Oyama VI, Levy M, Horton CL, Fleischman R. The growth response of mammalian cells in tissue culture to L-glutamine and L-glutamic acid. J Biol Chem. 1956;218(2):607-16. Epub 1956/02/01. PubMed PMID: 13295214.
19. DeBerardinis RJ, Mancuso A, Daikhin E, Nissim I, Yudkoff M, Wehrli S, et al. Beyond aerobic glycolysis: transformed cells can engage in glutamine metabolism that exceeds the requirement for protein and nucleotide synthesis. Proc Natl Acad Sci U S A. 2007;104(49):19345-50. Epub 2007/11/23. doi: 10.1073/pnas.0709747104. PubMed PMID: 18032601; PubMed Central PMCID: PMCPMC2148292.

20. Coloff JL, Murphy JP, Braun CR, Harris IS, Shelton LM, Kami K, et al. Differential Glutamate Metabolism in Proliferating and Quiescent Mammary Epithelial Cells. Cell Metab. 2016;23(5):867-80. Epub 2016/05/03. doi: 10.1016/j.cmet.2016.03.016. PubMed PMID: 27133130.
21. Reid MA, Kong M. Adaptation to metabolic stress: insights into a paradoxical Q. Cell Cycle. 2013;12(12):1807-8. Epub 2013/05/28. doi: 10.4161/cc.25113. PubMed PMID: 23708515; PubMed Central PMCID: PMCPMC3735684.
22. Nicklin P, Bergman P, Zhang B, Triantafellow E, Wang H, Nyfeler B, et al. Bidirectional transport of amino acids regulates mTOR and autophagy. Cell. 2009;136(3):521-34. Epub 2009/02/11. doi: 10.1016/j.cell.2008.11.044. PubMed PMID: 19203585; PubMed Central PMCID: PMCPMC3733119.
23. Yanagida O, Kanai Y, Chairoungdua A, Kim DK, Segawa H, Nii T, et al. Human L-type amino acid transporter 1 (LAT1): characterization of function and expression in tumor cell lines. Biochim Biophys Acta. 2001;1514(2):291-302. Epub 2001/09/15. doi: 10.1016/s0005-2736(01)00384-4. PubMed PMID: 11557028.
24. Wang R, Dillon CP, Shi LZ, Milasta S, Carter R, Finkelstein D, et al. The transcription factor Myc controls metabolic reprogramming upon T lymphocyte activation. Immunity. 2011;35(6):871-82. Epub 2011/12/27. doi: 10.1016/j.immuni.2011.09.021. PubMed PMID: 22195744; PubMed Central PMCID: PMCPMC3248798.
25. Wise DR, DeBerardinis RJ, Mancuso A, Sayed N, Zhang XY, Pfeiffer HK, et al. Myc regulates a transcriptional program that stimulates mitochondrial glutaminolysis and leads to glutamine addiction. Proc Natl Acad Sci U S A. 2008;105(48):18782-7. Epub 2008/11/27. doi: 10.1073/pnas.0810199105. PubMed PMID: 19033189; PubMed Central PMCID: PMCPMC2596212.
26. Eberhardy SR, Farnham PJ. c-Myc mediates activation of the cad promoter via a post-RNA polymerase II recruitment mechanism. J Biol Chem. 2001;276(51):48562-71. Epub 2001/10/24. doi: 10.1074/jbc.M109014200. PubMed PMID: 11673469.
27. Gao P, Tchernyshyov I, Chang T-C, Lee Y-S, Kita K, Ochi T, et al. c-Myc suppression of miR-23a/b enhances mitochondrial glutaminase expression and glutamine metabolism. Nature. 2009;458(7239):762-5. doi: http://www.nature.com/nature/journal/v458/n7239/suppinfo/nature07823_S1.html.
28. Mannava S, Grachtchouk V, Wheeler LJ, Im M, Zhuang D, Slavina EG, et al. Direct role of nucleotide metabolism in C-MYC-dependent proliferation of melanoma cells. Cell Cycle. 2008;7(15):2392-400. Epub 2008/08/05. doi: 10.4161/cc.6390. PubMed PMID: 18677108; PubMed Central PMCID: PMCPMC3744895.
29. Son J, Lyssiotis CA, Ying H, Wang X, Hua S, Ligorio M, et al. Glutamine supports pancreatic cancer growth through a KRAS-regulated metabolic pathway. Nature. 2013;496(7443):101-5. Epub 2013/03/29. doi: 10.1038/nature12040. PubMed PMID: 23535601; PubMed Central PMCID: PMCPMC3656466.
30. Kim JW, Tchernyshyov I, Semenza GL, Dang CV. HIF-1-mediated expression of pyruvate dehydrogenase kinase: a metabolic switch required for cellular adaptation to hypoxia. Cell Metab. 2006;3(3):177-85. Epub 2006/03/07. doi: 10.1016/j.cmet.2006.02.002. PubMed PMID: 16517405.
31. Papandreou I, Cairns RA, Fontana L, Lim AL, Denko NC. HIF-1 mediates adaptation to hypoxia by actively downregulating mitochondrial oxygen consumption. Cell Metab. 2006;3(3):187-97. Epub 2006/03/07. doi: 10.1016/j.cmet.2006.01.012. PubMed PMID: 16517406.
32. Metallo CM, Gameiro PA, Bell EL, Mattaini KR, Yang J, Hiller K, et al. Reductive glutamine metabolism by IDH1 mediates lipogenesis under hypoxia. Nature. 2011;481:380. doi: 10.1038/nature10602 https://www.nature.com/articles/nature10602#supplementary-information.
33. Mullen AR, Wheaton WW, Jin ES, Chen P-H, Sullivan LB, Cheng T, et al. Reductive carboxylation supports growth in tumour cells with defective mitochondria. Nature. 2011;481:385. doi: 10.1038/nature10642 https://www.nature.com/articles/nature10642#supplementary-information.
34. Kamphorst JJ, Nofal M, Commisso C, Hackett SR, Lu W, Grabocka E, et al. Human pancreatic cancer tumors are nutrient poor and tumor cells actively scavenge extracellular protein. Cancer Res. 2015;75(3):544-53. Epub 2015/02/04. doi: 10.1158/0008-5472.can-14-2211. PubMed PMID: 25644265; PubMed Central PMCID: PMCPMC4316379.
35. Pan M, Reid MA, Lowman XH, Kulkarni RP, Tran TQ, Liu X, et al. Regional glutamine deficiency in tumours promotes dedifferentiation through inhibition of histone demethylation. Nat Cell Biol. 2016. Epub 2016/09/13. doi: 10.1038/ncb3410. PubMed PMID: 27617932.
36. Denkert C, Budczies J, Weichert W, Wohlgemuth G, Scholz M, Kind T, et al. Metabolite profiling of human colon carcinoma – deregulation of TCA cycle and amino acid turnover. Molecular Cancer. 2008;7:72-. doi: 10.1186/1476-4598-7-72. PubMed PMID: PMC2569965.
37. Roberts E, Frankel S. Free amino acids in normal and neoplastic tissues of mice as studied by paper chromatography. Cancer Res. 1949;9(11):645-8, 3 pl. Epub 1949/11/01. PubMed PMID: 15392817.

38. Reid MA, Wang WI, Rosales KR, Welliver MX, Pan M, Kong M. The B55alpha subunit of PP2A drives a p53-dependent metabolic adaptation to glutamine deprivation. Mol Cell. 2013;50(2):200-11. Epub 2013/03/19. doi: 10.1016/j.molcel.2013.02.008. PubMed PMID: 23499005.
39. Tran TQ, Lowman XH, Reid MA, Mendez-Dorantes C, Pan M, Yang Y, et al. Tumor-associated mutant p53 promotes cancer cell survival upon glutamine deprivation through p21 induction. Oncogene. 2016. Epub 2016/10/11. doi: 10.1038/onc.2016.360. PubMed PMID: 27721412.
40. Lowman XH, Hanse EA, Yang Y, Ishak Gabra MB, Tran TQ, Li H, et al. p53 Promotes Cancer Cell Adaptation to Glutamine Deprivation by Upregulating Slc7a3 to Increase Arginine Uptake. Cell Reports. 2019;26(11):3051-60.e4. doi: 10.1016/j.celrep.2019.02.037.
41. Yang Y, Ishak Gabra MB, Hanse EA, Lowman XH, Tran TQ, Li H, et al. MiR-135 suppresses glycolysis and promotes pancreatic cancer cell adaptation to metabolic stress by targeting phosphofructokinase-1. Nature Communications. 2019;10(1):809. doi: 10.1038/s41467-019-08759-0.
42. Reid MA, Lowman XH, Pan M, Tran TQ, Warmoes MO, Ishak Gabra MB, et al. IKKbeta promotes metabolic adaptation to glutamine deprivation via phosphorylation and inhibition of PFKFB3. Genes Dev. 2016;30(16):1837-51. Epub 2016/09/03. doi: 10.1101/gad.287235.116. PubMed PMID: 27585591; PubMed Central PMCID: PMCPMC5024682.
43. Zhang J, Fan J, Venneti S, Cross JR, Takagi T, Bhinder B, et al. Asparagine plays a critical role in regulating cellular adaptation to glutamine depletion. Mol Cell. 2014;56(2):205-18. Epub 2014/09/23. doi: 10.1016/j.molcel.2014.08.018. PubMed PMID: 25242145; PubMed Central PMCID: PMCPMC4224619.
44. Commisso C, Davidson SM, Soydaner-Azeloglu RG, Parker SJ, Kamphorst JJ, Hackett S, et al. Macropinocytosis of protein is an amino acid supply route in Ras-transformed cells. Nature. 2013;497(7451):633-7. Epub 2013/05/15. doi: 10.1038/nature12138. PubMed PMID: 23665962; PubMed Central PMCID: PMCPMC3810415.
45. Tajiri H, Uruno T, Shirai T, Takaya D, Matsunaga S, Setoyama D, et al. Targeting Ras-Driven Cancer Cell Survival and Invasion through Selective Inhibition of DOCK1. Cell Rep. 2017;19(5):969-80. Epub 2017/05/04. doi: 10.1016/j.celrep.2017.04.016. PubMed PMID: 28467910.
46. Gao X, Reid MA, Kong M, Locasale JW. Metabolic interactions with cancer epigenetics. Mol Aspects Med. 2016. Epub 2016/09/14. doi: 10.1016/j.mam.2016.09.001. PubMed PMID: 27620316.
47. Suvà ML, Riggi N, Bernstein BE. Epigenetic Reprogramming in Cancer. Science. 2013;339(6127):1567-70. doi: 10.1126/science.1230184.
48. Fardi M, Solali S, Farshdousti Hagh M. Epigenetic mechanisms as a new approach in cancer treatment: An updated review. Genes Dis. 2018;5(4):304-11. Epub 2018/12/29. doi: 10.1016/j.gendis.2018.06.003. PubMed PMID: 30591931; PubMed Central PMCID: PMCPMC6303480.
49. Greer EL, Shi Y. Histone methylation: a dynamic mark in health, disease and inheritance. Nat Rev Genet. 2012;13(5):343-57. Epub 2012/04/05. doi: 10.1038/nrg3173. PubMed PMID: 22473383; PubMed Central PMCID: PMCPMC4073795.
50. Mosammaparast N, Shi Y. Reversal of histone methylation: biochemical and molecular mechanisms of histone demethylases. Annu Rev Biochem. 2010;79:155-79. Epub 2010/04/09. doi: 10.1146/annurev.biochem.78.070907.103946. PubMed PMID: 20373914.
51. Fong CY, Morison J, Dawson MA. Epigenetics in the hematologic malignancies. Haematologica. 2014;99(12):1772-83. Epub 2014/12/05. doi: 10.3324/haematol.2013.092007. PubMed PMID: 25472952; PubMed Central PMCID: PMCPMC4258753.
52. Morin RD, Mendez-Lago M, Mungall AJ, Goya R, Mungall KL, Corbett RD, et al. Frequent mutation of histone-modifying genes in non-Hodgkin lymphoma. Nature. 2011;476(7360):298-303. Epub 2011/07/29. doi: 10.1038/nature10351. PubMed PMID: 21796119; PubMed Central PMCID: PMCPMC3210554.
53. Nikoloski G, Langemeijer SM, Kuiper RP, Knops R, Massop M, Tonnissen ER, et al. Somatic mutations of the histone methyltransferase gene EZH2 in myelodysplastic syndromes. Nat Genet. 2010;42(8):665-7. Epub 2010/07/06. doi: 10.1038/ng.620. PubMed PMID: 20601954.
54. Locasale JW. Serine, glycine and one-carbon units: cancer metabolism in full circle. Nat Rev Cancer. 2013;13(8):572-83. Epub 2013/07/05. doi: 10.1038/nrc3557. PubMed PMID: 23822983; PubMed Central PMCID: PMCPMC3806315.
55. Kooistra SM, Helin K. Molecular mechanisms and potential functions of histone demethylases. Nat Rev Mol Cell Biol. 2012;13(5):297-311. Epub 2012/04/05. doi: 10.1038/nrm3327. PubMed PMID: 22473470.
56. Mentch Samantha J, Mehrmohamadi M, Huang L, Liu X, Gupta D, Mattocks D, et al. Histone Methylation Dynamics and Gene Regulation Occur through the Sensing of One-Carbon Metabolism. Cell Metabolism. 2015;22(5):861-73. doi: 10.1016/j.cmet.2015.08.024.

57. McDonald OG, Li X, Saunders T, Tryggvadottir R, Mentch SJ, Warmoes MO, et al. Epigenomic reprogramming during pancreatic cancer progression links anabolic glucose metabolism to distant metastasis. Nat Genet. 2017;49(3):367-76. Epub 2017/01/17. doi: 10.1038/ng.3753. PubMed PMID: 28092686; PubMed Central PMCID: PMCPMC5695682.
58. Klose RJ, Zhang Y. Regulation of histone methylation by demethylimination and demethylation. Nat Rev Mol Cell Biol. 2007;8(4):307-18. Epub 2007/03/08. doi: 10.1038/nrm2143. PubMed PMID: 17342184.
59. Roesch A, Mueller AM, Stempfl T, Moehle C, Landthaler M, Vogt T. RBP2-H1/JARID1B is a transcriptional regulator with a tumor suppressive potential in melanoma cells. Int J Cancer. 2008;122(5):1047-57. Epub 2007/11/02. doi: 10.1002/ijc.23211. PubMed PMID: 17973255.
60. Lu C, Ward PS, Kapoor GS, Rohle D, Turcan S, Abdel-Wahab O, et al. IDH mutation impairs histone demethylation and results in a block to cell differentiation. Nature. 2012;483(7390):474-8. Epub 2012/02/22. doi: 10.1038/nature10860. PubMed PMID: 22343901; PubMed Central PMCID: PMCPMC3478770.
61. Lu C, Thompson Craig B. Metabolic Regulation of Epigenetics. Cell Metabolism. 2012;16(1):9-17. doi: http://dx.doi.org/10.1016/j.cmet.2012.06.001.
62. Shen H, Laird Peter W. Interplay between the Cancer Genome and Epigenome. Cell. 2013;153(1):38-55. doi: https://doi.org/10.1016/j.cell.2013.03.008.
63. Grandy RA, Whitfield TW, Wu H, Fitzgerald MP, VanOudenhove JJ, Zaidi SK, et al. Genome-Wide Studies Reveal that H3K4me3 Modification in Bivalent Genes Is Dynamically Regulated during the Pluripotent Cell Cycle and Stabilized upon Differentiation. Molecular and Cellular Biology. 2016;36(4):615-27. doi: 10.1128/mcb.00877-15.
64. Prickaerts P, Adriaens ME, Beucken Tvd, Koch E, Dubois L, Dahlmans VEH, et al. Hypoxia increases genome-wide bivalent epigenetic marking by specific gain of H3K27me3. Epigenetics & Chromatin. 2016;9:46. doi: 10.1186/s13072-016-0086-0. PubMed PMID: PMC5080723.
65. Shen X, Liu Y, Hsu Y-J, Fujiwara Y, Kim J, Mao X, et al. EZH1 Mediates Methylation on Histone H3 Lysine 27 and Complements EZH2 in Maintaining Stem Cell Identity and Executing Pluripotency. Molecular Cell. 2008;32(4):491-502. doi: https://doi.org/10.1016/j.molcel.2008.10.016.
66. Spangle Jennifer M, Dreijerink Koen M, Groner Anna C, Cheng H, Ohlson Carolynn E, Reyes J, et al. PI3K/AKT Signaling Regulates H3K4 Methylation in Breast Cancer. Cell Reports. 2016;15(12):2692-704. doi: http://dx.doi.org/10.1016/j.celrep.2016.05.046.
67. Li L, Li W. Epithelial–mesenchymal transition in human cancer: Comprehensive reprogramming of metabolism, epigenetics, and differentiation. Pharmacology & Therapeutics. 2015;150:33-46. doi: https://doi.org/10.1016/j.pharmthera.2015.01.004.
68. Carey BW, Finley LW, Cross JR, Allis CD, Thompson CB. Intracellular alpha-ketoglutarate maintains the pluripotency of embryonic stem cells. Nature. 2015;518(7539):413-6. Epub 2014/12/10. doi: 10.1038/nature13981. PubMed PMID: 25487152; PubMed Central PMCID: PMCPMC4336218.
69. Cheng T, Sudderth J, Yang C, Mullen AR, Jin ES, Mates JM, et al. Pyruvate carboxylase is required for glutamine-independent growth of tumor cells. Proc Natl Acad Sci U S A. 2011;108(21):8674-9. Epub 2011/05/11. doi: 10.1073/pnas.1016627108. PubMed PMID: 21555572; PubMed Central PMCID: PMCPMC3102381.
70. Marin-Valencia I, Yang C, Mashimo T, Cho S, Baek H, Yang X-L, et al. Analysis of Tumor Metabolism Reveals Mitochondrial Glucose Oxidation in Genetically Diverse Human Glioblastomas in the Mouse Brain In Vivo. Cell Metabolism. 2012;15(6):827-37. doi: https://doi.org/10.1016/j.cmet.2012.05.001.
71. Vande Voorde J, Ackermann T, Pfetzer N, Sumpton D, Mackay G, Kalna G, et al. Improving the metabolic fidelity of cancer models with a physiological cell culture medium. Science Advances. 2019;5(1):eaau7314. doi: 10.1126/sciadv.aau7314.
72. Kung HN, Marks JR, Chi JT. Glutamine synthetase is a genetic determinant of cell type-specific glutamine independence in breast epithelia. PLoS Genet. 2011;7(8):e1002229. Epub 2011/08/20. doi: 10.1371/journal.pgen.1002229. PubMed PMID: 21852960; PubMed Central PMCID: PMCPMC3154963.
73. Pavlova NN, Hui S, Ghergurovich JM, Fan J, Intlekofer AM, White RM, et al. As Extracellular Glutamine Levels Decline, Asparagine Becomes an Essential Amino Acid. Cell Metab. 2018;27(2):428-38 e5. Epub 2018/01/18. doi: 10.1016/j.cmet.2017.12.006. PubMed PMID: 29337136; PubMed Central PMCID: PMCPMC5803449.
74. Tajan M, Hock AK, Blagih J, Robertson NA, Labuschagne CF, Kruiswijk F, et al. A Role for p53 in the Adaptation to Glutamine Starvation through the Expression of SLC1A3. Cell Metab. 2018;28(5):721-36 e6. doi: 10.1016/j.cmet.2018.07.005. PubMed PMID: 30122553; PubMed Central PMCID: PMC6224545.
75. Klose RJ, Kallin EM, Zhang Y. JmjC-domain-containing proteins and histone demethylation. Nature Reviews Genetics. 2006;7(9):715-27. doi: 10.1038/nrg1945.

76. Davidson SM, Papagiannakopoulos T, Olenchock BA, Heyman JE, Keibler MA, Luengo A, et al. Environment Impacts the Metabolic Dependencies of Ras-Driven Non-Small Cell Lung Cancer. Cell Metab. 2016;23(3):517-28. Epub 2016/02/09. doi: 10.1016/j.cmet.2016.01.007. PubMed PMID: 26853747; PubMed Central PMCID: PMCPMC4785096.
77. Sellers K, Fox MP, Bousamra M, II, Slone SP, Higashi RM, Miller DM, et al. Pyruvate carboxylase is critical for non–small-cell lung cancer proliferation. The Journal of Clinical Investigation. 2015;125(2):687-98. doi: 10.1172/JCI72873.
78. Fahr MJ, Kornbluth J, Blossom S, Schaeffer R, Klimberg VS. Harry M. Vars Research Award. Glutamine enhances immunoregulation of tumor growth. JPEN J Parenter Enteral Nutr. 1994;18(6):471-6. Epub 1994/11/01. doi: 10.1177/0148607194018006471. PubMed PMID: 7602720.
79. Klimberg VS, Souba WW, Salloum RM, Plumley DA, Cohen FS, Dolson DJ, et al. Glutamine-enriched diets support muscle glutamine metabolism without stimulating tumor growth. Journal of Surgical Research. 1990;48(4):319-23. doi: https://doi.org/10.1016/0022-4804(90)90066-B.
80. Kuhn KS, Muscaritoli M, Wischmeyer P, Stehle P. Glutamine as indispensable nutrient in oncology: experimental and clinical evidence. Eur J Nutr. 2010;49(4):197-210. Epub 2009/11/26. doi: 10.1007/s00394-009-0082-2. PubMed PMID: 19936817.
81. Søndergaard JN, Nazarian R, Wang Q, Guo D, Hsueh T, Mok S, et al. Differential sensitivity of melanoma cell lines with BRAFV600Emutation to the specific Raf inhibitor PLX4032. Journal of Translational Medicine. 2010;8(1):39. doi: 10.1186/1479-5876-8-39.
82. Hernandez-Davies JE, Tran TQ, Reid MA, Rosales KR, Lowman XH, Pan M, et al. Vemurafenib resistance reprograms melanoma cells towards glutamine dependence. Journal of Translational Medicine. 2015;13(1):210. doi: 10.1186/s12967-015-0581-2.
83. Dankort D, Curley DP, Cartlidge RA, Nelson B, Karnezis AN, Damsky WE, Jr., et al. Braf(V600E) cooperates with Pten loss to induce metastatic melanoma. Nat Genet. 2009;41(5):544-52. doi: 10.1038/ng.356. PubMed PMID: 19282848; PubMed Central PMCID: PMC2705918.
84. Ho VW, Leung K, Hsu A, Luk B, Lai J, Shen SY, et al. A Low Carbohydrate, High Protein Diet Slows Tumor Growth and Prevents Cancer Initiation. Cancer Research. 2011;71(13):4484-93. doi: 10.1158/0008-5472.can-10-3973.
85. Gray-Schopfer V, Wellbrock C, Marais R. Melanoma biology and new targeted therapy. Nature. 2007;445:851. doi: 10.1038/nature05661.
86. Hugo W, Zaretsky JM, Sun L, Song C, Moreno BH, Hu-Lieskovan S, et al. Genomic and Transcriptomic Features of Response to Anti-PD-1 Therapy in Metastatic Melanoma. Cell. 2016;165(1):35-44. doi: 10.1016/j.cell.2016.02.065. PubMed PMID: 26997480; PubMed Central PMCID: PMC4808437.
87. Weinstein D, Leininger J, Hamby C, Safai B. Diagnostic and Prognostic Biomarkers in Melanoma. The Journal of Clinical and Aesthetic Dermatology. 2014;7(6):13-24. PubMed PMID: PMC4086529.
88. Fischer GM, Vashisht Gopal YN, McQuade JL, Peng W, DeBerardinis RJ, Davies MA. Metabolic strategies of melanoma cells: Mechanisms, interactions with the tumor microenvironment, and therapeutic implications. Pigment Cell & Melanoma Research. 2018;31(1):11-30. doi: doi:10.1111/pcmr.12661.
89. Lyssiotis CA, Kimmelman AC. Metabolic Interactions in the Tumor Microenvironment. Trends in Cell Biology. 2017;27(11):863-75. doi: 10.1016/j.tcb.2017.06.003.
90. Liu P-S, Wang H, Li X, Chao T, Teav T, Christen S, et al. [alpha]-ketoglutarate orchestrates macrophage activation through metabolic and epigenetic reprogramming. Nat Immunol. 2017;18(9):985-94. doi: 10.1038/ni.3796 http://www.nature.com/ni/journal/v18/n9/abs/ni.3796.html#supplementary-information.
91. Sciacovelli M, Gonçalves E, Johnson TI, Zecchini VR, da Costa ASH, Gaude E, et al. Fumarate is an epigenetic modifier that elicits epithelial-to-mesenchymal transition. Nature. 2016;537:544. doi: 10.1038/nature19353
https://www.nature.com/articles/nature19353#supplementary-information.
92. Tran TQ, Lowman XH, Kong M. Molecular Pathways: Metabolic Control of Histone Methylation and Gene Expression in Cancer. Clin Cancer Res. 2017;23(15):4004-9. Epub 2017/04/14. doi: 10.1158/1078-0432.ccr-16-2506. PubMed PMID: 28404599; PubMed Central PMCID: PMCPMC5553983.
93. Cantor JR, Abu-Remaileh M, Kanarek N, Freinkman E, Gao X, Louissaint A, et al. Physiologic Medium Rewires Cellular Metabolism and Reveals Uric Acid as an Endogenous Inhibitor of UMP Synthase. Cell. 2017;169(2):258-72.e17. doi: https://doi.org/10.1016/j.cell.2017.03.023.
94. Sayegh J, Cao J, Zou MR, Morales A, Blair LP, Norcia M, et al. Identification of small molecule inhibitors of Jumonji AT-rich interactive domain 1B (JARID1B) histone demethylase by a sensitive high throughput screen.

The Journal of biological chemistry. 2013;288(13):9408-17. Epub 02/13. doi: 10.1074/jbc.M112.419861. PubMed PMID: 23408432.
95. Wang L, Chang J, Varghese D, Dellinger M, Kumar S, Best AM, et al. A small molecule modulates Jumonji histone demethylase activity and selectively inhibits cancer growth. Nat Commun. 2013;4:2035. Epub 2013/06/26. doi: 10.1038/ncomms3035. PubMed PMID: 23792809; PubMed Central PMCID: PMCPMC3724450.
96. Kwong LN, Costello JC, Liu H, Jiang S, Helms TL, Langsdorf AE, et al. Oncogenic NRAS signaling differentially regulates survival and proliferation in melanoma. Nature Medicine. 2012;18(10):1503-10. doi: 10.1038/nm.2941.
97. Metzner T, Bedeir A, Held G, Peter-Vörösmarty B, Ghassemi S, Heinzle C, et al. Fibroblast growth factor receptors as therapeutic targets in human melanoma: synergism with BRAF inhibition. The Journal of investigative dermatology. 2011;131(10):2087-95. Epub 07/14. doi: 10.1038/jid.2011.177. PubMed PMID: 21753785.
98. Joseph EW, Pratilas CA, Poulikakos PI, Tadi M, Wang W, Taylor BS, et al. The RAF inhibitor PLX4032 inhibits ERK signaling and tumor cell proliferation in a V600E BRAF-selective manner. Proceedings of the National Academy of Sciences. 2010;107(33):14903-8. doi: 10.1073/pnas.1008990107.
99. Melis GC, ter Wengel N, Boelens PG, van Leeuwen PA. Glutamine: recent developments in research on the clinical significance of glutamine. Current Opinion in Clinical Nutrition & Metabolic Care. 2004;7(1):59-70. PubMed PMID: 00075197-200401000-00011.
100. Maddocks ODK, Athineos D, Cheung EC, Lee P, Zhang T, van den Broek NJF, et al. Modulating the therapeutic response of tumours to dietary serine and glycine starvation. Nature. 2017;544(7650):372-6. Epub 2017/04/21. doi: 10.1038/nature22056. PubMed PMID: 28425994.
101. Martuscello RT, Vedam-Mai V, McCarthy DJ, Schmoll ME, Jundi MA, Louviere CD, et al. A Supplemented High-Fat Low-Carbohydrate Diet for the Treatment of Glioblastoma. Clinical Cancer Research. 2016;22(10):2482-95. doi: 10.1158/1078-0432.ccr-15-0916.
102. Xia S, Lin R, Jin L, Zhao L, Kang HB, Pan Y, et al. Prevention of Dietary-Fat-Fueled Ketogenesis Attenuates BRAF V600E Tumor Growth. Cell Metab. 2017;25(2):358-73. doi: 10.1016/j.cmet.2016.12.010. PubMed PMID: 28089569; PubMed Central PMCID: PMC5299059.
103. Kanarek N, Keys HR, Cantor JR, Lewis CA, Chan SH, Kunchok T, et al. Histidine catabolism is a major determinant of methotrexate sensitivity. Nature. 2018;559(7715):632-6. doi: 10.1038/s41586-018-0316-7.
104. Hopkins BD, Pauli C, Du X, Wang DG, Li X, Wu D, et al. Suppression of insulin feedback enhances the efficacy of PI3K inhibitors. Nature. 2018;560(7719):499-503. doi: 10.1038/s41586-018-0343-4.
105. Hensley Christopher T, Faubert B, Yuan Q, Lev-Cohain N, Jin E, Kim J, et al. Metabolic Heterogeneity in Human Lung Tumors. Cell. 2016;164(4):681-94. doi: http://dx.doi.org/10.1016/j.cell.2015.12.034.
106. Eales KL, Hollinshead KER, Tennant DA. Hypoxia and metabolic adaptation of cancer cells. Oncogenesis. 2016;5:e190. doi: 10.1038/oncsis.2015.50.
107. Yoo CB, Jones PA. Epigenetic therapy of cancer: past, present and future. Nature Reviews Drug Discovery. 2006;5:37. doi: 10.1038/nrd1930.
108. Li S, Shen L, Chen KN. Association between H3K4 methylation and cancer prognosis: A meta-analysis. Thorac Cancer. 2018;9(7):794-9. Epub 2018/05/09. doi: 10.1111/1759-7714.12647. PubMed PMID: 29737623; PubMed Central PMCID: PMCPMC6026618.
109. Lewis R, Li YD, Hoffman L, Hashizume R, Gravohac G, Rice G, et al. Global Reduction of H3K4me3 Improves Chemotherapeutic Efficacy for Pediatric Ependymomas. Neoplasia. 2019;21(6):505-15. doi: https://doi.org/10.1016/j.neo.2019.03.012.
110. Vatrinet R, Leone G, De Luise M, Girolimetti G, Vidone M, Gasparre G, et al. The α-ketoglutarate dehydrogenase complex in cancer metabolic plasticity. Cancer & Metabolism. 2017;5(1):3. doi: 10.1186/s40170-017-0165-0.
111. Nazarian R, Shi H, Wang Q, Kong X, Koya RC, Lee H, et al. Melanomas acquire resistance to B-RAF(V600E) inhibition by RTK or N-RAS upregulation. Nature. 2010;468:973. doi: 10.1038/nature09626 https://www.nature.com/articles/nature09626#supplementary-information.
112. Carugo A, Genovese G, Seth S, Nezi L, Rose Johnathon L, Bossi D, et al. In Vivo Functional Platform Targeting Patient-Derived Xenografts Identifies WDR5-Myc Association as a Critical Determinant of Pancreatic Cancer. Cell Reports. 2016;16(1):133-47. doi: http://dx.doi.org/10.1016/j.celrep.2016.05.063.
113. Liu X, Sadhukhan S, Sun S, Wagner GR, Hirschey MD, Qi L, et al. High-Resolution Metabolomics with Acyl-CoA Profiling Reveals Widespread Remodeling in Response to Diet. Mol Cell Proteomics. 2015;14(6):1489-500. Epub 2015/03/22. doi: 10.1074/mcp.M114.044859. PubMed PMID: 25795660; PubMed Central PMCID: PMCPMC4458715.

CHAPTER 2: IKKβ activates p53 to promote cancer cell adaptation to glutamine deprivation

Background:

Previously, IKK complex was shown to be activated in response to nutrient starvation as well as increased ROS levels upon glutamine deprivation. These studies highlight the important role of IKKβ activation upon stress to promote metabolic adaptation independent of NF-κB. However, there remains a gap in our understanding of the changes in IKKβ downstream signaling events that lead to cell survival upon metabolic stress. This chapter will provide evidence for the activation of p53 and its downstream genes in an IKKβ dependent manner under low levels of glutamine. This is especially important since p53 has been established as a key regulator of metabolic adaptation in response to various stress conditions. Moreover, the identified mechanism would expand our understanding of how cancer cells could potentially develop resistance to glutamine metabolism targeted inhibitors. This chapter has been adapted from a publication (Ishak Gabra et al., Oncogenesis, 2018)

IKKβ activates p53 to promote cancer cell adaptation to glutamine deprivation

Mari B. Ishak Gabra[1], Ying Yang[1], Xazmin H. Lowman[1], Michael A. Reid[2], Thai Q. Tran[1], and Mei Kong[1*]

1Department of Molecular Biology and Biochemistry; School of Biological Sciences, University of California, Irvine, Irvine, CA 92697, USA

2 Department of Pharmacology and Cancer Biology, Duke University School of Medicine, Durham, NC 27708, USA

*Corresponding Author:

Mei Kong

Department of Molecular Biology and Biochemistry

School of Biological Sciences, University of California, Irvine

Irvine, CA 92697

Phone: 949-824-5244

meik1@uci.edu

Abstract

One of the hallmarks of cancer is the ability to reprogram cellular metabolism to increase the uptake of necessary nutrients such as glucose and glutamine. Driven by oncogenes, cancer cells have increased glutamine uptake to support their highly proliferative nature. However, as cancer cells continue to replicate and grow, they lose access to vascular tissues and deplete local supply of nutrients and oxygen. We previously showed that many tumor cells situate in a low glutamine microenvironment in vivo, yet the mechanisms of how they are able to adapt to this metabolic stress are still not fully understood. Here, we report that IκB kinase β (IKKβ) is needed to promote survival and its activation is accompanied by phosphorylation of the metabolic sensor, p53, in response to glutamine deprivation. Knockdown of IKKβ decreases the level of wildtype and mutant p53 phosphorylation and its transcriptional activity, indicating a novel relationship between IKKβ and p53 in mediating cancer cell survival in response to glutamine withdrawal. Phosphopeptide mass spectrometry analysis further reveals that IKKβ phosphorylates p53 on Ser392 to facilitate its activation upon glutamine deprivation, independent of the NF-κB pathway. The results of this study offer an insight into the metabolic reprogramming in cancer cells that is dependent on a previously unidentified IKKβ-p53 signaling axis in response to glutamine depletion. More importantly, this study highlights a new therapeutic strategy for cancer treatment and advances our understanding of adaptive mechanisms that could lead to resistance to current glutamine targeting therapies.

Keywords:

IKKβ, p53, metabolic stress, glutamine

Introduction

The increased importance of glutamine uptake driven by oncogenes in cancer cells makes targeting glutamine metabolism an appealing approach for improved cancer therapy [1-3]. Glutamine, a non-essential amino acid, can be utilized by highly proliferative cancer cells to support cancer growth by replenishing the tricarboxylic acid (TCA) cycle intermediates, and providing a nitrogen source for the biosynthesis of other amino acids and nucleotides [4-6]. Moreover, glutamine can combat cellular oxidative stress as it supports the synthesis of the antioxidant, glutathione (GSH) [7]. However, as tumors continue to grow, increased glutamine demand and poor vascularization lead to its depletion in the microenvironment [8]. Multiple in vivo studies, including our recent publication, reveal that glutamine is among the amino acids depleted in the core of several xenograft tumors including melanoma, pancreatic adenocarcinoma, and colorectal cancer [9-11]. Therefore, cancer cells develop mechanisms to survive periods of nutrient starvation as new vascularization is developed. We recently reported that cancer cells are able to survive glutamine deprivation through the activation of cell cycle arrest genes mediated by p53, or metabolic reprogramming of glycolytic enzymes, but other mechanisms can also contribute to cell survival [12, 13]. Thus, understanding the molecular mechanisms of how cancer cells attain this metabolic reprogramming and promote survival in a glutamine poor environment needs to be fully understood in order to increase the efficacy of targeting glutamine metabolism therapeutically.

Recently, several studies have shown that the tumor suppressor p53 plays a critical role in the aberrant metabolism in cancer and can orchestrate cellular adaptions to metabolic stress [14-17]. For instance, p53 was shown to upregulate oxidative phosphorylation and modulate antioxidants in lung cancer cells in response to glycolytic stress [18]. This role was further demonstrated by

the activation of p53 upon glucose starvation and its regulation of TIGAR, a novel regulator of glycolytic genes, in response to this metabolic stress [19]. Similarly, serine or glutamine deprivation have been shown to activate p53 to promote survival through the induction of downstream genes such as the cyclin dependent kinase inhibitor, p21 [13, 20]. Thus, it has become apparent that p53 acts as a master metabolic regulator, which can promote cancer cell survival in response to metabolic stress through multiple mechanisms.

The activation of the I-kappa-B-kinase (IKK) complex and the nuclear factor kappa B (NF-κB) subunits is implicated in the inflammatory response, cell survival, and cancer [21-23]. Despite the homology between the IKK complex kinases, IKKα and IKKβ, the IKKβ subunit is required for the rapid activation of NF-κB in response to stimuli, and is shown to phosphorylate other substrates directly, such as BAD, p85α, and β-catenin, independent of the IKK complex [24-26]. Recent studies reveal a role for IKKβ in sensing metabolic stress. For instance, IKKβ is activated upon leucine starvation and promotes feedback inhibition of the PI3K/AKT signaling pathway [27]. Moreover, the IKK complex regulates oxidative phosphorylation in normal and cancer cells by upregulating mitochondrial synthesis of cytochrome c oxidase 2 when glucose levels are low [28]. IKKβ is also activated upon glutamine deprivation, and inhibits PFKFB3, a major driver of glycolysis, to regulate cellular metabolic adaptation [29].

Even though several studies demonstrate the activation of IKKβ and p53 under low glutamine conditions to promote cellular adaptation, the mechanism of how these major metabolic sensors interact to promote cell survival upon metabolic stress remains unknown. Here, we show that IKKβ modulates the activity of p53 in response to glutamine depletion to promote cancer cell adaptation. We further demonstrate that IKKβ phosphorylates p53 on Ser392 to enhance its transcriptional activity, independent of the NF-κB pathway. Our data provide a mechanistic

insight into the role of an IKKβ-p53 signaling axis that mediates cancer survival in the nutrient deprived tumor microenvironment.

Results

Glutamine deprivation induced p53 activation is IKKβ dependent

Previously, we reported that IKKβ is phosphorylated at Ser177 in response to low glutamine to downregulate glycolysis [29]. To further confirm the role of IKKβ in mediating cell survival, we stably knocked down IKKβ in HT1080 cells using shRNA and cultured IKKβ-deficient and control cells in glutamine free medium. Consistently, we found that IKKβ-deficient cells were more sensitive to glutamine deprivation (Fig. 1a). Since p53 is known to be phosphorylated in response to glutamine deprivation and its phosphorylation is reversed by the use of antioxidants [12], we asked whether IKKβ and p53 are acting synergistically to mediate cell survival. To test this, we cultured Ras-transformed 3T3 mouse embryonic fibroblast (MEF) cells with wild type, Ikkα -/- or Ikkβ -/- alleles in glutamine free medium for 24 hours. p53 phosphorylation on Ser18 was observed in control and IKKα knockout cells in response to glutamine starvation. In contrast, the increase in p53 phosphorylation was blocked in IKKβ knockout cells (Fig. 1b). Consistently, HT1080 cells transiently transfected with siRNA against scrambled control, IKKα, or IKKβ and cultured in glutamine free medium for 24 hours show that only the loss of IKKβ decreased the levels of p53 phosphorylation at Ser15 (Fig. 1b). This attenuation in p53 phosphorylation in IKKβ-deficient cells prompted us to investigate whether the loss of IKKβ affected the transcription activity of p53. Thus, we evaluated the expression levels of CDKN1A and GADD45A in MEF and HT1080 cells cultured in glutamine free medium. Interestingly, we found significant induction of these p53-target genes in control cells that is lost in IKKβ-deficient cells (Fig 1c. d), suggesting the requirement for IKKβ in p53 activation under low

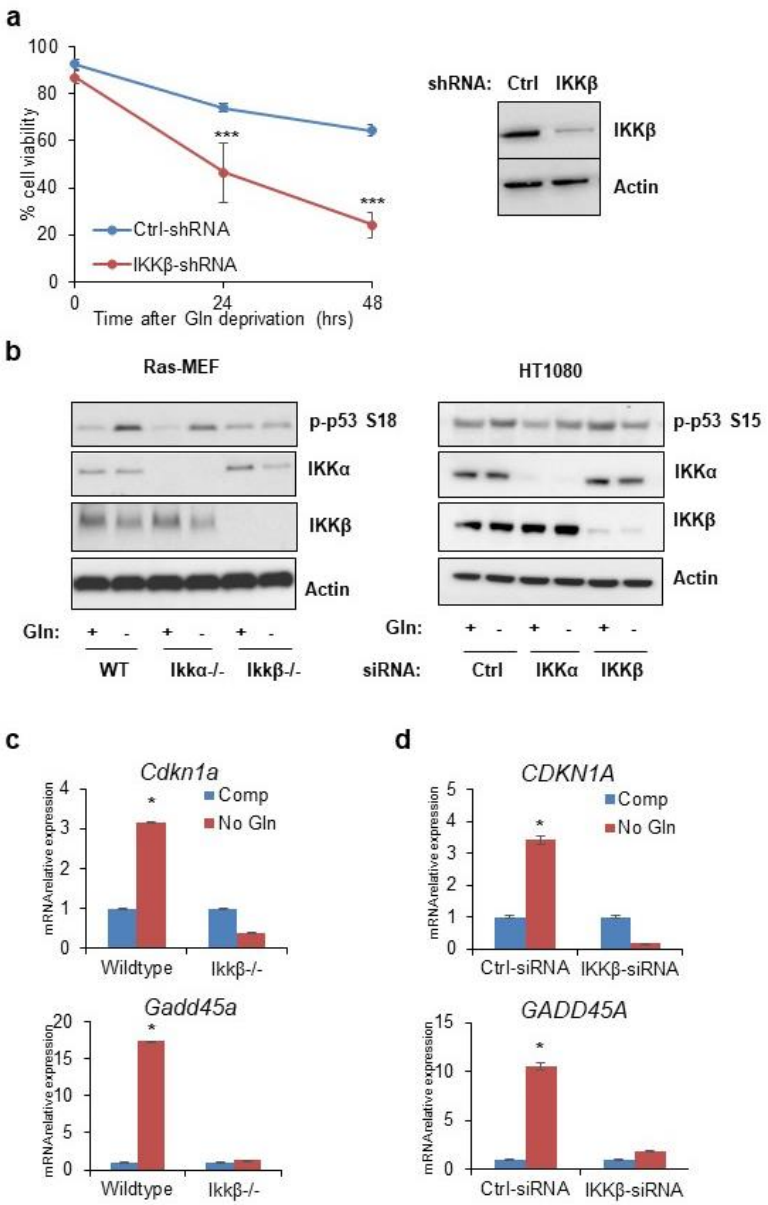

Figure 1: Glutamine deprivation induced p53 activation is IKKβ dependent. (a) HT1080 transduced with control (Ctrl) or IKKβ shRNA were cultured in glutamine free medium for 24 and 48 hours. Cell viability was assessed by PI exclusion. Cell lysate was collected for western blotting with the indicated antibodies. (b) Western blot analysis of wildtype (WT), *Ikkα* $^{-/-}$ or *Ikkβ* $^{-/-}$ MEFs and HT1080 cells transiently transfected with siRNA against scrambled control, IKKα, or IKKβ cultured in complete and glutamine (Gln) free medium overnight and cell lysate was used for immunoblotting using the antibodies indicated. (c) Wild type and *Ikkβ* $^{-/-}$ MEFs were cultured in complete (Comp) or glutamine free (No Gln) media overnight and mRNA was extracted for qPCR analysis of p53-target genes. (d) HT1080 cells transiently transfected with siRNA against scramble control or IKKβ were cultured in complete or glutamine free media overnight. mRNA was extracted, and expression of p53-target genes was determined using qPCR. a, c, and d represent means $\pm$ s.d. of triplicates from three independent experiments (*p<0.05, **p<0.01, ***p<0.001 using Student's *t*-test).

glutamine conditions.

Mutant p53 activation is also dependent on IKKβ under low glutamine

The p53 protein is mutated in over 50% of all human cancer, with a high prevalence in mutation of the DNA-binding domain [30, 31]. More importantly, mutant p53 (mutp53) has been shown to gain oncogenic functions through its transcriptional activity, which promotes cancer tumorgenicity [32]. We have previously shown that mutp53 is phosphorylated upon glutamine deprivation and subsequently leads to the induction of CDKN1A, which was necessary for the survival of cancer cells [13]. Therefore, we tested two cell lines with mutation in p53, the triplenegative breast cancer cell line, MDA-MB-231, and the pancreatic cancer cell line, MIA PaCa-2, with Arg280 and Arg248 mutation respectively to see whether loss of IKKβ affects the activation of mutp53. Similar to HT1080 cells, we transfected both MDA-MB-231 and MIA PaCa-2 cells with siRNA against scrambled control, IKKα, and IKKβ and incubated cells in control and glutamine free medium overnight. Strikingly, mutp53 activation by phosphorylation at Ser15 was lost in IKKβ knockdown cells but not in control or IKKα knockdown cells (Fig. 2a, c). This decrease in mutp53 phosphorylation was also accompanied by a loss in the induction of p53-target genes CDKN1A and GADD45A (Fig. 2b, d). These data further suggest an important correlation between IKKβ and p53 activation, indiscriminate of wildtype or mutant p53, upon glutamine deprivation.

p53 activation upon glutamine deprivation is NF-κB independent

Next, we sought to determine whether IKKβ activated p53 through the NF-κB pathway. IKKβ is known to be a master regulator of several NF-κB subunits including RelA (p65), a dominant NF-κB transactivating subunit [33]. Therefore, we tested whether p65 knockdown affected p53

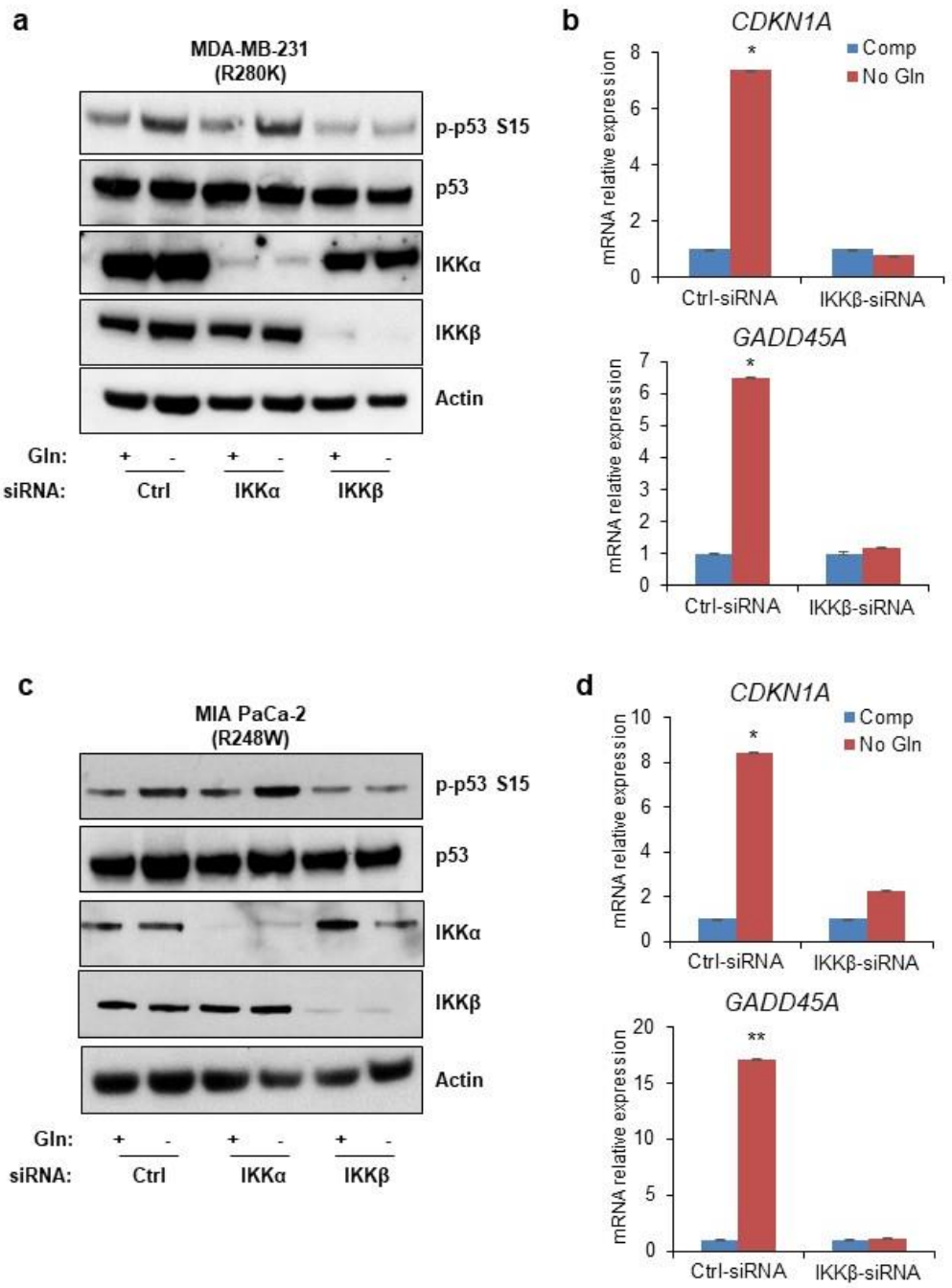

Figure 2: Mutant p53 activation is also dependent on IKKβ under low glutamine. (a, c) Western blot analysis of MDA-MB-231 and MIA PaCa-2 cells transiently transfected with siRNA against scramble control (Ctrl), IKKα, or IKKβ cultured in complete and glutamine (Gln)-free media overnight. Cell lysate was used for immunoblotting using the antibodies indicated. (b,d) MDA-MB-231 and MIA PaCa-2 cells transiently transfected with siRNA against scrambled control or IKKβ were cultured in complete (Comp) or glutamine-free (No Gln) media overnight. mRNA was extracted, and expression of p53-target genes was determined using qPCR. b and d represent means ± s.d. of triplicates from three independent experiments (*p<0.05, **p<0.01, ***p<0.001 using Student's *t*-test).

phosphorylation and induction of p53-target genes upon glutamine deprivation. Consistent with our previous results, the loss of IKKβ significantly attenuated the phosphorylation of p53. Interestingly, HT1080 transiently transfected with siRNA against p65 showed an increase in the phosphorylation of p53 upon glutamine withdrawal to similar level as the scramble control (Fig. 3a). Moreover, the expression of p53-target genes, CDKN1A and GADD45A, was significantly induced in p65 knockdown cells cultured in glutamine free medium overnight, similar to control

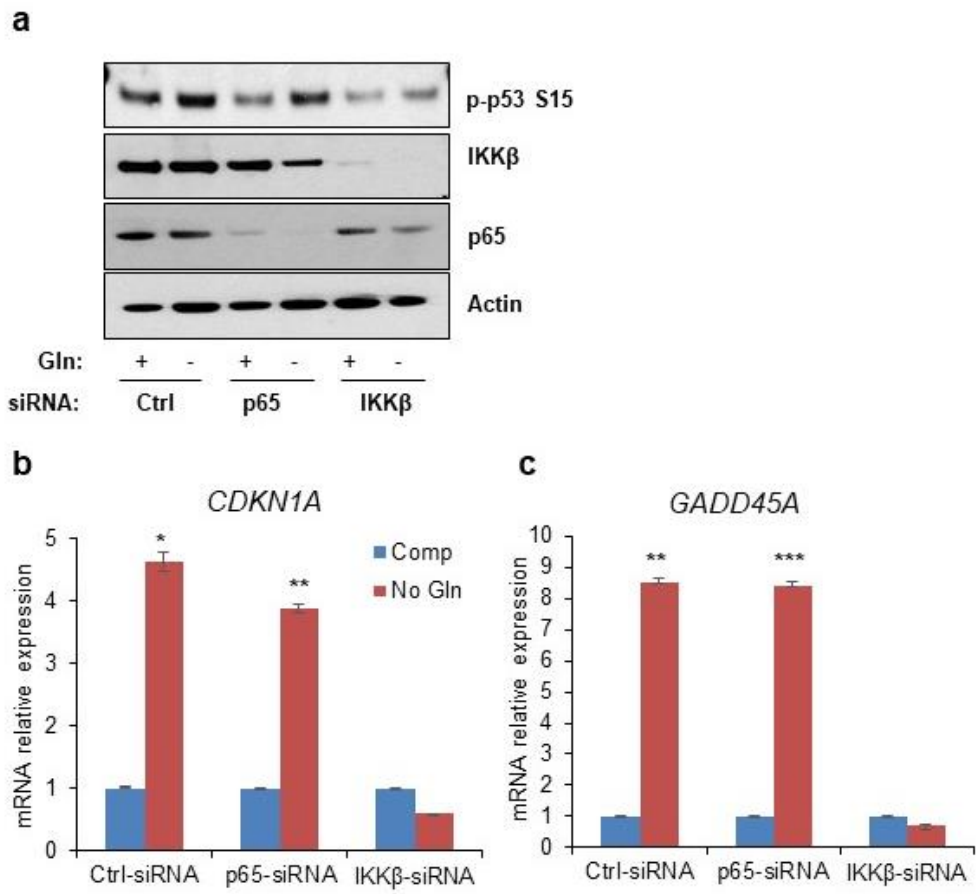

Figure 3: p53 activation upon glutamine deprivation is NF-κB independent. (a) HT1080 cells transiently transfected with siRNA against scrambled control (Ctrl), p65, or IKKβ cultured in complete or glutamine (Gln)-free media overnight. Cell lysate was used for immunoblotting using the antibodies indicated. (b, c) HT1080 cells transiently transfected with siRNA against scramble control, p65, or IKKβ were cultured in complete (Comp) or glutamine-free (No Gln) media overnight. mRNA was extracted, and expression of p53-target genes was determined using qPCR. b and c represent means $\pm$ s.d. of triplicates from three independent experiments (*p<0.05, **p<0.01, ***p<0.001 using Student's *t*-test).

cells (Fig. 3b). Meanwhile, IKKβ knockdown cells lost this induction of p53 downstream genes. These data suggest that IKKβ is regulating the phosphorylation of p53 independent of NF-κB transactivation.

IKKβ phosphorylates p53 on Ser392 in response to low glutamine

Since IKKβ has been previously shown to directly phosphorylate its substrates, we tested whether IKKβ could phosphorylate p53 under glutamine deprivation. Thus, we overexpressed Flag-tagged IKKβ in 293T cells and starved cells of glutamine overnight followed by immunoprecipitation using anti-Flag conjugated agarose beads to purify IKKβ-interacting proteins. We found that p53 interacts directly with IKKβ, albeit rather weakly, which could be due to the transient nature of the kinase-substrate interaction (Fig. 4a). To further confirm this finding, we transiently co-expressed HA-tagged IKKβ and p53 in 293T cells and cultured these cells in glutamine free medium. Cells were collected at 0, 0.5, 1, 3, and 6 hours and lysates were immunoprecipitated using anti-p53 antibody. Interestingly, IKKβ interaction with p53 appeared as early as 1 hour post glutamine withdrawal followed by its dissociation at 6 hours (Fig. 4b). Next, to identify which residue on p53 is phosphorylated by IKKβ, we performed an in vitro kinase assay using recombinant GST- IKKβ, which is constitutively active, and recombinant GST-p53 followed by phosphopeptide mapping using mass spectrometry. We found that p53 was phosphorylated on Ser392 in the c-terminal domain (Fig. 4c, d). To confirm the phosphorylation of p53 on Ser392 by IKKβ, we performed an in vitro kinase assay followed by immunoblotting and found that IKKβ phosphorylated GST-IκBα, a known IKKβ substrate, and GST-p53 on Ser392, but not on Ser15 (Fig. 4e). Taken together, these results indicate that IKKβ phosphorylates p53 on Ser392 as an early response to glutamine deprivation and possibly later facilitates its phosphorylation at Ser15 and transcriptional activity.

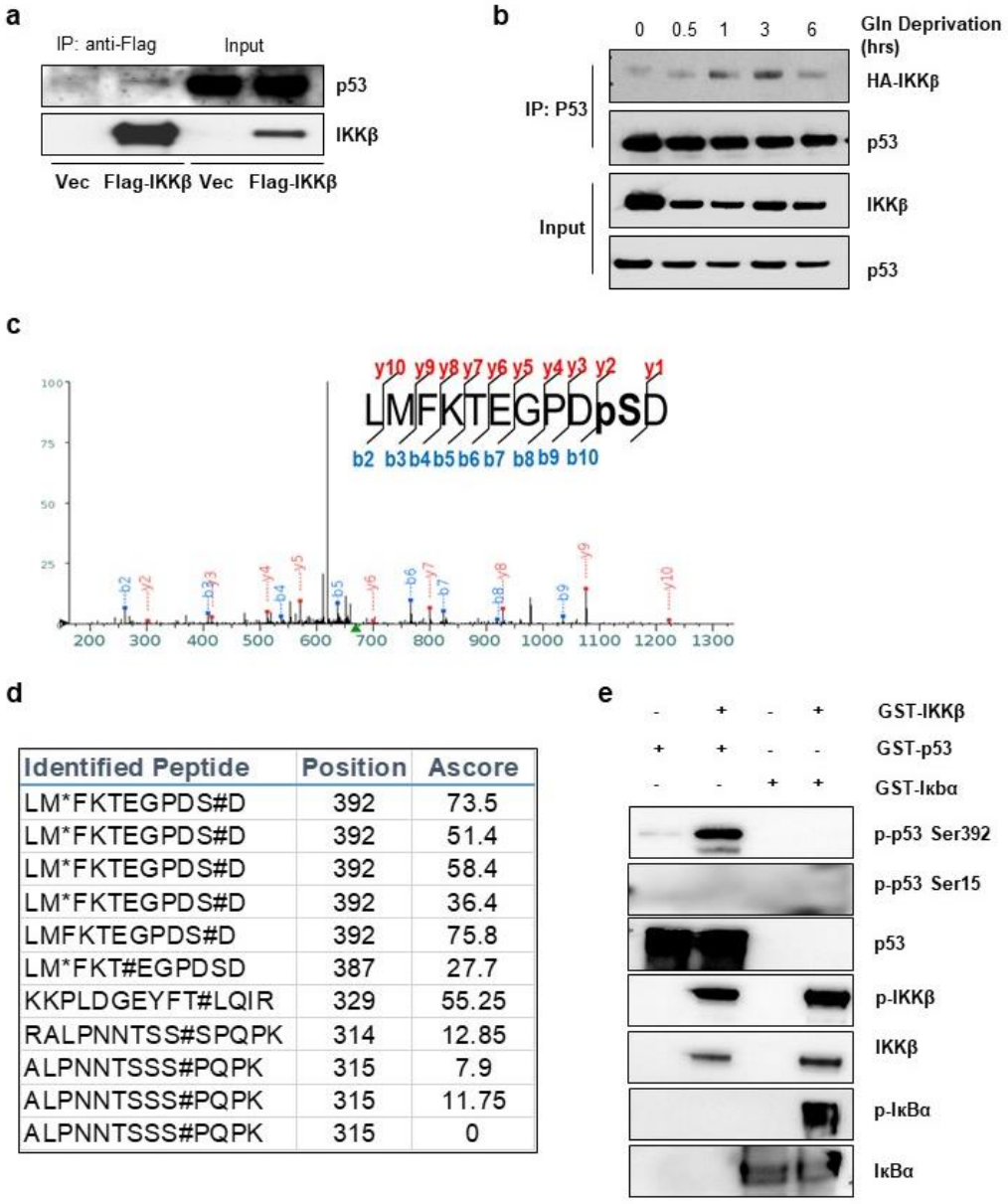

Identified Peptide	Position	Ascore
LM*FKTEGPDS#D	392	73.5
LM*FKTEGPDS#D	392	51.4
LM*FKTEGPDS#D	392	58.4
LM*FKTEGPDS#D	392	36.4
LMFKTEGPDS#D	392	75.8
LM*FKT#EGPDSD	387	27.7
KKPLDGEYFT#LQIR	329	55.25
RALPNNTSS#SPQPK	314	12.85
ALPNNTSSS#PQPK	315	7.9
ALPNNTSSS#PQPK	315	11.75
ALPNNTSSS#PQPK	315	0

Figure 4: IKKβ phosphorylates p53 at Ser392 in response to low glutamine. (a) 293T cells transiently expressing vector (Vec) or Flag- IKKβ were cultured in glutamine-free medium overnight and immunoprecipitated with anti-Flag conjugated beads followed by immunoblotting with the indicated antibodies. (b) 293T cells transiently expressing HA- IKKβ and wild type p53 were cultured in glutamine free medium for 0, 0.5, 1, 3, and 6 hours. Cell lysate was immunoprecipitated with anti-p53 antibody followed by immunoblotting with the indicated antibodies. (c) Kinase assay using recombinant GST- IKKβ and recombinant GST-p53 was performed followed by SDS-PAGE and phosphopeptide mapping. Mass spectra of identified phosphopeptide sequence on Ser392 of p53 is presented. (d) Identified phosphopeptides (as described in c) with positions on p53 and confidence score (A score) are presented. (e) Kinase assay using recombinant GST- IKKβ and recombinant GST-p53 or GST-IκBα (positive control) was performed followed by immunoblotting with the indicated antibodies.

Low glutamine induces phosphorylation of p53 on Ser392

Phosphorylation of p53 on Ser392 is shown to increase in response to various stimuli, such as treatment with genotoxic inducing agents, UV irradiation, and the MDM2 inhibitor Nutlin-3a [34]. Therefore, to illustrate that phosphorylation of p53 on Ser392 is induced in response to glutamine deprivation, we cultured HT1080 cells in complete medium, glutamine free medium, and complete medium with doxorubicin (Doxo), a DNA damaging reagent used as a positive control, and compared the phosphorylation of p53 on Ser392 by western blotting. Phosphorylation of p53 on Ser392 was induced in response to glutamine deprivation at a similar level to the genotoxic stress caused by Doxo treatment (Fig. 5a). Next, we wanted to evaluate the persistence of this phosphorylation with prolonged glutamine starvation by culturing HT1080 cells with no glutamine and collecting cell lysate over the course of 18 hours. Interestingly, phosphorylation on Ser392 seemed to increase with prolonged glutamine withdrawal, corresponding also with an increase in Ser15 phosphorylation, indicating its importance in mediating cellular response upon this metabolic stress (Fig. 5b). To determine the role of IKKβ in glutamine deprivation-induced p53 phosphorylation on Ser392, we compared wildtype Rastransformed MEF with Ikkβ -/- MEF cells. Similarly, the phosphorylation of p53 on Ser389 (the analog of Ser392 in human p53) in wildtype cells seemed to increase with glutamine deprivation over time and was completely abolished by the loss of IKKβ in Ikkβ -/- MEF cells (Fig. 5c).

Concurrently, phosphorylation of p53 on Ser18 also increased over time upon glutamine deprivation. However, the level of p53 Ser18 phosphorylation in Ikkβ -/- MEF cells was delayed, with a decreased level at 18 hours compared to wildtype cells. Furthermore, the phosphorylation

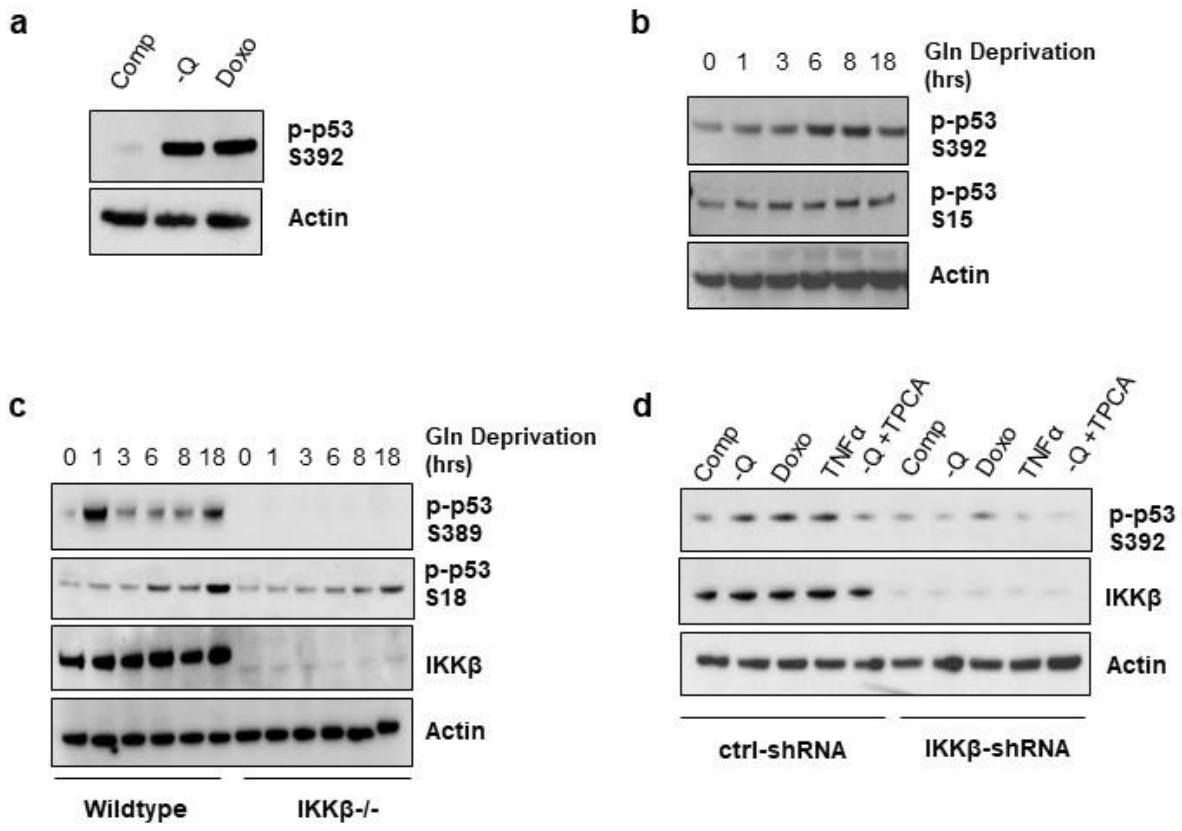

Figure 5: Low glutamine induces phosphorylation of p53 on Ser392. (a) HT1080 cells cultured in complete medium (Comp), glutamine-free (-Q) medium or complete medium with 2μM Doxorubicin (Doxo) overnight. Cell lysate was collected for immunoblotting using the indicated antibodies. (b) Time course of p53 phosphorylation on Ser392 using HT1080 cells cultured in glutamine free medium for 0, 1, 3, 6, 8, and 18 hours. Cell lysate was collected for immunoblotting using the indicated antibodies. (c) Time course of p53 activation on Ser389 using wild type and Ikkβ -/- MEFs cultured in glutamine (Gln) free medium for 0, 1, 3, 6, 8 and 18 hours. Cell lysate was collected for immunoblotting using indicated antibodies. (d) HT1080 cells transduced with shRNA against control (Ctrl) or IKKβ were cultured in complete medium, glutamine free medium, complete medium with 2μM Doxo, or glutamine free medium with 200nM TPCA-1 (-Q+TPCA) for 6 hours, or complete medium with 15ng/ml TNFα for 15 min. Cell lysate was collected for immunoblotting with indicated antibodies.

of p53 on Ser392 was dependent on IKKβ activity since it was induced in HT1080 cells treated with TNFα, which is known to activate IKKβ [35], and was attenuated when cells were cultured in low glutamine with the addition of TPCA-1, an IKKβ inhibitor (Fig. 5d) [36]. Consistently, the phosphorylation on Ser392 was completely lost in HT1080 IKKβ knockdown cells treated with the same conditions (Fig. 5d). These results demonstrate that low glutamine conditions lead

to the phosphorylation of p53 on Ser392 in an IKKβ dependent manner.

Phosphorylation of p53 on Ser392 is required for p53 activation upon glutamine deprivation

To further investigate how Ser392 phosphorylation affects p53 activity upon glutamine deprivation, we ectopically expressed both wild type and S392A mutant p53 in the p53-null prostate cancer cells, PC3. We then cultured wildtype and S392A expressing PC3 cells along with null cells in glutamine free medium and collected cell lysate at 0, 3, and 6 hours. Interestingly, we found that the expression of the p53 point mutant, S392A, hampered the phosphorylation of p53 on Ser392 and Ser15 in response to glutamine withdrawal (Fig. 6a). We next assessed whether the mutation on Ser392 would affect the transcriptional activity of p53. Thus, we expressed wildtype and S392A p53 in PC3 and cultured these cells under no glutamine for 6 hours. Consistently, the expression levels of CDKN1A and GADD45A increased upon glutamine deprivation in wildtype p53 expressing cells (Fig. 6b, c). However, this induction was attenuated by the mutation on Ser392, further suggesting that the phosphorylation of p53 on this residue plays a role in the transcriptional activity of p53 in response to low glutamine. Next, we wondered if mutation on Ser392 would affect the role p53 plays in survival. We expressed wild type and S392A p53 in PC3 and assessed cell viability after 48 hours in glutamine free medium. Indeed, S392A p53 expressing cells had significantly less cell viability compared to wild type (Fig. 6d). This data further supports a model, in which activation of IKKβ in response to glutamine deprivation leads to the phosphorylation of p53 on Ser392, which is required for p53 activity in the transcription of downstream target genes and in promoting cancer cell survival (Fig. 6e).

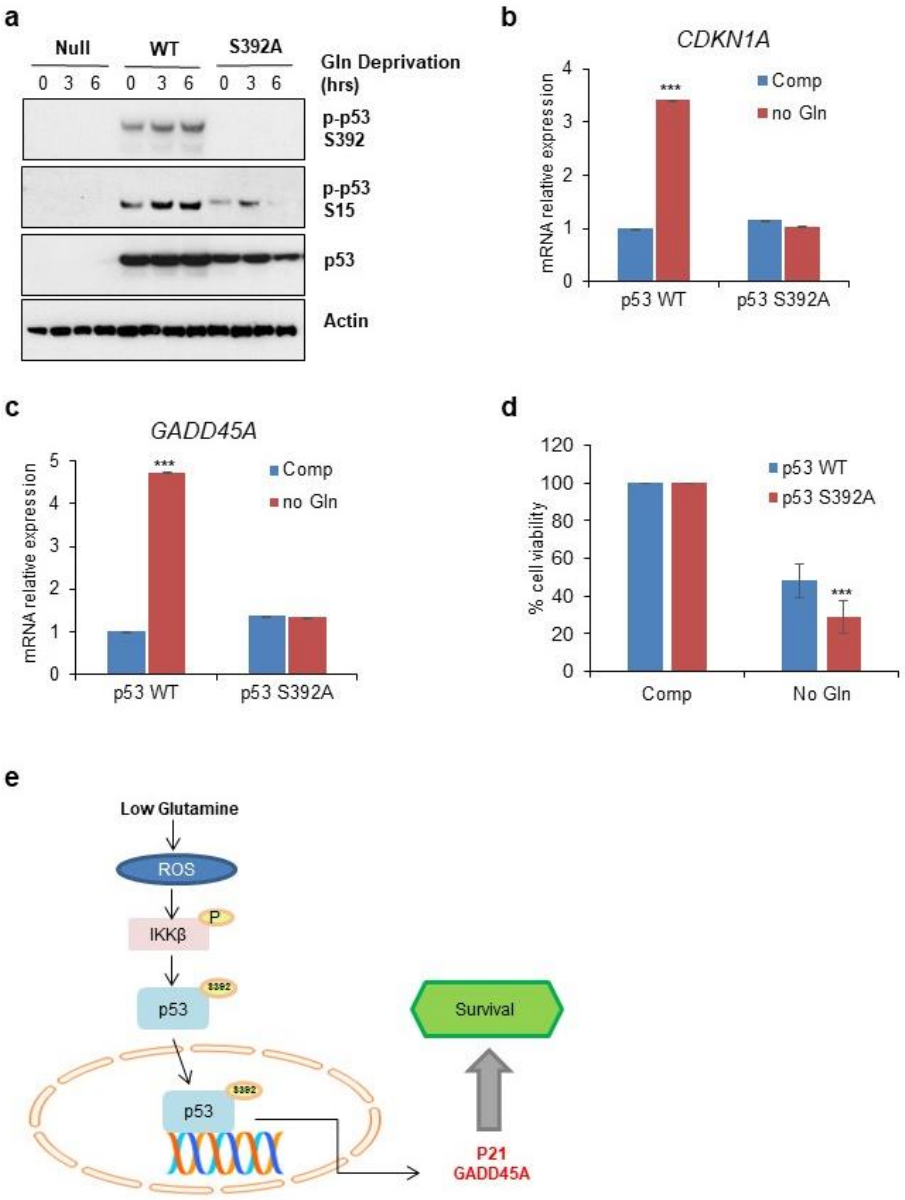

Figure 6: Phosphorylation of p53 on Ser392 is required for p53 activation upon glutamine deprivation. (a) Western blot analysis of p53-null PC3 cells and PC3 cells transiently expressing wild type p53 (WT) or Flag-p53 S392A cultured in glutamine free medium for 0, 3, and 6 hours. Cell lysates were collected for immunoblotting with the indicated antibodies. (b, c) PC3 transiently expressing wild-type p53 (WT) or Flag-p53 S392A were cultured in glutamine free medium for 6 hours. mRNA was extracted, and expression of p53-target genes was determined using qPCR. (d) PC3 transiently expressing p53 WT or Flag-p53 S392A were cultured in glutamine-free medium for 48 hours. Cell viability was assessed using trypan blue exclusion assay at time 0 or 48 hours of glutamine deprivation. (e) Schematic showing molecular mechanism by which cells survive glutamine deprivation via the suggested IKKβ-p53 signaling axis. b, c, and d represent means $\pm$ s.d. of triplicates from three independent experiments (*p<0.05, **p<0.01, ***p<0.001
using Student's *t*-test).

Discussion

IKKβ and the NF-κB pathway have been implicated in cancer cell response to metabolic stress and their activation is necessary for cancer cell survival [27]. Similarly, p53 has been shown to regulate glycolysis, cell cycle arrest, and expression of metabolic enzymes to promote survival in many cancer models [17, 37, 38]. As these pathways function to promote survival in cancer, it is critical to delineate whether IKKβ and p53 work synergistically or independently to combat metabolic stress or induce therapeutic resistance to drugs targeting glutamine metabolism. Here, we demonstrate a role for IKKβ in phosphorylating p53 upon glutamine depletion to promote cancer cell survival. Loss of IKKβ in cancer cells harboring both wild type and mutant variants of p53 significantly reduced the phosphorylation of p53 and its transcriptional activity under low glutamine. Specifically, these results indicate that IKKβ can phosphorylate p53 on Ser392 in response to glutamine depletion and induce its transcriptional activity. Additionally, the mutation of Ser392 residue attenuated the activation of p53 and sensitized cancer cells to glutamine deprivation. This study highlights a new IKKβ-p53 signaling axis that is critical to cancer cell adaptation to metabolic stress.

Previously, there have been several studies indicating crosstalk between the IKKβ/ NF-κB pathway and p53 stabilization and activation. For instance, under genotoxic conditions, IKKβ acts as a regulator of p53 via the association with β-TrCP1 in MEF cells to destabilize its protein levels, independent of Mdm2, and the loss of IKKβ via chemical inhibition in lung adenocarcinoma cells reduced proliferation and invasion in these cells, and was accompanied by the stabilization of p53 [39, 40]. Moreover, several studies link the activity of the DNA damage kinase, ATM, to the activation of the IKK complex and NF-κB under genotoxic stimuli [41, 42]. These studies indicate the dynamic nature of p53 regulation by the IKK complex that is highly

dependent on the type of stress. The realization that cancer cells experience metabolic stress in vivo prompted further investigation into the connection between the IKK pathway and p53. Interestingly, the activation of the NF-κB pathway is necessary to regulate p53 activity and protects cells against glucose starvation, while the loss of p53 leads to the upregulation of GLUT3 expression and glycolysis by the hyperactivation of NF-κB [21, 28]. These studies further indicate the existence of a feedback loop connecting the activity of the IKKβ/ NF-κB pathway and p53 in modulating cancer metabolism. Therefore, the connection between IKKβ and p53, which are both activated in cancer, in response to glutamine starvation and other metabolic stress needs to be fully understood.

Post-translational modification of p53 is rapid and results in its stabilization in response to various stress stimuli [43]. The phosphorylation of p53 on the highly conserved residue, Ser392 (Ser389 in mice), was shown to have a role in site-specific DNA binding, formation of the p53 tetramer, and inducing cell arrest [44-46]. Additionally, a mutation of Ser392 to alanine was sufficient in disrupting p53 localization to the nucleus and its degradation in response to DNA damage [47, 48]. Later studies indicated p53 has a basal level of phosphorylation on Ser392 in unstressed cells that increases when exposed to various stress conditions, such as irradiation, UV exposure, and etoposide treatment. To date, several kinases of Ser392 under genotoxic stress were identified such as CK2 and p38 MAPK, but other kinases that are resistant to CK2 inhibition remain to be identified [49-51]. More importantly, the phosphorylation of p53 on Ser392 in response to metabolic stress and the kinases that catalyze this phosphorylation remains to be elucidated. Our study provides an unprecedented signaling pathway connecting IKKβ to p53 phosphorylation on Ser392 in response to glutamine deprivation as a mechanism of survival in cancer cells.

The connection between the phosphorylation of p53 on Ser392 and Ser15 and their effect on p53 activity remains unclear in literature. p53 activation by Ser15 phosphorylation was observed in several cancer cell lines when cultured under metabolic stress. For instance, serine and glutamine withdrawal induced phosphorylation of p53 and its activation [12, 20]. Similarly, glucose starvation and nutrient stress led to the activation of p53 by phosphorylation on Ser15 [28]. Our findings suggest that the phosphorylation of p53 on Ser392 is required for its activity and role in cell survival upon glutamine withdrawal. Thus, it would be interesting to unveil whether Ser392 is also critical for p53 phosphorylation on Ser15 and its activity under different metabolic stress conditions. It is also possible that IKKβ could be activating p53 at Ser392 as an early response to glutamine deprivation followed by a later induction of Ser15 phosphorylation and p53 activity. However, more studies would be needed to further understand the regulation of p53 and its phosphorylation on both Ser15 and Ser392 in response to metabolic stress.

Our findings indicate that an IKKβ-p53 signaling axis could promote tumor growth despite glutamine deprivation. Furthermore, IKKβ knockdown affected the phosphorylation and activity of both wild type and mutant p53 when cells were cultured in glutamine free medium. As more in vivo studies reveal glutamine depleted niches due to rapid glutamine consumption by cancer or poor vascularization networks, it is important to understand how cells adapt to this metabolic stress in order to develop better therapeutic strategies. Therefore, future experiments will further investigate the attenuation of p53 phosphorylation by targeting IKKβ in vivo through combination treatment using IKKβ inhibitors and glutaminase inhibitors in cancer cells harboring wild type or mutant p53. This study highlights the potential efficacy of a combination therapeutic strategy in targeting cancer growth and identifies a potential resistance mechanism to ongoing clinical trials that use glutaminase inhibitors.

Materials and methods

Reagents and Plasmids

Antibodies to IKKβ (8943), IKKα (2682), p-p53 S15 (9284), p-p53 S392 (9281), p-p65 (3033), p65 (3987), p-Iκbα (2859), Iκbα (4814) were from Cell Signaling (Danvers, MA, USA), beta actin (A1978) was from Sigma (St. Louis, MO, USA), and p53 DO-1 (SC126) was from Santa Cruz Biotechnology (Dallas, TX, USA). Recombinant active GST- IKKβ (31176) was purchased from Active Motif (Carlsbad, CA, USA). Recombinant GST-p53 (14-865) was purchased from Millipore (Temecula, CA, USA). Recombinant GST- IκBα (P323-30G) was purchased from SignalChem (Richmond, BC, Canada). pcDNA3.0-p53wt (69003), pCMV2-Flag- IKKβ (11103) were purchased from Addgene (Cambridge, MA, USA). pUNO1-HA-IKKβ was purchased from InvivoGen (puno1ha-hikkb). pcDNA3.0-Flag-p53 S392A was custom ordered from SignalChem. Doxorubicin (Doxo) (D2141) was purchased from Sigma (St. Louis, MO, USA). TPCA-1 (15115) was purchased from PerkinElmer (Waltham, MA, USA). Lipofectamine RNAiMAX and Lipofectamine 2000 transfection reagents were purchased from Life Technologies (Carlsbad, CA, USA). TRC human IKKβ shRNA (TRCN0000018917) was purchased from Dharmacon (Lafayetter, CO, USA) and pLKO.1 scramble (1864) was purchased from Addgene.

Cell Culture

HT1080, MIA PaCa-2, MDA-MB-231, PC3, and 293T cell lines were purchased from American Type Culture Collection (ATCC, Manassas, VA, USA). Wild type, Ikkα -/- or Ikkβ -/- mouse embryonic fibroblasts (MEFs) were kindly provided by Dr. Michael Karin's laboratory at University of California, San Diego. All cells were cultured in Dulbecco's modified Eagle's medium (DMEM, Corning) containing 25mM glucose and 4mM L-glutamine supplemented with 10% fetal bovine serum (FBS), 100 U/ml penicillin, and 100 ug/ml streptomycin (Gemini Bio-

Products). PC3 cells were cultured in RPMI 1640 medium supplemented with 10% FBS and 100 U/ml penicillin, and 100 ug/ml streptomycin. All cells were regularly tested for mycoplasma. For glutamine free medium, DMEM without L-glutamine (11960, Life Technologies) was supplemented with 10% dialyzed FBS (Gemini Bio-Products). Cell viability was either determined using propidium iodide exclusion flow cytometry or using trypan blue exclusion counted by TC20 automated cell counter (Bio-Rad, Hercules, CA, USA).

siRNA and shRNA silencing

Cells were transiently transfected according to manufacturer's protocol with on-target SMARTpool control siRNA (D-001810-10-20) and siRNA targeting human IKKβ (L-003503-00-0005), human IKKα (L-0034733-00-0005), human p65 (L-003533-00-0005) purchased from Dharmacon. For stable gene silencing, HT1080 cells were generated via lentiviral mediated gene transfer followed by puromycin selection.

Quantitative Real-time Polymerase-chain Reaction

Total RNA was extracted and purified using Trizol reagent (Life Technologies, Carlsbad, CA, USA) according to manufacturer's guidelines. 1ug RNA was used for qScript cDNA Synthesis Kit (Quanta Biosciences, Beverly, MA, USA). qRT-PCR analyses were performed with SYBR Green PCR (Quanta Biosciences) using CFX Connect Real-Time PCR Detection System (Bio-Rad, Hercules, CA, USA). The following forward and reverse primers were generated to check gene expression: HUMAN (F: forward, R: reverse) ACTIN-F: 5′-CACCAACTGGGAGGACAT-3′ R: 5′-GCACAGCCT GGATAGCAAC-3′; CDKN1A-F: 5′-AGGTGGACCTGGAGACTCTCAG-3′ R: 5′-TCCTCTTGGAGAAGATCA GCCG-3′; GADD45A-F: 5′-CTGGAGGAAGTGC TCAGCAAAG-3′ R: 5′-AGAGCCACA TCTCTGTCGTCGT-3′: 18S-F 5′-CCCGTTGAACCCCATTCGTGA-3′; R: 5′-

GCCTCACTAAACCATCCAATCGG-3′, MOUSE Cdkn1a-F: 5’-TCGCTGTCTTGCACTCTGGTG-3’; R: 5’-CCAATCTGCGCTTGGAGTGATAG-3’; Gadd45a-F: 5’-GCCACATCCCGGTCGTCGTC-3’; R: 5’-CGCACCATTACGGTCGGCGT-3’; 18S F: 5’-CGCTTCCTTACCTGGTTGAT-3’ R: 5’-GAGCGACCAAAGGAACCATA-3’.

Western Blotting and Immunoprecipitation

Cells were lysed in buffer (50 mM Tris-HCL [pH 7.4], 5 mM Sodium Fluoride, 5 mM Sodium Pyrophosphate, 1 mM EDTA, 1 mM EGTA, 250 mM Mannitol, 1% [v/v] Triton X-100) containing protease inhibitor complex (Roche) and phosphatase inhibitor (Life Technologies). Equal amounts of protein were loaded on precast NuPAGE Bis-Tris Gels (Life Technologies) followed by transfer onto nitrocellulose. For co-immunoprecipitation, one 15-cm plate containing 80% cell confluency was used for each experimental condition. Cells lysate was scrapped with lysis buffer (150 mM KCl, 0.2% [v/v] NP-40, 10% [v/v] glycerol, 20 mM Tris at pH 7.5, 0.5mM DTT) with protease inhibitor complex (Roche) and phosphatase inhibitor (Life Technologies) on ice. Equal amounts of lysate (500µg to 1mg) were immunoprecipitated with 4µg of anti-p53 (Santa Cruz). Protein G agarose or anti-Flag conjugated agarose beads (20µl) were added to each tube and rotated at 4°C for 24 hours. Beads were washed four times with lysis buffer and resuspended in SDS loading dye and boiled for immunoblotting.

Kinase Assay

Recombinant active GST- IKKβ was incubated for 30 min at 30°C with: kinase buffer, 200 µM ATP (Cell Signaling), and the specified recombinant proteins (GST-p53 or GST- IκBα). The reaction was quenched with 10uL of SDS loading dye and was separated by SDS-PAGE. For phospho-peptide mass spectrometry, the reaction was repeated using the same protocol with the addition of gel drying at 80°C for 2 hours, followed by coomassie blue staining. The respective

p53 band was excised from gel and sent for mass spectrometry analysis.

Statistics

Data are represented as means + standard deviation; statistical analysis were done in Excel. A two-tailed Student's t-test was used to determine the statistical significance with *$p<0.05$, **$p<0.01$, ***$p<0.001$.

Acknowledgments

We thank members of the Kong laboratory for helpful comments on the manuscript. This work was supported by National Institutes of Health (NIH)/R01CA183989 to MK. MK is the Pew Scholar in Biomedical Sciences and American Cancer Society Research Scholar (RSG-16-085-01-TBE).

Author contributions

M.B.G performed most of the experiments, analyzed the data, prepared figures and wrote the manuscript. M.A.R contributed to several experiments included in figures 1 and 2. Y.Y., X.H.L., and T.Q.T. contributed to experimental design, data analysis, and manuscript editing. M.K. conceived and designed experiments and contributed manuscript writing.

Competing interests

The authors declare no competing interests.

References

1. Hao, Y., et al., *Oncogenic PIK3CA mutations reprogram glutamine metabolism in colorectal cancer.* Nat Commun, 2016. **7**.
2. Le, A., et al., *Glucose-Independent Glutamine Metabolism via TCA Cycling for Proliferation and Survival in B Cells.* Cell Metabolism, 2012. **15**(1): p. 110-121.
3. Son, J., et al., *Glutamine supports pancreatic cancer growth through a KRAS-regulated metabolic pathway.* Nature, 2013. **496**(7443): p. 101-5.
4. Boroughs, L.K. and R.J. DeBerardinis, *Metabolic pathways promoting cancer cell survival and growth.* Nat Cell Biol, 2015. **17**(4): p. 351-359.
5. Coloff, J.L., et al., *Differential Glutamate Metabolism in Proliferating and Quiescent Mammary Epithelial Cells.* Cell Metab, 2016. **23**(5): p. 867-80.
6. DeBerardinis, R.J., et al., *The Biology of Cancer: Metabolic Reprogramming Fuels Cell Growth and Proliferation.* Cell Metabolism, 2008. **7**(1): p. 11-20.
7. Jin, L., et al., *Glutamate Dehydrogenase 1 Signals through Antioxidant Glutathione Peroxidase 1 to Regulate Redox Homeostasis and Tumor Growth.* Cancer Cell, 2015. **27**(2): p. 257-270.
8. Reid, M.A. and M. Kong, *Dealing with hunger: Metabolic stress responses in tumors.* J Carcinog, 2013. **12**: p. 17.
9. Denkert, C., et al., *Metabolite profiling of human colon carcinoma – deregulation of TCA cycle and amino acid turnover.* Molecular Cancer, 2008. **7**: p. 72-72.
10. Kamphorst, J.J., et al., *Human pancreatic cancer tumors are nutrient poor and tumor cells actively scavenge extracellular protein.* Cancer Res, 2015. **75**(3): p. 544-53.
11. Pan, M., et al., *Regional glutamine deficiency in tumours promotes dedifferentiation through inhibition of histone demethylation.* Nat Cell Biol, 2016.
12. Reid, M.A., et al., *The B55alpha subunit of PP2A drives a p53-dependent metabolic adaptation to glutamine deprivation.* Mol Cell, 2013. **50**(2): p. 200-11.
13. Tran, T.Q., et al., *Tumor-associated mutant p53 promotes cancer cell survival upon glutamine deprivation through p21 induction.* Oncogene, 2016.
14. Assaily, W., et al., *ROS-mediated p53 induction of Lpin1 regulates fatty acid oxidation in response to nutritional stress.* Mol Cell, 2011. **44**(3): p. 491-501.
15. Dai, Q., et al., *Two p53-related metabolic regulators, TIGAR and SCO2, contribute to oroxylin Amediated glucose metabolism in human hepatoma HepG2 cells.* Int J Biochem Cell Biol, 2013. **45**(7): p. 1468-78.
16. Green, D.R. and J.E. Chipuk, *p53 and metabolism: Inside the TIGAR.* Cell, 2006. **126**(1): p. 30-2.
17. Jiang, P., et al., *p53 regulates biosynthesis through direct inactivation of glucose-6-phosphate dehydrogenase.* Nat Cell Biol, 2011. **13**(3): p. 310-6.
18. Sinthupibulyakit, C., et al., *p53 Protects lung cancer cells against metabolic stress.* Int J Oncol, 2010. **37**(6): p. 1575-81.
19. Bensaad, K., et al., *TIGAR, a p53-inducible regulator of glycolysis and apoptosis.* Cell, 2006. **126**(1): p. 107-20.
20. Maddocks, O.D., et al., *Serine starvation induces stress and p53-dependent metabolic remodelling in cancer cells.* Nature, 2013. **493**(7433): p. 542-6.
21. Kawauchi, K., et al., *p53 regulates glucose metabolism through an IKK-NF-[kappa]B pathway and inhibits cell transformation.* Nat Cell Biol, 2008. **10**(5): p. 611-618.
22. Lee, D.F., et al., *IKK beta suppression of TSC1 links inflammation and tumor angiogenesis via the mTOR pathway.* Cell, 2007. **130**(3): p. 440-55.
23. Liu, J., et al., *Inflammation Improves Glucose Homeostasis through IKKβ-XBP1s Interaction.* Cell, 2016. **167**(4): p. 1052-1066.e18.

24. Hacker, H. and M. Karin, *Regulation and function of IKK and IKK-related kinases.* Sci STKE, 2006. **2006**(357): p. re13.
25. Yan, J., et al., *Inactivation of BAD by IKK inhibits TNFalpha-induced apoptosis independently of NF-kappaB activation.* Cell, 2013. **152**(1-2): p. 304-15.
26. Lamberti, C., et al., *Regulation of beta-catenin function by the IkappaB kinases.* J Biol Chem, 2001. **276**(45): p. 42276-86.
27. Comb, W.C., et al., *p85alpha SH2 domain phosphorylation by IKK promotes feedback inhibition of PI3K and Akt in response to cellular starvation.* Mol Cell, 2012. **45**(6): p. 719-30.
28. Mauro, C., et al., *NF-kappaB controls energy homeostasis and metabolic adaptation by upregulating mitochondrial respiration.* Nat Cell Biol, 2011. **13**(10): p. 1272-9.
29. Reid, M.A., et al., *IKKbeta promotes metabolic adaptation to glutamine deprivation via phosphorylation and inhibition of PFKFB3.* Genes Dev, 2016. **30**(16): p. 1837-51.
30. Kandoth, C., et al., *Mutational landscape and significance across 12 major cancer types.* Nature, 2013. **502**(7471): p. 333-339.
31. Muller, P.A. and K.H. Vousden, *p53 mutations in cancer.* Nat Cell Biol, 2013. **15**(1): p. 2-8.
32. Zhou, G., et al., *Gain-of-function mutant p53 promotes cell growth and cancer cell metabolism via inhibition of AMPK activation.* Mol Cell, 2014. **54**(6): p. 960-74.
33. Perkins, N.D., *Integrating cell-signalling pathways with NF-κB and IKK function.* Nature Reviews Molecular Cell Biology, 2007. **8**: p. 49.
34. Cox, M.L. and D.W. Meek, *Phosphorylation of serine 392 in p53 is a common and integral event during p53 induction by diverse stimuli.* Cellular Signalling, 2010. **22**(3): p. 564-571.
35. Chen, G., P. Cao, and D.V. Goeddel, *TNF-induced recruitment and activation of the IKK complex require Cdc37 and Hsp90.* Mol Cell, 2002. **9**(2): p. 401-10.
36. Podolin, P.L., et al., *Attenuation of Murine Collagen-Induced Arthritis by a Novel, Potent, Selective Small Molecule Inhibitor of IκB Kinase 2, TPCA-1 (2-[(Aminocarbonyl)amino]-5-(4-fluorophenyl)-3-thiophenecarboxamide), Occurs via Reduction of Proinflammatory Cytokines and Antigen-Induced T Cell Proliferation.* Journal of Pharmacology and Experimental Therapeutics, 2005. **312**(1): p. 373-381.
37. Wanka, C., J.P. Steinbach, and J. Rieger, *Tp53-induced glycolysis and apoptosis regulator (TIGAR) protects glioma cells from starvation-induced cell death by up-regulating respiration and improving cellular redox homeostasis.* J Biol Chem, 2012. **287**(40): p. 33436-46.
38. Won, K.Y., et al., *Regulatory role of p53 in cancer metabolism via SCO2 and TIGAR in human breast cancer.* Hum Pathol, 2012. **43**(2): p. 221-8.
39. Xia, Y., et al., *Phosphorylation of p53 by IkappaB kinase 2 promotes its degradation by beta-TrCP.* Proc Natl Acad Sci U S A, 2009. **106**(8): p. 2629-34.
40. Yang, P.-M., et al., *Loss of IKKβ activity increases p53 stability and p21 expression leading to cell cycle arrest and apoptosis.* Journal of Cellular and Molecular Medicine, 2010. **14**(3): p. 687-698.
41. Wu, Z.-H., et al., *Molecular Linkage Between the Kinase ATM and NF-κB Signaling in Response to Genotoxic Stimuli.* Science, 2006. **311**(5764): p. 1141-1146.
42. Yoshida, K., et al., *ATM-dependent nuclear accumulation of IKK-α plays an important role in the regulation of p73-mediated apoptosis in response to cisplatin.* Oncogene, 2007. **27**: p. 1183.
43. Bode, A.M. and Z. Dong, *Post-translational modification of p53 in tumorigenesis.* Nat Rev Cancer, 2004. **4**(10): p. 793-805.
44. Milne, D.M., R.H. Palmer, and D.W. Meek, *Mutation of the casein kinase II phosphorylation site abolishes the anti-proliferative activity of p53.* Nucleic Acids Research, 1992. **20**(21): p. 5565-5570.
45. Sakaguchi, K., et al., *Phosphorylation of serine 392 stabilizes the tetramer formation of tumor suppressor protein p53.* Biochemistry, 1997. **36**(33): p. 10117-24.

46. Hupp, T.R., et al., *Regulation of the specific DNA binding function of p53.* Cell, 1992. **71**(5): p. 875-886.
47. Du, C., H. Wu, and R.P. Leng, *UBE4B targets phosphorylated p53 at serines 15 and 392 for degradation.* Oncotarget, 2016. **7**(3): p. 2823-2836.
48. Kim, Y.-Y., et al., *Modification of serine 392 is a critical event in the regulation of p53 nuclear export and stability.* FEBS Letters, 2004. **572**(1-3): p. 92-98.
49. Blaydes, J.P. and T.R. Hupp, *DNA damage triggers DRB-resistant phosphorylation of human p53 at the CK2 site.* Oncogene, 1998. **17**(8): p. 1045-52.
50. Huang, C., et al., *p38 kinase mediates UV-induced phosphorylation of p53 protein at serine 389.* J Biol Chem, 1999. **274**(18): p. 12229-35.
51. Keller, D.M., et al., *A DNA damage-induced p53 serine 392 kinase complex contains CK2, hSpt16, and SSRP1.* Mol Cell, 2001. **7**(2): p. 283-92.

CHAPTER 3: Dietary glutamine supplementation suppresses epigenetically-activated oncogenic pathways to inhibit melanoma tumor growth

Background

We previously demonstrated that core regions of solid tumors experience lower levels of glutamine and glutamine-derived αKG, an essential cofactor for histone demethylases. As a result, these cancer cells exhibit histone hypomethylation leading to the upregulation of dedifferentiation genes and resistance to targeted therapeutics. Thus, in this chapter, we investigate whether glutamine supplementation could affect tumor growth through epigenetic reprogramming and contribute to a differentiated state. These results demonstrate the potential for using dietary glutamine supplementation as a novel therapeutic direction to impede tumor growth while enhancing therapeutic response by exploiting the connection between cellular metabolites and epigenetics to control gene expression.

Dietary glutamine supplementation suppresses epigenetically-activated oncogenic pathways to inhibit melanoma tumour growth

Mari B. Ishak Gabra[1], Ying Yang[1], Haiqing Li[2,3], Parijat Senapati[4], Eric A. Hanse[1], Xazmin H. Lowman[1], Thai Q. Tran[1], Lishi Zhang[5], Linda T. Doan[6], Xiangdong Xu[7], Dustin E. Schones[4], David A. Fruman[1], and Mei Kong[1*]

[1]Department of Molecular Biology and Biochemistry; School of Biological Sciences, University of California, Irvine, Irvine, CA 92697, USA

[2]Center for Informatics, City of Hope National Medical Center, Duarte, CA, 91010, USA

[3]Department of Computational & Quantitative Medicine, Beckman Research Institute, City of Hope Medical Center, Duarte, CA, USA

[4]Department of Diabetes and Metabolic Disease, Beckman Research Institute of City of Hope Cancer Center, Duarte, CA 91010, USA

[5]Institute for Clinical and Translational Science, University of California, Irvine, CA 92687

[6] UCI Health Dermatology Center, Irvine, CA 92697, USA

[7]Department of Pathology, University of California San Diego, La Jolla, California 92093, USA

*Corresponding Author:

Mei Kong

Department of Molecular Biology and Biochemistry

School of Biological Sciences, University of California, Irvine

Irvine, CA 92697

Phone: 949-824-5244

meik1@uci.edu

Abstract:

Tumour cells adapt to nutrient deprivation *in vivo*, yet strategies targeting the nutrient poor microenvironment remain unexplored. We recently found, in melanoma, tumour cells often experience low glutamine levels, which induce histone hypermethylation, promote dedifferentiation, and increase resistance to BRAF inhibitors. These findings raise the possibility that increased glutamine levels can be detrimental to melanoma tumours. Here, we show that dietary glutamine supplementation significantly inhibits melanoma tumour growth, prolongs survival in transgenic mouse model, and increases sensitivity to BRAF targeted inhibitors in both melanoma xenograft and patient-derived xenograft (PDX) models. Notably, metabolomic analysis reveals that dietary uptake of glutamine effectively increases the concentration of glutamine and its downstream metabolite, αKG, in serum and tumours, without increasing biosynthetic intermediates necessary for cell proliferation. Mechanistically, we find that glutamine supplementation uniformly alters the transcriptome and suppresses expression of many melanoma-associated genes. Our data further demonstrate that increase in intra-tumoural αKG concentration, following glutamine supplementation, drives hypomethylation of H3K4me3, thereby suppressing epigenetically-activated oncogenic pathways in melanoma. Therefore, our findings provide important evidence that glutamine supplementation can serve as a potential dietary intervention to block melanoma tumour growth and sensitize tumours to targeted therapy via epigenetic reprogramming.

Keywords: melanoma, glutamine supplementation, metabolism, and epigenetics.

Introduction

Despite the fact that glutamine is the most abundant amino acid in serum, several studies indicate solid tumours, such as melanoma, pancreatic cancer, and colorectal cancer, reside in a glutamine deprived microenvironment (34-36). As a result, tumour cells must develop strategies to adapt to glutamine deprivation for tumourigenesis to persist. For instance, tumour cells can undergo metabolic reprogramming to utilize other carbon sources, like asparagine and aspartate, to promote cell survival (21, 73, 74). In melanoma, low glutamine in the core regions led to the depletion of α-ketoglutarate (αKG), a key cofactor for the Jumonji-domain-containing (JmjC) histone demethylases (JHDMs), which catalyze the removal of methyl marks from histones (35, 75). This low glutamine-induced histone hypermethylation promoted melanoma tumour dedifferentiation and resistance to BRAF inhibitors. These results suggest that low glutamine in the tumour microenvironment, similar to hypoxia, may drive cancer progression and augment resistance to treatment via epigenetic regulation. However, whether increased glutamine levels *in vivo* can be detrimental to melanoma cells, which have well adapted to a low glutamine environment, remains unknown.

In vitro conditioned cancer cells convert glucose to lactate and rely on glutamine to replenish tricarboxylic acid (TCA) cycle intermediates (8). However, in contrast to previous *in vitro* results, accumulating evidence from *in vivo* experiments demonstrate that glutamine is not an essential nutritional source to support tumour growth. For instance, *in vivo* trace-labeling studies, in lung cancer patients and animal models, indicated minimal utilization of glutamine in the TCA cycle with glucose and lactate identified as the main contributors to TCA intermediates (76, 77). Similarly, human glioblastoma cells relied more on glucose to support anapleorotic and biosynthetic pathways and led to accumulation of glucose-derived glutamine in the tumours *in*

vivo (70). Furthermore, as *in vitro* conditions rely on the use of culturing medium with excess nutrients, a recent study used a modified medium, in combination with hypoxia, to reproduce the *in vivo* metabolic environment and demonstrate that an increase in glutamine consumption does not predict its essentiality for growth (71). Therefore, a more objective evaluation of how glutamine can affect tumour growth *in vivo* is needed.

Here, using several patient-derived melanoma tumour models, we found that glutamine supplementation suppressed epigenetically-activated oncogenic pathways and inhibited melanoma tumour growth. Importantly, dietary glutamine supplementation increased survival in a transgenic melanoma model and improved therapeutic response to BRAF inhibition. Our work highlights the importance of understanding the *in vivo* effect of glutamine on melanoma tumour growth for better therapeutic strategies targeting the nutrient poor tumour microenvironment.

Results

Dietary glutamine supplementation inhibits melanoma tumour growth *in vivo*

To test the effect of glutamine supplementation on melanoma tumour growth, we used a diet supplemented with 20% glutamine compared to control diet (Fig. 1a). We based the diet composition on previous clinical studies demonstrating benefits to using up to 30 grams per day in patients and *in vivo* studies with 20-30% glutamine supplementation in rodent diet (78-80). We found the rate of change in tumour volume was significantly different between high glutamine supplementation and control diet groups when mice were placed on high glutamine diet one week after subcutaneous xenograft injections of the patient-derived M229 cells, which harbor a BRAF V600E mutation and *PTEN* deletion (Fig. 1b-d) (81). Using a linear mixed model, we observed a difference in growth rate of 70 mm^3 per week (95% CI: 48-92, $P < 0.001$)

a

Product	Control (kcal%)	High Gln (kcal%)
Glutamine	0	20
Purified amino acids	18	18
Carbohydrate	66	46
Fat	16	16
Total	100	100

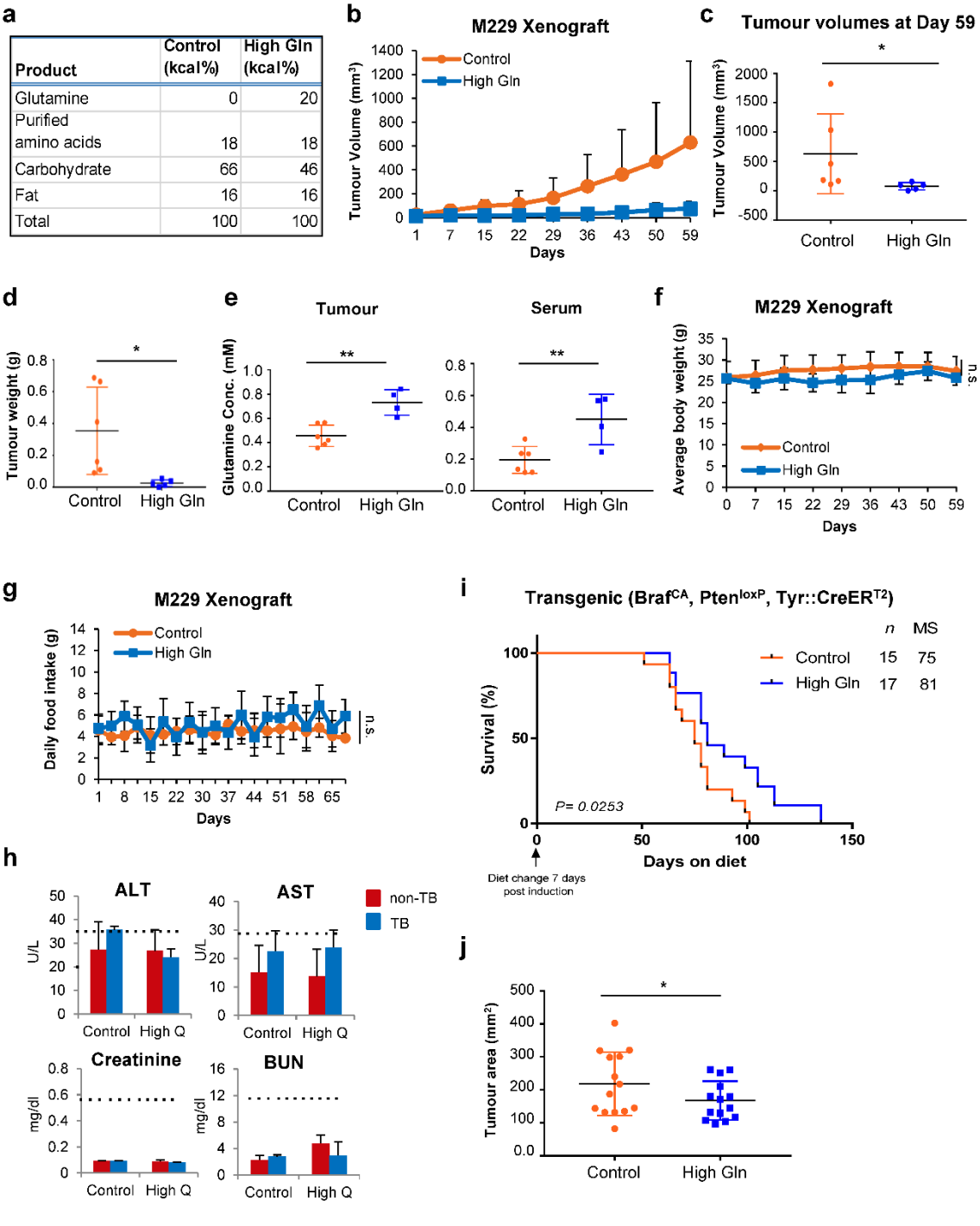

Figure 1. Dietary glutamine supplementation inhibits melanoma tumour growth *in vivo.* a. Percentage of kcal of main food groups in purified amino acid control diet compared to glutamine supplemented (High Gln) diet. **b.** Nude mice with subcutaneous injection of M229 cells received control or high glutamine (High Gln) diet one-week post injection. Tumours were measured twice weekly (Control, *n*=6; High Gln, *n*=5). **c.** Final tumour volumes at day 59 in control and High Gln diet groups. *P* value calculated using Mann-Whitney test. **d.** M229 xenograft tumour weights post-mortem. **e.** Glutamine concentration from M229 tumours and nude mice serum measured by EIA kit (*n*=6 for Control and *n*=4 for High Gln biological replicates). **f, g.** Body weight (**f**) and food intake (**g**) of nude mice injected with M229 xenografts (Control, n=6; High Gln, n=5). **h.** Blood from M229 tumour-bearing (TB) and non-TB nude mice fed control or glutamine supplemented (High Q) diet. Blood was collected by cardiac puncture and analysed for liver and kidney function evaluation by EIA kit. (Control non-TB *n*=2, Control TB *n*=4, High Q non-TB *n*=4, High Q TB *n*=4, biological replicates performed in triplicates). **i.** B6.BRaf^{CA}, Pten^{loxP}, Tyr::Cre^{ERT2} tri-allelic transgenic mice placed on control or glutamine supplemented (High Gln) diet one-week post 4-hydroxytamoxifen topical administration until clinical end point. *P* value calculated by Mantel-Cox test. **j.** B6.BRaf^{CA}, Pten^{loxP}, Tyr::Cre^{ERT2} tumour areas post mortem**.** Data represent means and error bars are s.d. *P* value calculated by *t*-test (unpaired, two-tailed) unless specified otherwise, *p<0.05, **p<0.01, ***p<0.001, n.s. not significant.

between the two diet groups. Moreover, supplementation of glutamine in the diet significantly increased the concentration of glutamine in serum and tumours (Fig. 1e), without any significant difference in body weight, food intake, or liver and kidney physiological functions (Fig. 1f-h). Since mutant NRAS is known to drive glutamine dependency in melanoma(82), we investigated the effect of glutamine supplementation in HMCB xenografts, which express BRAF wildtype and mutant NRAS, and found that increased glutamine intake hindered growth in these tumours compared to control diet group (Supplementary Fig. 1a, b). To further test glutamine supplementation on mice melanoma models, we used B16 xenografts and observed a similar confounding inhibitory effect on tumour growth (Supplementary Fig. 1c). Moreover, we sought to test whether increased dietary glutamine can extend the survival rate of tumour bearing mice in a spontaneous, more aggressive, mouse melanoma model, B6.BRaf^{CA}, Pten^{loxP}, Tyr::Cre^{ERT2} tri-allelic transgenic mice placed on control or glutamine supplemented diet one week after administering 4-hydroxytamoxifen to induce melanoma tumours(83). We found that dietary

glutamine supplementation modestly, albeit significantly, extended the survival in these mice and reduced overall tumour burden (Fig. 1i, j).

Dietary and oral glutamine intake effectively hinders melanoma tumour progression

To maintain isocaloric intake, glutamine supplementation in diet resulted in a 20% reduction in carbohydrate content (Fig. 1a). Low carbohydrate diet has previously been shown to affect growth in prostate cancer, we sought to confirm that the observed effect on tumour growth was specific to glutamine supplementation, and not the reduction in dietary carbohydrates(84). Thus, we designed another control diet to replace the 20% glutamine increase with equal increase in all purified amino acids already present in rodent diet (labelled "Amino Acids" diet) and equal percentage of carbohydrates (Fig. 2a, Supplementary Data 1). Consistently, high glutamine in diet led to significant reduction in M229 xenograft tumour volumes. Importantly, increasing amino acids in the diet did not have an effect on tumour growth. These results suggest that the observed change in melanoma tumour growth is specific to the increased glutamine, and not the decrease in the kcal percentage of carbohydrate, in the diet (Fig. 2b, c). Notably, serum glutamine levels were significantly increased only by glutamine supplementation in diet and no difference in body weight or food intake was observed between the diet groups (Fig. 2d-f). We also found glutamine supplementation in drinking water was as effective in deterring melanoma tumour growth as dietary glutamine intake (Fig. 2g-j). Together, these data demonstrate that glutamine supplementation via food or water is sufficient to inhibit melanoma tumour growth.

Glutamine supplementation impedes growth in wildtype and mutant BRAF melanoma PDX tumours

To further test the effect of increased dietary glutamine on larger, established tumours, as often seen in patients, we used two melanoma PDX models with different genetic background,

a

Product	Control (% kcal)	High Gln (% kcal)	Amino Acids (% kcal)
Glutamine	0	20	0
Purified amino acids	18	18	38
Carbohydrate	66	46	46
Fat	16	16	16
Total	100	100	100

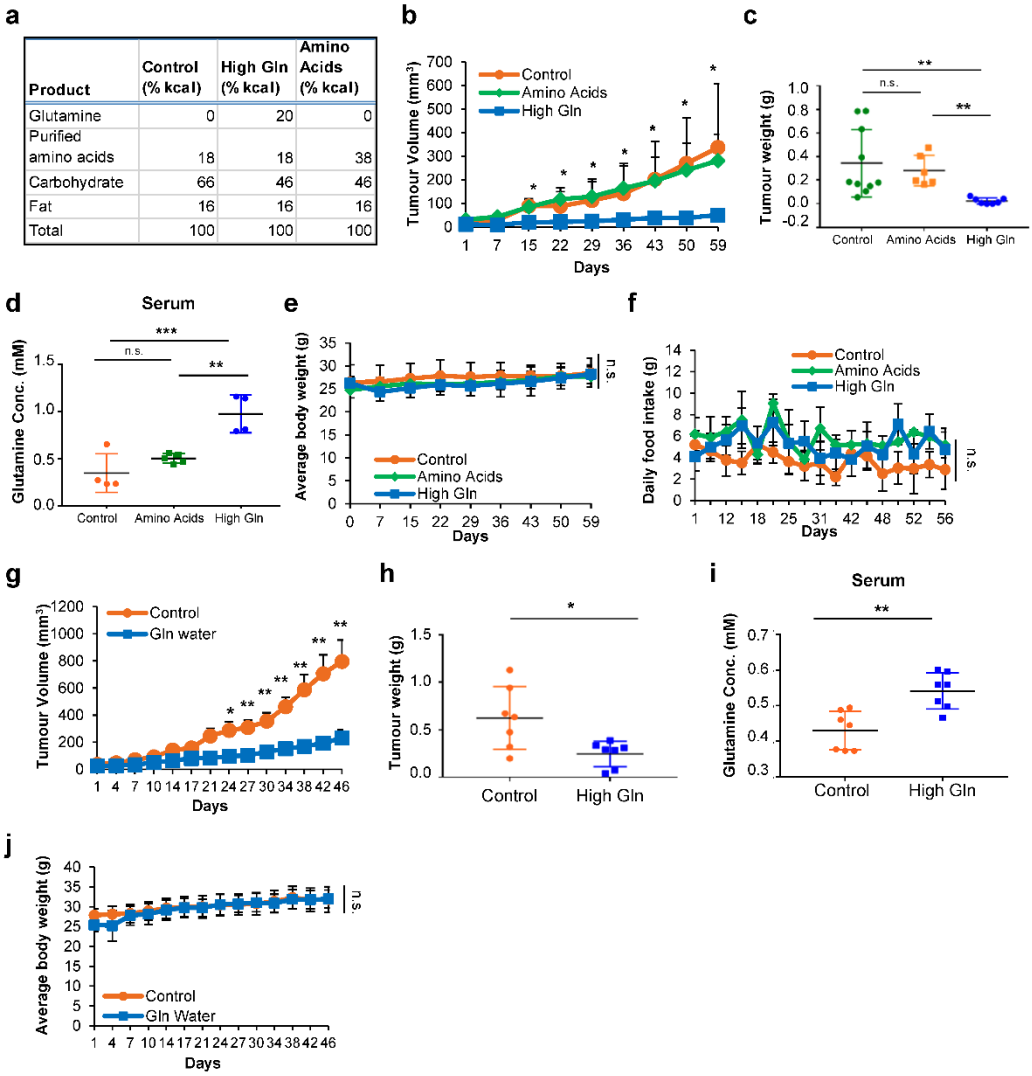

Figure 2. Dietary and oral glutamine intake effectively hinders melanoma tumour progression. a. Percentage of kcal of main food groups in Control and high glutamine (High Gln) diet compared to Amino Acids diet. **b.** Nude mice with M229 xenografts received Control, Amino Acids or High Gln diet. Tumours were measured twice weekly (Control, *n*=10; Amino Acids, *n*=6; High Gln, *n*=7). **c.** Tumour weights post-mortem. **d.** Glutamine concentration in serum measured by EIA kit (*n*= biological replicates performed in triplicates). **e, f.** Nude mice with subcutaneous injection of M229 cells receiving control, amino acids or High Gln diet were weighed (**e**) and monitored for food intake (**f**) (Control, *n*=10; amino acids, *n*=6; High Gln, *n*=7). **g.** Nude mice with subcutaneous injection of M229 cells placed on regular (control) water, or glutamine supplemented (Gln) water one-week post injection. Tumours were measured twice weekly (Control, *n*=7; High Gln, *n*=7). **h.** Tumour weights post-mortem. **i.** Glutamine concentration in serum measured by EIA kit (*n*= biological replicates performed in triplicates). **j.** Nude mice with subcutaneous injection of M229 cells placed on control water or Gln water were weighed twice weekly. Data represent means and error bars are s.d. **b-f,** *P* value calculated using one-way ANOVA followed by post-hoc Tukey's HSD test. **g-j,** *P* value calculated by *t*-test (unpaired, two-tailed), *p<0.05, **p<0.01, ***p<0.001, n.s. not significant.

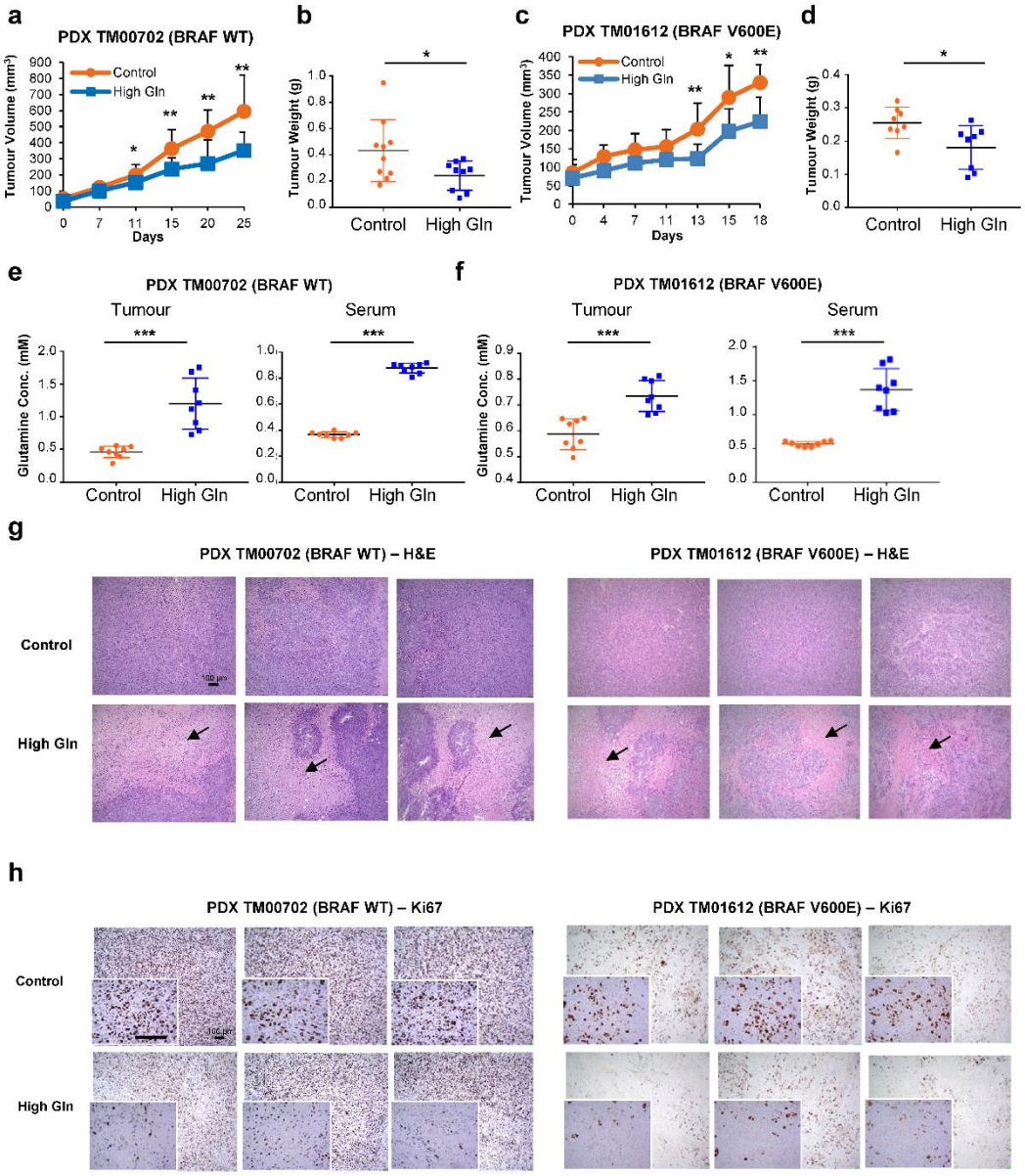

Figure 3. Glutamine supplementation impedes growth in wildtype and mutant BRAF melanoma PDX tumours. a. NSG mice with subcutaneous implantation of melanoma PDX tumour TM00702 (Control, *n*=10; High Gln, *n*=9) received control or high glutamine (High Gln) diet and tumours were measured twice weekly. **b.** Tumour weights post-mortem. **c.** NSG mice with subcutaneous implantation of melanoma PDX tumour TM01612 (Control, *n*=8; High Gln, *n*=8) received control or High Gln diet and tumours were measured twice weekly. **d.** Tumour weights post-mortem. **e, f.** Glutamine concentration in PDX TM00702 (**e**) and TM01612 (**f**) serum and tumours measured by EIA kit (*n*=8 biological replicates). **g.** Cross-sections of PDX_TM00702 (left) and PDX_TM01612 (right) tumours were H&E stained. Scale bar = 100µm at 10x. Arrows indicate regions of necrosis/apoptosis. **h.** Cross-sections of PDX_TM00702 (left) and PDX_TM01612 (right) tumours were Ki67 stained (Control, *n*=3; High Gln, *n*=3). Scale bar = 100µm. Data represent means and error bars are s.d. *P* value calculated by *t*-test (unpaired, two-tailed), *p<0.05, **p<0.01, ***p<0.001, n.s. not significant.

PDX_TM00702 (with wild type BRAF) and PDX_TM01612 (with BRAF V600E mutation), and placed mice on either control or glutamine rich diet when tumours reached an average of 50 mm^3. Interestingly, we found that dietary glutamine supplementation significantly reduced tumour growth in both melanoma PDX models regardless of BRAF status (Fig. 3a, b and 3c, d). Consistently, we did not observe any significant difference in body weight or food intake in mice with PDX_TM00702 tumours (Supplementary Fig. 2a, b). However, mice with PDX_TM01612 tumours exhibited weight loss in both dietary groups with no difference in food intake, which concluded this study at day 18 (Supplementary Fig. 2c, d). Serum and tumour tissues from both models showed increased glutamine levels in mice receiving the experimental diet (Fig. 3e, f), while having inconsistent or no effect on other amino acids (Supplementary Fig. 3). In addition to the marked difference in tumour volumes, cross-sections of PDX tumours from mice fed with glutamine supplemented diet appeared to have more necrotic or apoptotic regions by haematoxylin and eosin staining (Fig. 3g) accompanied by decreased proliferation by Ki67 staining compared to control (Fig. 3h and Supplementary Fig. 2e).

Glutamine supplementation downregulates expression of melanoma-associated oncogenes

Low glutamine levels in tumour regions have been shown to induce upregulation of melanoma dedifferentiation genes via the inhibition of the αKG-dependent JHDMs (35). We tested whether dietary glutamine supplementation is affecting growth through transcriptomic alternations by performing RNA-sequencing analysis in PDX melanoma tumours. We compared differentially expressed genes (DEGs) coupled with pathway enrichment and GSEA analyses in control versus high glutamine tumours. From DEGs analysis, we observed a major and uniform change in the gene expression profile in all tumours from glutamine fed mice with an observed overall down-regulation of genes as a result of high glutamine levels (Fig. 4a and Supplementary Data 2).

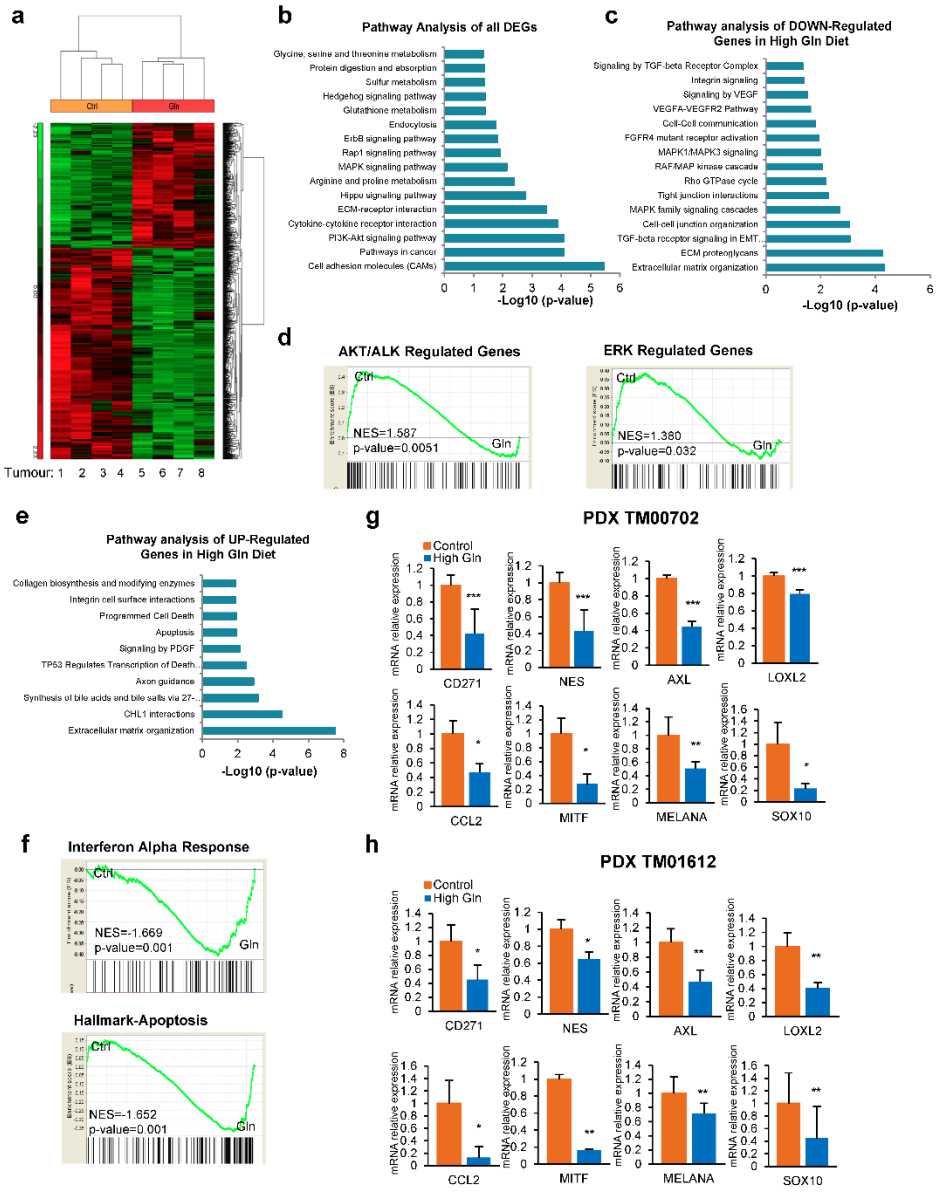

Figure 4. **Glutamine supplementation downregulates expression of melanoma-associated oncogenes. a.** Cluster and heat map of differentially expressed genes (DEGs) in PDX_TM00702 tumours from control (Ctrl) or glutamine supplementation (Gln) mice groups (*n*=4, biological replicates). **b.** Pathway enrichment analysis of all DEGs (p<0.05 and FDR<0.05) in Gln versus Ctrl groups with foldchange = $\pm$1.5. **c.** Pathway enrichment analysis of DEGs downregulated in Gln versus Ctrl groups with foldchange $\geq$ 1.5, p<0.05 and FDR<0.05. **d.** GSEA analysis in control (Ctrl) versus glutamine supplemented (Gln) tumours. **e.** Pathway enrichment analysis of DEGs upregulated in Gln versus Ctrl groups with foldchange $\leq$ -1.5, p<0.05 and FDR<0.05. **f.** GSEA analysis in control (Ctrl) versus glutamine supplemented (Gln) tumours. **g, h.** Melanoma-associated oncogenes expression in PDX_TM00702 (**g**) and PDX_TM01612 (**h**) tumours verified by qPCR. (*n*=3, biological replicates performed in triplicates). Data represent means and error bars are s.d. *P* value calculated by *t*-test (unpaired, two-tailed). *p<0.05, **p<0.01, ***p<0.001.

Broad pathway enrichment analyses revealed several pathways impacted by glutamine supplementation (Fig. 4b). Specifically, significantly down-regulated gene sets (p<0.05, FDR<0.05) indicated a downregulation in major oncogenic pathways in mice groups receiving dietary glutamine supplementation (Fig. 4c). Moreover, GSEA analyses demonstrate control tumours, but not tumours from mice supplemented with glutamine, have stronger enrichments for AKT and ERK related genes, both of which are major melanoma oncogenic signalling pathways (Fig. 4d) (85). In comparison, up-regulated genes (p<0.05, FDR<0.05) in tumours from mice group receiving glutamine supplementation show significant changes in pathways related to apoptosis regulation (Fig. 4e, f and Supplementary Data 2). Furthermore, qPCR analysis of melanoma oncogenic genes (CD271, NES, AXL, LOXL2, MITF, MELANA, SOX10) and the melanoma chemotactic gene,CCL2, showed significant down-regulation and a change in downstream signalling of these genes by glutamine supplementation in both PDX tumour models (Fig. 4g, 4h, and Supplementary Fig 2f) (86, 87). These data indicate that glutamine supplementation suppresses tumour growth via global repression of melanoma oncogenic genes.

Dietary glutamine supplementation increases intra-tumoural α-ketoglutarate but not biosynthetic intermediates

We next analyzed metabolites from tumour tissues by liquid chromatography-mass spectrometry (LC-MS) to evaluate changes in tumour metabolism as a result of the high glutamine diet. As expected, glutamine supplementation resulted in significant changes in several metabolites, particularly in metabolites downstream of glutaminolysis including αKG (Fig. 5a, b). Pathway analysis of significantly changed metabolites (p<0.05, FDR<0.05) indicated an increase in pathways directly linked to glutamine, such as nucleotides and glutathione metabolism, in

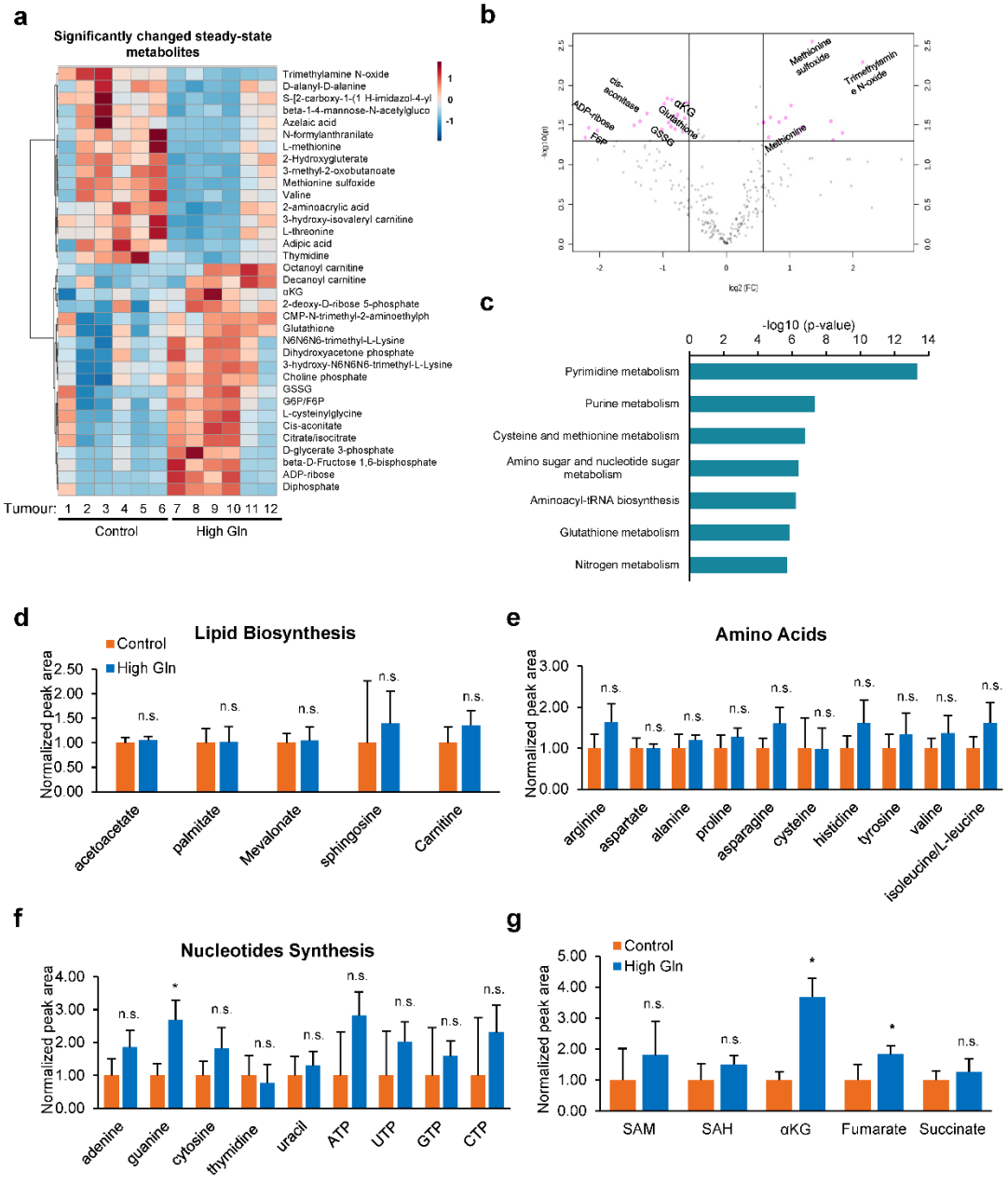

Figure 5. **Dietary glutamine supplementation increases intra-tumoural α-ketoglutarate but not biosynthetic intermediates. a.** Heat map of metabolites measured by LC-MS in PDX_TM00702 tumours ($p<0.05$, $n=6$, biological replicates). **b.** Volcano plot of significantly changed metabolites. **c.** Pathway analysis on significantly changed ($p<0.05$, and FDR<0.05) metabolites in control versus high glutamine PDX_TM00702 tumours. **d,e,f.** Peak area of selected metabolites related to lipid biosynthesis, amino acids, and nucleotide synthesis normalized to control tumours. **g.** Peak area of epigenetic-related metabolites normalized to control tumours. Data represent means and error bars are s.d., *P* value calculated by *t*-test (unpaired, two-tailed). *$p<0.05$, n.s. not significant.

tumours from mice receiving glutamine supplementation (Fig. 5c and Supplementary Data 3). Despite the increase in nucleotide metabolism, tumours from mice supplemented with glutamine were not rapidly proliferating or increasing in size (Fig. 3a, h). Thus, to further confirm that glutamine supplementation is not contributing to biosynthetic pathways necessary for cell proliferation *in vivo*, we evaluated levels of cellular substrates for lipid, amino acids, and nucleotides biosynthesis (88, 89). The metabolite profile of each of these pathways revealed no significant change in their levels as a result of increased glutamine (Fig. 5d-f). Alternatively, glutamine supplementation could be inhibiting melanoma tumour growth through metabolite-driven gene expression based on the change observed in transcriptomic profile of these tumours (Fig. 4a). This is consistent with previous studies linking glutamine levels to gene expression via αKG-mediated epigenetic reprogramming (62, 90). Thus, we examined all metabolites that were previously linked to epigenetics modifications, such as *S*-adenosyl methionine (SAM), *S*-adenosylhomocysteine (SAH), and the TCA cycle intermediates αKG, fumarate, and succinate (46, 56, 91, 92). We found αKG is the most increased metabolite in tumours from mice fed with high glutamine diet (Fig. 5g and Supplementary Fig. 4a). These results indicate that significant increase in αKG could be mediating transcriptomic changes as a result of the increase in glutamine in the tumour microenvironment.

High glutamine deters melanoma progression through decreasing H3K4me3 dependent gene expression

αKG is a necessary cofactor for several JHDM enzymes that mediate the demethylation of histones H3 on lys4, lys27 and lys9 thereby affecting access of transcriptional machinery to gene loci (58, 62, 90). Histone immunoblots from PDX_TM00702, PDX_TM01612, and M229 xenograft tumours revealed a decrease in H3K4me3, H3K27me3, and H3K9me3 levels as a

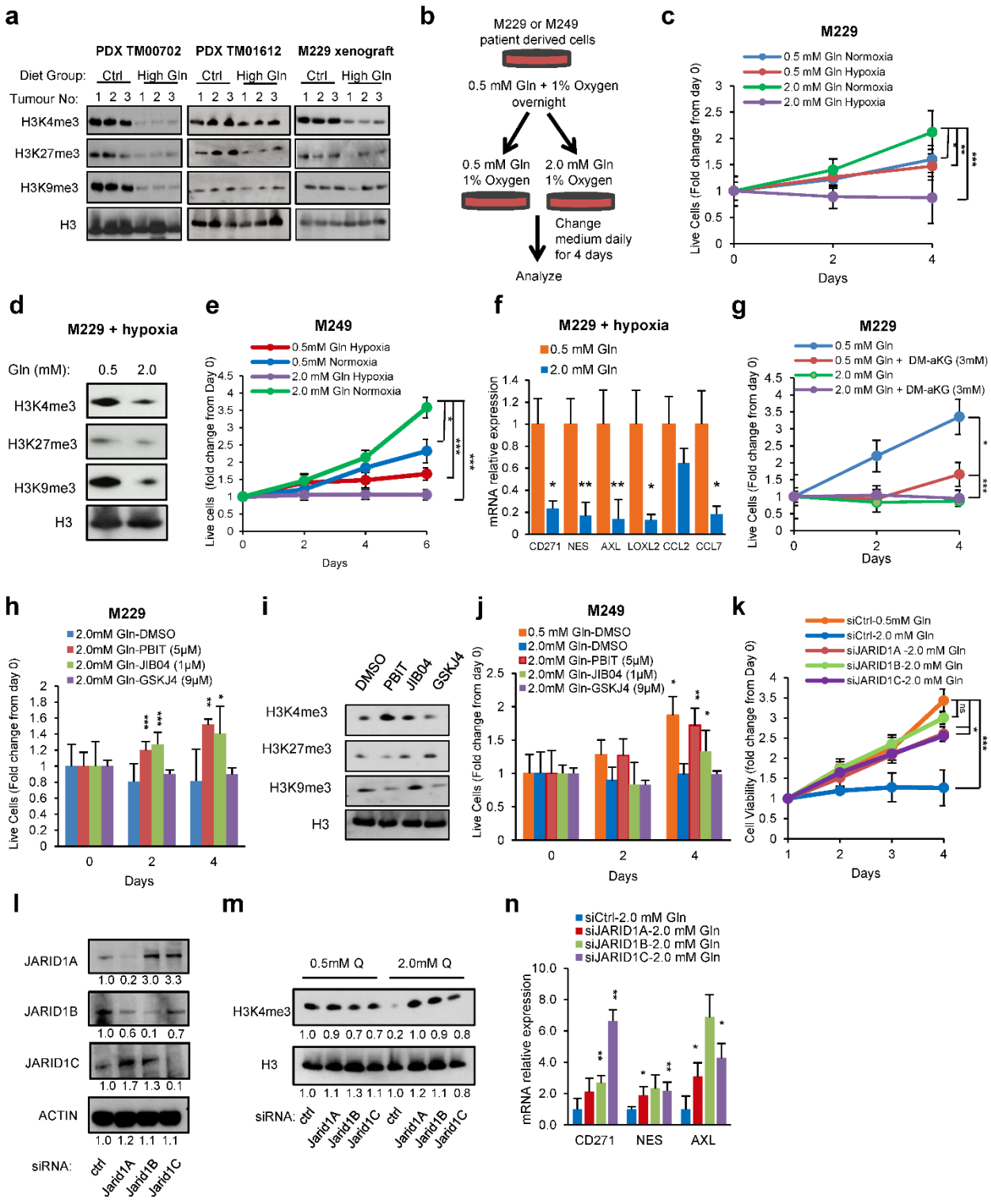
a
PDX TM00702
PDX TM01612
M229 xenograft
Diet Group: Ctrl High Gln Ctrl High Gln Ctrl High Gln
Tumour No: 1 2 3 1 2 3 1 2 3 1 2 3 1 2 3 1 2 3
H3K4me3
H3K27me3
H3K9me3
H3
b
M229 or M249
patient derived cells
0.5 mM Gln + 1% Oxygen
overnight
0.5 mM Gln
1% Oxygen
2.0 mM Gln
1% Oxygen
Change
medium daily
for 4 days
Analyze
c
M229
0.5 mM Gln Normoxia
0.5 mM Gln Hypoxia
2.0 mM Gln Normoxia
2.0 mM Gln Hypoxia
Live Cells (Fold change from day 0)
Days
d
M229 + hypoxia
Gln (mM): 0.5 2.0
H3K4me3
H3K27me3
H3K9me3
H3
e
M249
0.5mM Gln Hypoxia
0.5mM Normoxia
2.0 mM Gln Hypoxia
2.0 mM Gln Normoxia
Live cells (fold change from Day 0)
Days
f
M229 + hypoxia
0.5 mM Gln
2.0 mM Gln
mRNA relative expression
CD271 NES AXL LOXL2 CCL2 CCL7
g
M229
0.5 mM Gln
0.5 mM Gln + DM-aKG (3mM)
2.0 mM Gln
2.0 mM Gln + DM-aKG (3mM)
Live Cells (Fold change from day 0)
Days
h
M229
2.0mM Gln-DMSO
2.0mM Gln-PBIT (5μM)
2.0mM Gln-JIB04 (1μM)
2.0mM Gln-GSKJ4 (9μM)
Live Cells (Fold change from day 0)
Days
i
DMSO
PBIT
JIB04
GSKJ4
H3K4me3
H3K27me3
H3K9me3
H3
j
M249
0.5 mM Gln-DMSO
2.0mM Gln-DMSO
2.0mM Gln-PBIT (5μM)
2.0mM Gln-JIB04 (1μM)
2.0mM Gln-GSKJ4 (9μM)
Live Cells (Fold change from day 0)
Days
k
siCtrl-0.5mM Gln
siCtrl-2.0 mM Gln
siJARID1A -2.0 mM Gln
siJARID1B-2.0 mM Gln
siJARID1C-2.0 mM Gln
Cell Viability (fold change from Day 0)
Days
l
JARID1A
1.0 0.2 3.0 3.3
JARID1B
1.0 0.6 0.1 0.7
JARID1C
1.0 1.7 1.3 0.1
ACTIN
1.0 1.2 1.1 1.1
siRNA: ctrl Jarid1A Jarid1B Jarid1C
m
0.5mM Q
2.0mM Q
H3K4me3
1.0 0.9 0.7 0.7 0.2 1.0 0.9 0.8
H3
1.0 1.1 1.3 1.1 1.0 1.2 1.1 0.8
siRNA: ctrl Jarid1A Jarid1B Jarid1C ctrl Jarid1A Jarid1B Jarid1C
n
siCtrl-2.0 mM Gln
siJARID1A-2.0 mM Gln
siJARID1B-2.0 mM Gln
siJARID1C-2.0 mM Gln
mRNA relative expression
CD271 NES AXL

Figure 6. High glutamine deters melanoma progression through decreasing H3K4me3 dependent gene expression. a. Tumours from control (Ctrl) or glutamine supplemented (High Gln) groups were used for histone extraction and assessed by western blotting using the indicated histone antibodies. **b.** Schematic of modified cell culturing conditions *in vitro* to mimic tumour microenvironment. **c.** M229 cells culture in 96-well plate as in (**b**). Cell viability was assessed using CellTiter Glo assay (*n*=3, independent experiments). **d.** M229 cells, cultured as in (**b**), were lysed and used for histone extraction and immunoblotting with the indicated antibodies. **e.** M249 cells, cultured as in (**b**), were assessed using Trypan blue exclusion (*n*=3, independent cell cultures). **f.** M229 cells, cultured as in (**b**), were used for qPCR analysis (*n*=3, independent cell cultures). **g.** M229 cells cultured as in (**b**) with or without 3mM DM-αKG. Cell viability was assessed using CellTiter Glo assay (*n*=3, independent cell cultures). **h, i.** M229 cells cultured as in (**b**) and treated with DMSO, PBIT (5μM), JIB04 (1μM) or GSKJ4 (9μM). Cells were assessed for viability by CellTiter Glo assay (**h**) (*n*=3, independent experiments) or collected for western blotting using indicated antibodies (**i**). **j.** M249 cells cultured as in (**b**) and treated with DMSO, PBIT (5μM), JIB04 (1μM) or GSKJ4 (9μM). Live cell numbers were assessed using Trypan blue exclusion (*n*=3, independent experiments). **k, l.** M229 cells were transfected with siRNA against scramble control (siCtrl), JARID1A, JARID1B or JARID1C and cultured as in (**b**). Live cell numbers were assessed using Trypan blue exclusion (**k**) (*n*=3, independent cell cultures) or collected for immunoblotting as indicated (**l**). **m.** siCtrl, JARID1A, JARID1B or JARID1C were collected for histone extraction and immunoblotting. Immunoblots were quantified using ImageJ, and the graph represents the mean of each group divided by actin or total H3 histones normalized to the control treatment values. **n.** siCtrl, JARID1A, JARID1B or JARID1C cells cultured as in (**b**) were collected for qPCR analysis (*n*=3, independent cell cultures). Data represents means and error bars are s.d. *P* value calculated by *t*-test (unpaired, two-tailed). *p<0.05, **p<0.01, ***p<0.001.

result of glutamine supplementation (Fig. 6a). Notably, only the decrease in H3K4me3 was consistent across all tumour models. To further investigate whether high glutamine-induced melanoma growth inhibition is mediated by histone hypomethylation, we cultured two parental patient-derived melanoma cells, M229 and M249, in tumour-like conditions, under low glutamine (0.5mM) and 1% oxygen. We then proceeded to switch the medium to either low glutamine (0.5mM) or high glutamine (2.0mM), under hypoxic conditions, with the medium changed daily (Fig. 6b). Both M229 and M249 cells cultured under normoxia had increased rate of proliferation with higher glutamine concentration, in agreement with previous *in vitro* studies. However, we found that, using these patient-derived cells under more physiological oxygen levels, increased glutamine dramatically reduces cellular proliferation (Fig. 6c, e). This is in line

with several studies indicating that non-physiological culturing conditions can skew cancer cells metabolism (71, 93). Additionally, reduced histone methylation was observed in cells cultured with high glutamine under hypoxia, similar to the effect seen in melanoma tumours *in vivo* (Fig. 6d). As seen in the PDX tumours, the expression of melanoma associated genes were also decreased in M229 cells cultured with high glutamine under hypoxia (Fig. 6f). Moreover, to further confirm that the effect of high glutamine, under hypoxia, on viability is mediated through the increase in αKG-dependent demethylation of histones, we cultured cells in different glutamine concentrations with the addition of dimethyl-αKG. The addition of cell permeable dimethyl-αKG to cells cultured under low glutamine reduced cell viability and levels of H3K4me3 similar to the effect observed by high glutamine in the medium (Fig. 6g and Supplementary Fig. 3b). To further delineate which histone modification is critical in mediating the effect of glutamine supplementation, we treated cells cultured in high glutamine with JIB04 (a pan demethylases inhibitor), PBIT (an H3K4me3 demethylases inhibitor), or GSKJ4 (an H3K27me3 demethylase inhibitor) to determine if either of these histone marks are necessary for the effect of high glutamine (68, 94, 95). We found the pan inhibitor JIB04 effectively rescued cell viability in cells cultured in high glutamine. Importantly, the H3K4me3 demethylases inhibitor PBIT treatment alone was sufficient to rescue cell viability to a similar extent as the pan inhibitor, suggesting H3K4me3 is critical in the glutamine regulated modification of chromatin (Fig. 6h-j). In contrast, we did not observe an effect of JHDMs inhibition on growth in cells cultured under low glutamine (Supplementary Fig. 4c). In line with these results, we further tested several melanoma cell lines with different genetic background. We found that the response in these cell lines (HMCB, SK-MEL-2, WM-266-4, and M249R) was tightly correlated with the decrease in H3K4me3 as a result of increased glutamine levels under hypoxia (Supplementary

Fig. 4d, e). While the non-responding cell line, A375, had no change in H3K4me3 levels. PBIT specifically inhibits the JARID1 family demethylases, which include JARID1A, JARID1B, and JARID1C, that mediate the demethylation of H3K4me3 (94). Consistently, we found that knockdown of these enzymes rescued melanoma cells cultured under high glutamine, while having no effect on cells cultured in low glutamine (Fig. 6k-m and Supplementary Fig. 4f). Despite the increase in JARID1A expression in JARID1B and JARID1C knockdown cells, these cells still had better survival at high glutamine and an overall increase in levels of H3K4me3. Moreover, the knockdown of JARID1 demethylases induced the expression of melanoma related oncogenes, which are suppressed by increased levels of glutamine (Fig. 6n).

Reduction in H3K4me3 by dietary glutamine supplementation downregulates oncogenic pathways and cooperates with targeted therapies

As H3K4me3 is a marker for transcription initiation, we investigated whether downregulation of melanoma genes in tumours was directly linked to decrease in H3K4me3 levels. We performed H3K4me3 ChIP-sequencing and observed a significant decrease in H3K4me3 overall and near the promoter regions in PDX_TM00702 tumours from mice receiving glutamine supplementation (Fig. 7a, and Supplementary Fig. 5). GSEA analysis indicated glutamine supplementation affected H3K4me3 enrichment at genes involved in melanoma oncogenic pathways such as AKT and ERK, previously observed by RNA-seq analysis (Fig. 7b). Correlating downregulated DEGs by RNA-seq and genes with decreased H3K4me3 ChIP-seq enrichment at the promoter showed an overlap of 51 genes, which are involved in several oncogenic pathways such as RAS and FGFR4 signalling pathways (Fig. 7c, d)(96, 97). Importantly, we observed a significant decrease in H3K4me3 enrichment at the melanoma-associated genes, CD271, AXL, SOX10, and MITF (Fig. 7e). These results further suggest that

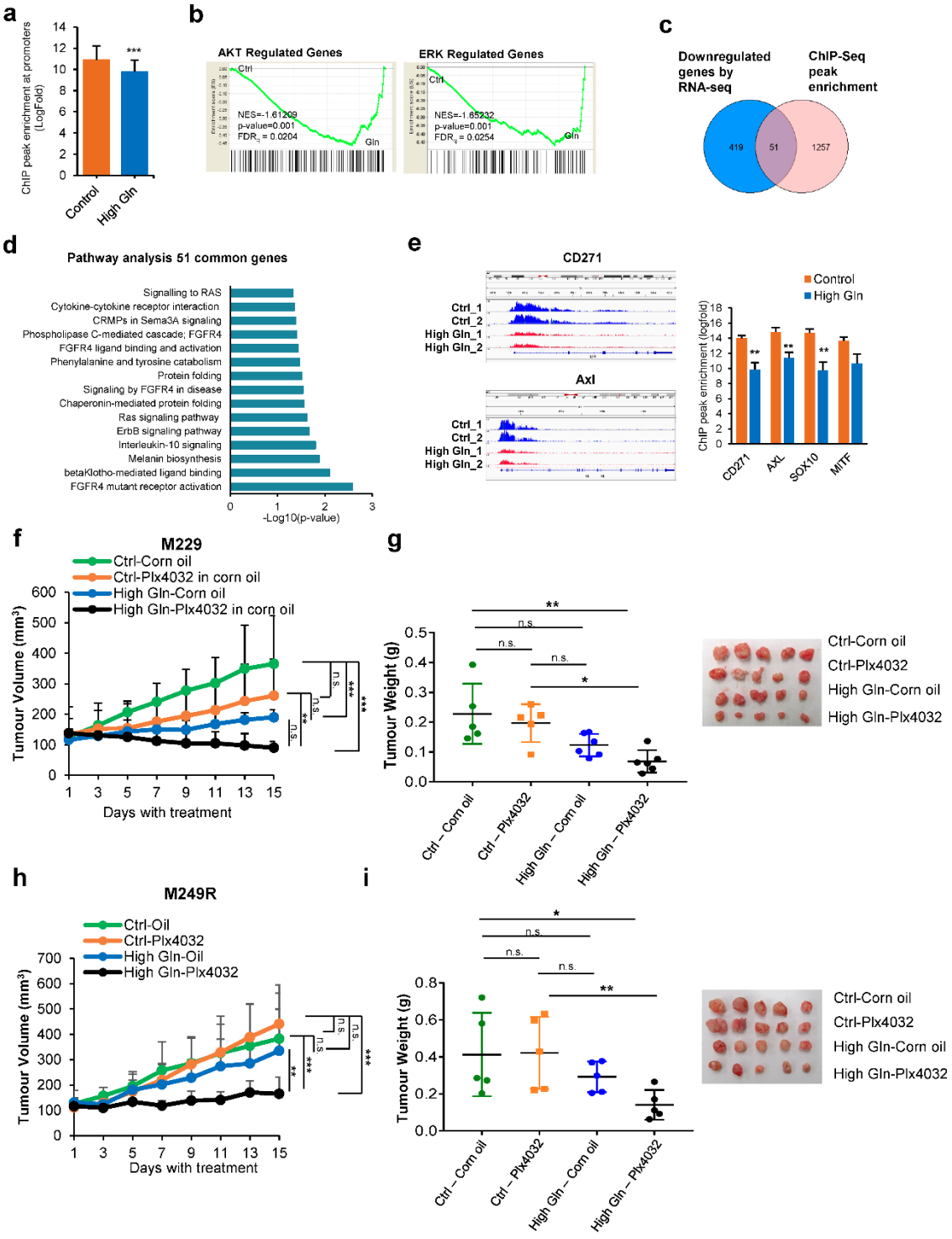
a
ChIP peak enrichment at promoters (LogFold)
Control
High Gln
b
AKT Regulated Genes
ERK Regulated Genes
NES=-1.61209
p-value=0.001
FDR = 0.0204
NES=-1.65232
p-value=0.001
FDR = 0.0254
c
Downregulated genes by RNA-seq
ChIP-Seq peak enrichment
419
51
1257
d
Pathway analysis 51 common genes
Signalling to RAS
Cytokine-cytokine receptor interaction
CRMPs in Sema3A signaling
Phospholipase C-mediated cascade; FGFR4
FGFR4 ligand binding and activation
Phenylalanine and tyrosine catabolism
Protein folding
Signaling by FGFR4 in disease
Chaperonin-mediated protein folding
Ras signaling pathway
ErbB signaling pathway
Interleukin-10 signaling
Melanin biosynthesis
betaKlotho-mediated ligand binding
FGFR4 mutant receptor activation
-Log10(p-value)
e
CD271
Axl
Ctrl_1
Ctrl_2
High Gln_1
High Gln_2
Control
High Gln
ChIP peak enrichment (logfold)
CD271
AXL
SOX10
MITF
f
M229
Ctrl-Corn oil
Ctrl-Plx4032 in corn oil
High Gln-Corn oil
High Gln-Plx4032 in corn oil
Tumour Volume (mm³)
Days with treatment
g
Tumour Weight (g)
Ctrl – Corn oil
Ctrl – Plx4032
High Gln – Corn oil
High Gln – Plx4032
Ctrl-Corn oil
Ctrl-Plx4032
High Gln-Corn oil
High Gln-Plx4032
h
M249R
Ctrl-Oil
Ctrl-Plx4032
High Gln-Oil
High Gln-Plx4032
Tumour Volume (mm³)
Days with treatment
i
Tumour Weight (g)
Ctrl – Corn oil
Ctrl – Plx4032
High Gln – Corn oil
High Gln – Plx4032
Ctrl-Corn oil
Ctrl-Plx4032
High Gln-Corn oil
High Gln-Plx4032

Figure 7. Reduction in H3K4me3 by dietary glutamine supplementation downregulates oncogenic pathways and cooperates with targeted therapies. a. PDX_TM00702 tumours were used for ChIP-sequencing analysis using H3K4me3 antibody. ChIP peaks average at promoter regions of associated genes (LogFC between ChIP and Input) in control and High Gln tumour samples (*n*=3, biological replicates per group performed in technical duplicates). **b.** GSEA analysis of H3K4me3 ChIP peak associated genes in control (Ctrl) versus glutamine supplemented (Gln) tumours. **c.** Venn diagram of DEGs downregulated in RNA-seq ($p<0.05$, FDR<0.05) and ChIP-seq gene peaks specific to promoter region in PDX-TM00702 tumours ($p<0.05$, LogFC=1.2). **d.** Pathway analysis of 51 common genes between RNA-seq and ChIP-seq ($p<0.05$). **e.** Representation (left) and quantitation (right) of average H3K4me3 peaks at promoter regions in melanoma associated oncogenes. **f.** Nude mice with M229 xenografts received control (Ctrl) or glutamine supplemented (High Gln) diets one-week post injection. When tumours reached an average of 100 mm^3 in volume, mice were treated with corn oil or 10 mg kg^{-1} PLX4032 in corn oil by oral gavage for 2 weeks. (Control-oil, *n*=5; Control-Plx4032, *n*=5; High Gln-oil, *n*=6; High Gln-Plx4032, *n*=6). **h.** Nude mice with M249R xenografts received control (Ctrl) or glutamine supplemented (High Gln) diets one-week post injection. When tumours reached an average of 100 mm^3 in volume, mice were treated with corn oil or 10 mg kg^{-1} PLX4032 in corn oil by oral gavage for 2 weeks. (Control-oil, *n*=5; Control-Plx4032, *n*=5; High Gln-oil, *n*=5; High Gln-Plx4032, *n*=5). Data represent mean and error bars are s.d. **g. i.** M229 and M249R xenograft tumours were weighed post mortem. **e.** *P* value calculated by *t*-test (unpaired, two-tailed). **f-i.** *P* value calculated by two-way or one-way ANOVA followed by post-hoc Tukey's multiple comparison test. *$p<0.05$, **$p<0.01$, ***$p<0.001$, n.s not significant.

high glutamine levels in the tumour microenvironment reduces H3K4me3-dependent transcription and affect the expression of critical melanoma-associated oncogenes. Since our RNA-seq and ChIP-seq analyses indicated that increased glutamine levels repressed the expression of melanoma oncogenes, we sought to test whether glutamine supplementation can cooperate with BRAF targeted therapies. We used the BRAF inhibitor, PLX4032, in M229 and PLX4032-resistant M249R xenograft tumours when tumours reached an average of 100 mm^3 in volume (98). Interestingly, tumours in mice fed with high glutamine diet were much more sensitive to PLX4032 treatment indicating combining these interventions could improve therapeutic response (Fig. 7g, h). More importantly, even though glutamine supplementation had a very modest effect on tumour growth in M249R tumours, these tumours exhibited significantly slower growth when glutamine supplementation was combined with PLX4032 treatment (Fig. 7h, i). These results indicate that glutamine supplementation in diet can potentially re-sensitize

tumours by downregulating MAPK and other oncogenic pathways that give rise to targeted resistance in melanoma.

Discussion

Our results show unprecedented evidence that glutamine supplementation can slow growth in melanoma tumours with different BRAF status by inhibiting epigenetically-activated oncogenic pathways. Taken with previous studies on glutamine supplementation to boost the immune response without any side effects, this highlights the potential benefit of glutamine supplementation in melanoma patients (79, 80, 99). Similarly, several studies have now explored the therapeutic benefits of disrupting the tumour microenvironment *in vivo*. For instance, dietary serine and glycine limitation or use of ketogenic diet effectively inhibited tumour growth in several models (100-102). In addition, supplementation with histidine or adopting a ketogenic regimen sensitized cancer to targeted treatments (103, 104). The effect of dietary intervention in treating several metabolic diseases, including cancer, has been gaining interest. Therefore, it is critical to scientifically examine how diet can serve as a molecular therapeutic tool in cancer treatments as part of a "personalized diet" for patients. Our current work focused on melanoma, and further work is needed to determine whether other solid tumours are also sensitive to glutamine supplementation.

In vitro studies showing glutamine can be utilized by tumour cells raise a concern that glutamine will provide nutritional support to promote tumour growth *in vivo*. Here, we found that glutamine supplementation increased several TCA intermediates; however, it was not directly utilized for growth and proliferation as indicated by Ki67 staining in melanoma tumours. Consistently, independent trace-labeling studies in human lung cancer indicated minimum glutamine utilization *in vivo* with glucose and lactate being the main contributors to the TCA cycle (76,

105). In addition, using a modified *in vitro* culturing system, which combines hypoxia and physiological levels of glutamine, we found patient-derived melanoma cells exhibit differential metabolism in normoxia compared to hypoxia, indicating that hypoxia in the tumour microenvironment greatly affect glutamine metabolism. In support with this, several studies highlighted that cells experiencing hypoxia or mitochondrial dysfunction have decreased glutamine oxidation and rely on carbon sources, other than glucose and glutamine, to supply metabolic intermediates under hypoxic conditions (32, 33, 106). These studies and others support the idea that, under low oxygen levels in the tumour microenvironment, glutamine supplementation may not increase tumour growth *in vivo*.

Accumulating evidence indicate that epigenetic modifications contribute to tumour progression and therapeutic responses (107). The reversible nature of epigenetic modifications led to the emergence of novel epigenetic therapeutics and several types of these medications have been approved by the FDA. Despite the success of these drugs in changing the epigenetics of various cancers, its efficacy in solid tumours is lagging behind. In melanoma, a solid tumour, how epigenetic reprogramming affect tumour growth is not well-studied. Our data indicate that expression of several oncogenic genes in melanoma tumours are regulated at the epigenetic level, particularly, by H3K4me3. Global increased H3K4me3 levels have been associated with metastasis and poor prognosis in cancer(108, 109). Thus, a regimen that can decrease levels of H3K4me3 would be clinically beneficial. More importantly, glutamine suppression of melanoma oncogenic pathways via global decrease in H3K4me3 levels can not only cooperate with, but re-sensitize resistant tumours to, targeted therapies. This data also suggests that developing inhibitors targeting H3K4me3 methyltransferases may inhibit melanoma tumour growth and sensitize tumours to current treatments.

Additionally, the availability of several metabolites has been long suspected to play a role in regulating enzymes that carry out several epigenetic modifications. Of which, αKG has been realized as a key glutamine-metabolite that regulate the activity of several JHDMs (92, 110). Although the specificity of each JARID1 enzyme to particular genes or regions in the genome remains unknown, the knockdown of JARID1A, JARID1B, and JARID1C in our study directly impacted the expression of several melanoma oncogenes. Notably, we observed an increase in the expression of JARID1A by the knockdown of JARID1B or JARID1C, however, these cells still exhibited an increase in H3K4me3. Despite the fact that our results suggest that the inhibition of H3K4me3 demethylation enzymes is able to reverse the effect of high glutamine on cell growth, we are not able to exclude the potential role of these demethylases in other cellular functions.

Taken together, our results provide a previously unidentified mechanism by which glutamine supplementation inhibits melanoma tumour growth and suggests a previously unrealized therapeutic avenue using glutamine supplementation in melanoma to cooperate with current therapies and potentially combat resistance mechanisms. Furthermore, our results provide important evidence that glutamine supplementation, rather than the nutrient limiting approaches, is a simple dietary intervention that has the potential to block melanoma tumour growth and potentiate the effects of anti-melanoma treatments by suppressing epigenetically-activated oncogenic pathways.

Materials and Methods

Cell culture. Patient-derived melanoma M229, M249, and M249R cells were obtained from Roger S. Lo's lab (UCLA)(111). B16-OVA cells were kindly provided by Roberto Tinoco's lab (UCI). HMCB, SK-MEL-2, A375, and WM-266-4 cells were purchased from ATCC. Cells were cultured at 37˚C in 5% CO_2 in Dulbecco's modified Eagle's medium (DMEM) with high glucose (4.5g/L) (DM-22, Omega, Tarzana, CA) supplemented with 10% dialyzed fetal bovine serum (FBS) (FB-07, Omega, Tarzana, CA), 100 units/mL of penicillin, and 100μg/mL of streptomycin (Gemini Bio-Products, Sacramento, CA) and either 0.5mM or 2.0mM L-glutamine (GS-60, Omega, Tarzana, CA). For hypoxia culture, cells were seeded in DMEM supplemented with 10% dialyzed FBS and 0.5mM glutamine under 1% O_2 in BioSpherix Xvivo system (Parish, NY, USA). After 24 hours, the medium was changed to DMEM supplemented with 10% dialyzed FBS and either 0.5 mM glutamine or 2.0 mM glutamine. Cells were incubated under hypoxic conditions for 4 days with the medium changed daily. Cells were tested for mycoplasma using MycoAlert mycoplasma detection kit (Lonza, Switzerland).

Histone extraction and western blotting. Tumour tissues and cells were used for histones extraction as previously described(35). Briefly, $3x10^6$ cells or 20mg of homogenized tissues (homogenized using Percellys Ceramic kit with Percellys 24 homogenizer) were lysed in hypotonic lysis buffer (10 mM HEPES, 10 mM KCl, 1.5 mM $MgCl_2$, 0.5 mM dithiothreitol) with protease inhibitor (Roche) on ice for 1 hour. Lysate was rotated at 4˚C overnight in a final concertation of 0.2N H_2SO_4. Samples were centrifuged, and supernatants were used for histone precipitation using 30%(w/v) TCA for 1 hour on ice. Pellet was washed with ice cold acetone and dissolved with water. For western blotting, cells or tumour tissues were lysed in RIPA buffer. Protein concentration was determined using BCA protein assay kit (Life

Technologies, Carlsbad, CA, USA). Blots were blocked for 1 hour in 5% non-fat milk in PBS with 0.05% Tween-20 and membranes were probed with primary antibodies overnight and horseradish-peroxidase-conjugated secondary antibodies (Bio-Rad, Hercules, CA, USA). Signal was visualized by Western Lightning Plus-ECL (PerkinElmer, Waltham, MA, USA). The antibodies used for western blotting can be found in Supplementary Table 2.

Cell viability assays. Cells were seeded in 96-well or 12-well plates and allowed to adhere overnight in 0.5mM glutamine medium. Afterwards, medium was changed to either medium containing 0.5mM or 2.0mM glutamine. Reagents such as DMSO and dimethyl-αKG were purchased from Sigma Aldrich (St. Louis, MO, USA) and PBIT, JIB04, and GSKJ4 were purchased from Tocris Bio-Techne (Minneapolis, MN, USA). Medium was replaced daily. Viable cell number was assessed by CellTiter Glo (Promega, Madison, WI, USA) or Trypan Blue exclusion and counted by TC20 automated cell counter (Bio-Rad, Hercules, CA, USA).

Animal models. All studies involving animals were performed according to and approved by the Institutional Animal Care and Use Committee (IACUC) protocols at the University of California, Irvine in compliance with ethical regulations. NCr Nude mice (nu/nu, male 4-week old, Taconic Bioscience) were used for xenograft studies and NSG mice (NOD scid gamma, male 4-week old, The Jackson Lab) were used for patient-derived xenografts (PDX) studies. For xenograft studies, 2×10^6 or 5×10^6 of M229 and M249R in 100 μl DMEM without FBS or antibiotics were injected subcutaneously into 6 weeks old male NCr Nude mice. Mice were on normal chow diet for one-week post xenograft injection. In mice melanoma model, $1x10^5$ B16 cells in 100 μl DMEM without FBS or antibiotics were injected subcutaneously into 6 weeks old male C57BL/6 mice and placed on diets immediately. Tumour bearing mice were placed randomly on control, glutamine rich or amino acids diets. For PDX studies, NSG mice were purchased from the

Jackson Lab carrying the TM00702 or TM01612 tumours. The tumours were excised, and small pieces were implanted subcutaneously in 6-week old male NSG mice as previously described (112). Mice were placed randomly into 2 dietary groups one-week post engraftment. Tumour size was measured every 2-3 days with callipers and tumour volume was calculated using the formula ½(length×width^2). Mice were euthanized when tumours reached 1 cm^3 in volume, upon ulceration/bleeding, drop in weight, or signs of lethargy. For PLX4032 treatment, when the tumour volume reached an average of 100mm^3, mice were placed randomly into 4 experimental groups and treated with corn oil (control) or PLX4032 (dissolved in DMSO and diluted in corn oil to 10 mg kg^{-1}) by oral gavage daily. Mice were euthanized after 2 weeks of treatment. The B6.BRaf^{CA}, Pten^{loxP}, Tyr::Cre^{ERT2} tri-allelic transgenic mouse model was purchased from the Jackson Lab (4 weeks old). Mixed male and female population were used. Activation of BRAF and *Pten* deletion were induced by topical administration of 4-hydroxytamoxifen (4-OHT) as previously described (83). Mice were placed into 2 dietary groups one week following 4-OHT administration. All mice were monitored to determine a humane clinical end point. Animals that died from illnesses unrelated to tumour growth were included as censored observations. Sample sizes for each animal study were estimated based on preliminary data or previous experience with these models predicting variance within each group.

Immunohistochemistry. After euthanization, tumours were collected and fixed in 10% formalin. Formalin-fixed, paraffin embedded blocks of melanoma PDX tumours were used for haematoxylin and eosin (H&E) and Ki67 staining. Slides were blindly evaluated by two independent pathologists to assess the extent of necrosis or apoptosis and Ki67 staining in tumours. Ki67 microscope images of PDX TM00702 and PDX TM01612 tumors were

quantified using Image Pro Plus software. % total area of pixels selected by threshold for the Ki67 stain was calculated using Image Pro's Count/Size tool.

Diets. All mice were kept on normal chow diet until the start of the experiments. Three diets were used in this study based on the OpenStandard diet with 15 kcal% fat with crystalline amino acids from Research Diets Inc (New Brunswick, NJ). The "Control diet" (A11112201) contained all essential amino acids and non-essential amino acids as specified by Research Diets. The "Glutamine supplemented diet" contained all amino acids equal to the control diet with the addition of 200g of glutamine. Corn starch content was adjusted to achieve the isocaloric intake. The "Amino acids diet" contained all amino acids equal to the control diet with a proportional increase in each amino acids to achieve the same total protein as the "Glutamine rich diet". For glutamine supplementation in drinking water, the amount of "Glutamine supplemented diet" food intake per day was calculated to be 0.5g per cage per day. The same amount of glutamine was dissolved in the drinking water and changed daily.

siRNA cell transfection. M229 cells were transiently transfected with siRNA according to manufacturer's protocol by Lipofectamine RNAiMAX (Life Technologies, Carlsbad, CA, USA) with on-target SMARTpool control siRNA (D-001810-10-20) and siRNA targeting human JARID1A (KDM5A) (L-003297-02-0005), human JARID1B (KDM5B) (L-003297-02-0005), human JARID1C (KDM5C) (L-010097-01-0005) purchased from Dharmacon (Lafayette, CO, USA). Transfected M229 cells were cultured in medium with 0.5 mM glutamine. Medium was changed to 2.0mM glutamine after 24 hours and changed daily for 4 days for cell viability or 3 days for mRNA extraction.

Glutamine extraction and measurement. Glutamine was extracted from 20-40mg of tumour tissues homogenized in 70% ethanol by a Percellys 24 homogenizer. After spinning down cell debris, the supernatant was evaporated to dryness and dissolved in distilled water (1ul water per mg of tissue). Glutamine concentration was determined by the EnzyChrom Glutamine kit (EGLN-100, BioAssay Systems, Hayward, CA, USA). Whole blood was collected from mice by cardiac puncture in BD vacutainer tubes (Fisher Scientific, Hampton, NH, USA) and centrifuged for 40 minutes at 2000 RPM to separate serum. Non-haemolyzed serum was used according to the manufacturer's protocol.

Physiological markers. Mouse liver functions were assessed by measuring serum alanine transaminase (ALT) and aspartate transaminase (AST) (EALT-100, EASTR-100, respectively, EnzyChrom, BioAssay Systems) according to manufacturer's protocol. Mouse kidney functions were assessed by measuring serum creatinine and blood urea nitrogen levels (BUN) (DICT-500, DIUR-500, respectively, Quantichrome, BioAssay Systems) according to manufacturer's protocol. Samples with insufficient volumes were diluted with assay buffer provided from the manufacturer. All assays were run with biological replicates in technical triplicates normalized to control levels.

Liquid chromatography-mass spectrometry (LC-MS). 10-15mg of tumour tissues were cut on dry ice and soaked in pre-cooled 80% methanol in HPLC-grade water. Samples were homogenized by Precellys 24 homogenizer using Percellys Ceramic kit. Samples were centrifuged at 4˚C for 15 mins and 500µL of supernatant was transferred to a new tube and evaporated to dryness at room temperature. For serum, 20µL was dissolved in 80µL ice cold HPLC-grade water. 400µL of cold HPLC-grade methanol were added to each sample (for a final concentration of 80% v/v). Samples were vortexed and left on ice for 10min. After

centrifugation, supernatant was transferred to new tube and evaporated to dryness using speed vacuum. The samples were prepared and analysed by LC-MS at Duke University as previously described (113). MetaboAnalyst was used to analyze significantly changed metabolites and generate heat map, PCA, and volcano plot (www.metaboanalyst.ca/).

RNA-sequencing library preparation. Total RNA was extracted using Trizol reagent (15596026, Life Technologies, Carlsbad, CA, USA) from tumour tissues. RNA sequencing libraries were prepared with Kapa RNA mRNA HyperPrep kit (Kapa Biosystems, Cat KR1352) according to the manufacturer's protocol. Briefly, 100 ng of total RNA from each sample was used for polyA RNA enrichment using magnetic oligo-dT beads. The enriched mRNA was fragmented using heat and magnesium and the first strand cDNA was made using random priming. The libraries were validated with the Agilent Bioanalyzer and quantified with Qubit. The RNA-seq sequence reads were mapped to *Homo sapiens* genome assembly GRCh37 (hg19) using open source RNA-seq alignment tool HISAT2. The alignment results were converted to RNA-seq gene expression measurement as RPKM (reads/kilo base of total exon length/million mapped) using Partek Genome Suite (v6.6) and normalized to gene models in the NCBI RefSeq database. Gln sample were compared with Control Sample group using ANOVA analysis with +/− 1.5 fold change (p value < 0.05, FDR<0.05) as the minimum threshold. Maximum expression < 0.5RPKM was used to filter and exclude very low expressing genes. Common genes between RNA-seq and ChIP-seq were analysed using IMPaLA version 11 pathway over-representation analysis.

Sequencing with Illumina Hiseq2500. Both RNA-seq and ChIP-seq Library templates were prepared for sequencing using cBot cluster generation system (Illumina, San Diego, CA, USA) with HiSeq SR Cluster V4 Kit. Sequencing run was performed in the single read mode of

51cycle of read1 and 7 cycles of index read using Illumina HiSeq 2500 with HiSeq SBS V4 Kits. Real-time analysis (RTA) 2.2.38 software was used to process the image analysis and base calling.

Quantitative Real-time PCR. Total RNA, from cell culture or tumour tissues, was extracted and purified using Trizol reagent (Life Technologies, Carlsbad, CA, USA) according to manufacturer's guidelines. 1ug RNA was used for qScript cDNA Synthesis Kit (Quanta Biosciences, Beverly, MA, USA). qPCR analyses were performed with SYBR Green PCR (Quanta Biosciences) using CFX Connect Real-Time PCR Detection System (Bio-Rad, Hercules, CA, USA). Expression results were normalized to β-actin levels and all qPCR amplifications were performed in triplicates and repeated in three independent experiments. The following forward and reverse primers were generated to check gene expression: HUMAN (F: forward, R: reverse) ACTIN-F: 5′-CACCAACTGGGAGGACAT-3′ R: 5′-GCACAGCCT GGATAGCAAC-3′; CD271-F: 5'-TTGGGGGCTTGCAAGTATGT-3' R: 5′-GTTTCAGGAGGGCCCAAGAA-3′; NES-F: 5′- CCCAACTTGGAGGGGAAGTC-3′ R: 5′-TCTCCCTCAGAGACTAGCGG-3′: AXL-F 5′-ATTCATTCCAAACCCCTGACT-3′; R: 5′-ACTGGTTAGTGATGGCCCTA-3′, LOXL2-F: 5'-CTGGTCAACAAGGCAAGAG-3'; R: 5'-AGGAATTCAGGGTCTTGCTA-3'; CCL2-F: 5'-CCAAAGAAGCTGTGATGTGA-3'; R: 5'-GCACTCTCTGACTCTAGGTTT-3'; CCL7-F: 5'-AAAATCCCTAAGCAGAGGCT-3' R: 5'-ACCTAGGACTGAGGTGTGAG-3'; MITF-F: 5'-GATCCTATGGACTGGGCTAT-3' R: 5'-CCAACCAAGGACATGAGAAT-3'; MELANA-F: 5'-AAGAAGGGTTTGATCATCGG-3' R: 5'-ACAGCCATTCATGAAAATACC-3'; SOX10-F: 5'-CCAGCTAAACCCATCTGG-3' R: 5'-CACACCAAGAGACGGTTG-3'.

Chromatin Immunoprecipitation (ChIP) sequencing library preparation. 10 mg of frozen tumour tissue was minced and cross-linked using 1% formaldehyde in PBS for 10 mins at room temperature. Cross-linking was stopped following centrifugation by resuspending the pellet in 125mM glycine in PBS for 5 minutes at RT. Pellets were washed twice with PBS followed by lysis in SDS lysis buffer [1% SDS, 10 mM ethylenediaminetetraacetic acid (EDTA), 50 mM Tris–HCl, pH 8] supplemented with protease inhibitors (Roche). Sonication was performed using Diagenode BioruptorR pico (Leige, Belgium) for 7 cycles (30 sec on/30 sec off) to produce DNA fragments of 100–300 bp in length. The sonicated lysate was centrifuged and diluted using 10 volumes of cold ChIP-dilution buffer (0.01% SDS, 1.1% Triton X-100, 1.2 mm EDTA, 16.7 mm Tris-HCl, pH 8, 167 mm NaCl). The pull-down was performed with anti-H3K4me3 antibody (Millipore Sigma, Burlington, MA, USA) and magnetic protein G Dynabeads (Cat. No. 10004D; Life Technologies, Carlsbad, CA, USA) overnight at 4˚C. Beads were washed with low salt buffer (0.1% SDS, 1% Triton X-100, 2 mm EDTA, 20 mm Tris–HCl, pH 8, and 150 mm NaCl), high salt buffer (0.1% SDS, 1% Triton X-100, 2 mm EDTA, 20 mm Tris–HCl, pH 8, and 500 mm NaCl), LiCl buffer (250 mm LiCl, 1% NP40, 1% NaDOC, 1 mm EDTA, and 10 mm Tris–HCl, pH 8), and twice with TE buffer(10 mmTris–HCl, pH 8, and 1 mm EDTA). Elution buffer (1% SDS and 100 mm NaHCO3). The DNA-protein complexes were then reverse cross-linked by adding 200 mmNaCl, 20 µg Proteinase K (Sigma Aldrich, St. Louis, MO, USA) and incubated at 65 °C for 4 h. Subsequently, 20 µg of RNaseA (Sigma Aldrich) was added and further incubated for 15 minutes at 37 °C. The immunoprecipitated DNA was extracted using phenol-chloroform and ethanol precipitation. Resultant ChIP DNA was quantified using Quant-iT™ dsDNA Assay Kit (Cat No. Q33120; ThermoFisher Scientific) and used for library preparation. ChIP-seq libraries were prepared with Kapa DNA HyperPrep Kit (Cat No. KK

8700, Kapa) according to the manufacturer's protocol. A 10 cycles of PCR was performed to produce the final sequencing library. The libraries were validated with the Agilent Bioanalyzer DNA High Sensitivity Kit and quantified with Qubit. The ChiP-Seq sequence reads were mapped to Homo sapiens genome assembly GRCh37 (hg19) using open source DNA-seq alignment tool BWA (v). High quality unique alignments were used with SAM Tag (XA:Z and SA:Z) as filter, and removed the duplicated alignments caused by PCR duplication using SAMTools (ver 0.1.19). The unmapped reads were removed using SAMTools based on the alignment quality tag (-F 4 -F 256). The cross-correlation of the reads aligned to both strands was tested as ChiP QC using R's SPP package (v1.13) before ChIP-seq peak calling using MACS2 (v2.1.2) with broad option to detect the H3K4me3 binding sites with FDR<0.005 cutoff.

GSEA analysis. Gene set enrichment analysis (GSEA) was performed against hallmarks and oncogenic signature gene set MSigDB database v6.2 database with dataset ranked from LogFC. (http://software.broadinstitute.org/gsea/msigdb).

Statistics. All *in vitro* experiments were repeated three independent times with at least technical triplicates. Results are shown as means; error bars represent standard deviation (s.d.) as specified in figure legends. Unpaired t-test, one-way or two-way ANOVA followed by post hoc test were used to determine the statistical significance of differences between means and were calculated in Microsoft Excel or GraphPad Prism (v7) software. Statistical comparison of the survival curves was calculated using GraphPad Prism (v7) software using Mantel-Cox (Log Ranks) test. (*P<0.05, **P<0.01, ***P<0.001, unless indicated separately).

Data availability. The authors declare that all data generated from this study are included in this publication and its supplementary information files. Data that support the findings of this study

have been deposited in the Gene Expression Omnibus (GEO) under accession code GSE125822.Source Data are also provided with the online version of the paper. All other datasets are available from the corresponding author upon request.

References:

1. Pan, M. et al. Regional glutamine deficiency in tumours promotes dedifferentiation through inhibition of histone demethylation. Nat Cell Biol (2016).
2. Kamphorst, J.J. et al. Human pancreatic cancer tumors are nutrient poor and tumor cells actively scavenge extracellular protein. Cancer research 75, 544-553 (2015).
3. Denkert, C. et al. Metabolite profiling of human colon carcinoma – deregulation of TCA cycle and amino acid turnover. Molecular Cancer 7, 72-72 (2008).
4. Pavlova, N.N. et al. As Extracellular Glutamine Levels Decline, Asparagine Becomes an Essential Amino Acid. Cell metabolism 27, 428-438 e425 (2018).
5. Reid, M.A. & Kong, M. Adaptation to metabolic stress: insights into a paradoxical Q. Cell cycle 12, 1807-1808 (2013).
6. Tajan, M. et al. A Role for p53 in the Adaptation to Glutamine Starvation through the Expression of SLC1A3. Cell metabolism 28, 721-736 e726 (2018).
7. Klose, R.J., Kallin, E.M. & Zhang, Y. JmjC-domain-containing proteins and histone demethylation. Nature Reviews Genetics 7, 715-727 (2006).
8. DeBerardinis, R.J., Lum, J.J., Hatzivassiliou, G. & Thompson, C.B. The Biology of Cancer: Metabolic Reprogramming Fuels Cell Growth and Proliferation. Cell metabolism 7, 11-20 (2008).
9. Davidson, S.M. et al. Environment Impacts the Metabolic Dependencies of Ras-Driven Non-Small Cell Lung Cancer. Cell metabolism 23, 517-528 (2016).
10. Sellers, K. et al. Pyruvate carboxylase is critical for non–small-cell lung cancer proliferation. The Journal of clinical investigation 125, 687-698 (2015).
11. Marin-Valencia, I. et al. Analysis of Tumor Metabolism Reveals Mitochondrial Glucose Oxidation in Genetically Diverse Human Glioblastomas in the Mouse Brain In Vivo. Cell metabolism 15, 827-837 (2012).
12. Vande Voorde, J. et al. Improving the metabolic fidelity of cancer models with a physiological cell culture medium. Science advances 5, eaau7314 (2019).
13. Fahr, M.J., Kornbluth, J., Blossom, S., Schaeffer, R. & Klimberg, V.S. Harry M. Vars Research Award. Glutamine enhances immunoregulation of tumor growth. JPEN. Journal of parenteral and enteral nutrition 18, 471-476 (1994).
14. Klimberg, V.S. et al. Glutamine-enriched diets support muscle glutamine metabolism without stimulating tumor growth. Journal of Surgical Research 48, 319-323 (1990).
15. Kuhn, K.S., Muscaritoli, M., Wischmeyer, P. & Stehle, P. Glutamine as indispensable nutrient in oncology: experimental and clinical evidence. European journal of nutrition 49, 197-210 (2010).
16. Søndergaard, J.N. et al. Differential sensitivity of melanoma cell lines with BRAFV600Emutation to the specific Raf inhibitor PLX4032. Journal of Translational Medicine 8, 39 (2010).
17. Hernandez-Davies, J.E. et al. Vemurafenib resistance reprograms melanoma cells towards glutamine dependence. Journal of Translational Medicine 13, 210 (2015).
18. Dankort, D. et al. Braf(V600E) cooperates with Pten loss to induce metastatic melanoma. Nature genetics 41, 544-552 (2009).
19. Ho, V.W. et al. A Low Carbohydrate, High Protein Diet Slows Tumor Growth and Prevents Cancer Initiation. Cancer research 71, 4484-4493 (2011).
20. Gray-Schopfer, V., Wellbrock, C. & Marais, R. Melanoma biology and new targeted therapy. Nature 445, 851 (2007).

21. Hugo, W. et al. Genomic and Transcriptomic Features of Response to Anti-PD-1 Therapy in Metastatic Melanoma. Cell 165, 35-44 (2016).
22. Weinstein, D., Leininger, J., Hamby, C. & Safai, B. Diagnostic and Prognostic Biomarkers in Melanoma. The Journal of Clinical and Aesthetic Dermatology 7, 13-24 (2014).
23. Fischer, G.M. et al. Metabolic strategies of melanoma cells: Mechanisms, interactions with the tumor microenvironment, and therapeutic implications. Pigment Cell & Melanoma Research 31, 11-30 (2018).
24. Lyssiotis, C.A. & Kimmelman, A.C. Metabolic Interactions in the Tumor Microenvironment. Trends in Cell Biology 27, 863-875 (2017).
25. Lu, C. & Thompson, Craig B. Metabolic Regulation of Epigenetics. Cell metabolism 16, 9-17 (2012).
26. Liu, P.-S. et al. [alpha]-ketoglutarate orchestrates macrophage activation through metabolic and epigenetic reprogramming. Nature immunology 18, 985-994 (2017).
27. Mentch, Samantha J. et al. Histone Methylation Dynamics and Gene Regulation Occur through the Sensing of One-Carbon Metabolism. Cell metabolism 22, 861-873 (2015).
28. Sciacovelli, M. et al. Fumarate is an epigenetic modifier that elicits epithelial-to-mesenchymal transition. Nature 537, 544 (2016).
29. Gao, X., Reid, M.A., Kong, M. & Locasale, J.W. Metabolic interactions with cancer epigenetics. Molecular aspects of medicine (2016).
30. Tran, T.Q., Lowman, X.H. & Kong, M. Molecular Pathways: Metabolic Control of Histone Methylation and Gene Expression in Cancer. Clinical cancer research : an official journal of the American Association for Cancer Research 23, 4004-4009 (2017).
31. Klose, R.J. & Zhang, Y. Regulation of histone methylation by demethylimination and demethylation. Nature reviews. Molecular cell biology 8, 307-318 (2007).
32. Cantor, J.R. et al. Physiologic Medium Rewires Cellular Metabolism and Reveals Uric Acid as an Endogenous Inhibitor of UMP Synthase. Cell 169, 258-272.e217 (2017).
33. Sayegh, J. et al. Identification of small molecule inhibitors of Jumonji AT-rich interactive domain 1B (JARID1B) histone demethylase by a sensitive high throughput screen. The Journal of biological chemistry 288, 9408-9417 (2013).
34. Wang, L. et al. A small molecule modulates Jumonji histone demethylase activity and selectively inhibits cancer growth. Nature communications 4, 2035 (2013).
35. Carey, B.W., Finley, L.W., Cross, J.R., Allis, C.D. & Thompson, C.B. Intracellular alpha-ketoglutarate maintains the pluripotency of embryonic stem cells. Nature 518, 413-416 (2015).
36. Kwong, L.N. et al. Oncogenic NRAS signaling differentially regulates survival and proliferation in melanoma. Nature medicine 18, 1503-1510 (2012).
37. Metzner, T. et al. Fibroblast growth factor receptors as therapeutic targets in human melanoma: synergism with BRAF inhibition. J Invest Dermatol 131, 2087-2095 (2011).
38. Joseph, E.W. et al. The RAF inhibitor PLX4032 inhibits ERK signaling and tumor cell proliferation in a V600E BRAF-selective manner. Proceedings of the National Academy of Sciences 107, 14903-14908 (2010).
39. Melis, G.C., ter Wengel, N., Boelens, P.G. & van Leeuwen, P.A. Glutamine: recent developments in research on the clinical significance of glutamine. Current Opinion in Clinical Nutrition & Metabolic Care 7, 59-70 (2004).
40. Maddocks, O.D.K. et al. Modulating the therapeutic response of tumours to dietary serine and glycine starvation. Nature 544, 372-376 (2017).

41. Martuscello, R.T. et al. A Supplemented High-Fat Low-Carbohydrate Diet for the Treatment of Glioblastoma. Clinical Cancer Research 22, 2482-2495 (2016).
42. Xia, S. et al. Prevention of Dietary-Fat-Fueled Ketogenesis Attenuates BRAF V600E Tumor Growth. Cell metabolism 25, 358-373 (2017).
43. Kanarek, N. et al. Histidine catabolism is a major determinant of methotrexate sensitivity. Nature 559, 632-636 (2018).
44. Hopkins, B.D. et al. Suppression of insulin feedback enhances the efficacy of PI3K inhibitors. Nature 560, 499-503 (2018).
45. Hensley, Christopher T. et al. Metabolic Heterogeneity in Human Lung Tumors. Cell 164, 681-694 (2016).
46. Eales, K.L., Hollinshead, K.E.R. & Tennant, D.A. Hypoxia and metabolic adaptation of cancer cells. Oncogenesis 5, e190 (2016).
47. Metallo, C.M. et al. Reductive glutamine metabolism by IDH1 mediates lipogenesis under hypoxia. Nature 481, 380 (2011).
48. Mullen, A.R. et al. Reductive carboxylation supports growth in tumour cells with defective mitochondria. Nature 481, 385 (2011).
49. Yoo, C.B. & Jones, P.A. Epigenetic therapy of cancer: past, present and future. Nature Reviews Drug Discovery 5, 37 (2006).
50. Li, S., Shen, L. & Chen, K.N. Association between H3K4 methylation and cancer prognosis: A meta-analysis. Thoracic cancer 9, 794-799 (2018).
51. Lewis, R. et al. Global Reduction of H3K4me3 Improves Chemotherapeutic Efficacy for Pediatric Ependymomas. Neoplasia 21, 505-515 (2019).
52. Vatrinet, R. et al. The α-ketoglutarate dehydrogenase complex in cancer metabolic plasticity. Cancer & metabolism 5, 3 (2017).
53. Nazarian, R. et al. Melanomas acquire resistance to B-RAF(V600E) inhibition by RTK or N-RAS upregulation. Nature 468, 973 (2010).
54. Carugo, A. et al. In Vivo Functional Platform Targeting Patient-Derived Xenografts Identifies WDR5-Myc Association as a Critical Determinant of Pancreatic Cancer. Cell reports 16, 133-147 (2016).
55. Liu, X. et al. High-Resolution Metabolomics with Acyl-CoA Profiling Reveals Widespread Remodeling in Response to Diet. Molecular & cellular proteomics : MCP 14, 1489-1500 (2015).1. Egeblad M, Nakasone ES, Werb Z. Tumors as organs: complex tissues that interface with the entire organism. Developmental cell. 2010;18(6):884-901. Epub 2010/07/16. doi: 10.1016/j.devcel.2010.05.012. PubMed PMID: 20627072; PubMed Central PMCID: PMCPMC2905377.
2. Hanahan D, Weinberg Robert A. Hallmarks of Cancer: The Next Generation. Cell.144(5):646-74. doi: 10.1016/j.cell.2011.02.013.
3. Yuneva Mariia O, Fan Teresa WM, Allen Thaddeus D, Higashi Richard M, Ferraris Dana V, Tsukamoto T, et al. The Metabolic Profile of Tumors Depends on Both the Responsible Genetic Lesion and Tissue Type. Cell metabolism. 2012;15(2):157-70. doi: https://doi.org/10.1016/j.cmet.2011.12.015.
4. Jain RK. Normalization of tumor vasculature: an emerging concept in antiangiogenic therapy. Science. 2005;307(5706):58-62. Epub 2005/01/08. doi: 10.1126/science.1104819. PubMed PMID: 15637262.
5. Xie H, Simon MC. Oxygen availability and metabolic reprogramming in cancer. The Journal of biological chemistry. 2017. Epub 2017/08/27. doi: 10.1074/jbc.R117.799973. PubMed PMID: 28842498.
6. Choi SY, Collins CC, Gout PW, Wang Y. Cancer-generated lactic acid: a regulatory, immunosuppressive metabolite? The Journal of pathology. 2013;230(4):350-5. Epub 2013/06/05. doi: 10.1002/path.4218. PubMed PMID: 23729358; PubMed Central PMCID: PMCPMC3757307.
7. San-Millan I, Brooks GA. Reexamining cancer metabolism: lactate production for carcinogenesis could be the purpose and explanation of the Warburg Effect. Carcinogenesis. 2017;38(2):119-33. Epub 2016/12/21. doi: 10.1093/carcin/bgw127. PubMed PMID: 27993896; PubMed Central PMCID: PMCPMC5862360.

8. DeBerardinis RJ, Lum JJ, Hatzivassiliou G, Thompson CB. The Biology of Cancer: Metabolic Reprogramming Fuels Cell Growth and Proliferation. Cell metabolism. 2008;7(1):11-20. doi: http://dx.doi.org/10.1016/j.cmet.2007.10.002.
9. Kroemer G, Pouyssegur J. Tumor Cell Metabolism: Cancer's Achilles' Heel. Cancer cell. 2008;13(6):472-82. doi: https://doi.org/10.1016/j.ccr.2008.05.005.
10. Warburg O. On respiratory impairment in cancer cells. Science. 1956;124(3215):269-70.
11. Zhu A, Lee D, Shim H. Metabolic positron emission tomography imaging in cancer detection and therapy response. Semin Oncol. 2011;38(1):55-69. Epub 2011/03/03. doi: 10.1053/j.seminoncol.2010.11.012. PubMed PMID: 21362516; PubMed Central PMCID: PMCPMC3075495.
12. Barthel A, Okino ST, Liao J, Nakatani K, Li J, Whitlock JP, Jr., et al. Regulation of GLUT1 gene transcription by the serine/threonine kinase Akt1. The Journal of biological chemistry. 1999;274(29):20281-6. Epub 1999/07/10. doi: 10.1074/jbc.274.29.20281. PubMed PMID: 10400647.
13. Wieman HL, Wofford JA, Rathmell JC. Cytokine stimulation promotes glucose uptake via phosphatidylinositol-3 kinase/Akt regulation of Glut1 activity and trafficking. Molecular biology of the cell. 2007;18(4):1437-46. Epub 2007/02/16. doi: 10.1091/mbc.e06-07-0593. PubMed PMID: 17301289; PubMed Central PMCID: PMCPMC1838986.
14. Guillaumond F, Leca J, Olivares O, Lavaut MN, Vidal N, Berthezene P, et al. Strengthened glycolysis under hypoxia supports tumor symbiosis and hexosamine biosynthesis in pancreatic adenocarcinoma. Proceedings of the National Academy of Sciences of the United States of America. 2013;110(10):3919-24. Epub 2013/02/15. doi: 10.1073/pnas.1219555110. PubMed PMID: 23407165; PubMed Central PMCID: PMCPMC3593894.
15. Faubert B, Li KY, Cai L, Hensley CT, Kim J, Zacharias LG, et al. Lactate Metabolism in Human Lung Tumors. Cell. 2017;171(2):358-71 e9. Epub 2017/10/07. doi: 10.1016/j.cell.2017.09.019. PubMed PMID: 28985563; PubMed Central PMCID: PMCPMC5684706.
16. Sonveaux P, Vegran F, Schroeder T, Wergin MC, Verrax J, Rabbani ZN, et al. Targeting lactate-fueled respiration selectively kills hypoxic tumor cells in mice. The Journal of clinical investigation. 2008;118(12):3930-42. Epub 2008/11/27. doi: 10.1172/jci36843. PubMed PMID: 19033663; PubMed Central PMCID: PMCPMC2582933.
17. Boroughs LK, DeBerardinis RJ. Metabolic pathways promoting cancer cell survival and growth. Nat Cell Biol. 2015;17(4):351-9. doi: 10.1038/ncb3124.
18. Eagle H, Oyama VI, Levy M, Horton CL, Fleischman R. The growth response of mammalian cells in tissue culture to L-glutamine and L-glutamic acid. The Journal of biological chemistry. 1956;218(2):607-16. Epub 1956/02/01. PubMed PMID: 13295214.
19. DeBerardinis RJ, Mancuso A, Daikhin E, Nissim I, Yudkoff M, Wehrli S, et al. Beyond aerobic glycolysis: transformed cells can engage in glutamine metabolism that exceeds the requirement for protein and nucleotide synthesis. Proceedings of the National Academy of Sciences of the United States of America. 2007;104(49):19345-50. Epub 2007/11/23. doi: 10.1073/pnas.0709747104. PubMed PMID: 18032601; PubMed Central PMCID: PMCPMC2148292.
20. Coloff JL, Murphy JP, Braun CR, Harris IS, Shelton LM, Kami K, et al. Differential Glutamate Metabolism in Proliferating and Quiescent Mammary Epithelial Cells. Cell metabolism. 2016;23(5):867-80. Epub 2016/05/03. doi: 10.1016/j.cmet.2016.03.016. PubMed PMID: 27133130.
21. Reid MA, Kong M. Adaptation to metabolic stress: insights into a paradoxical Q. Cell cycle. 2013;12(12):1807-8. Epub 2013/05/28. doi: 10.4161/cc.25113. PubMed PMID: 23708515; PubMed Central PMCID: PMCPMC3735684.
22. Nicklin P, Bergman P, Zhang B, Triantafellow E, Wang H, Nyfeler B, et al. Bidirectional transport of amino acids regulates mTOR and autophagy. Cell. 2009;136(3):521-34. Epub 2009/02/11. doi: 10.1016/j.cell.2008.11.044. PubMed PMID: 19203585; PubMed Central PMCID: PMCPMC3733119.
23. Yanagida O, Kanai Y, Chairoungdua A, Kim DK, Segawa H, Nii T, et al. Human L-type amino acid transporter 1 (LAT1): characterization of function and expression in tumor cell lines. Biochimica et biophysica acta. 2001;1514(2):291-302. Epub 2001/09/15. doi: 10.1016/s0005-2736(01)00384-4. PubMed PMID: 11557028.
24. Wang R, Dillon CP, Shi LZ, Milasta S, Carter R, Finkelstein D, et al. The transcription factor Myc controls metabolic reprogramming upon T lymphocyte activation. Immunity. 2011;35(6):871-82. Epub 2011/12/27. doi: 10.1016/j.immuni.2011.09.021. PubMed PMID: 22195744; PubMed Central PMCID: PMCPMC3248798.
25. Wise DR, DeBerardinis RJ, Mancuso A, Sayed N, Zhang XY, Pfeiffer HK, et al. Myc regulates a transcriptional program that stimulates mitochondrial glutaminolysis and leads to glutamine addiction. Proceedings of the National Academy of Sciences of the United States of America. 2008;105(48):18782-7. Epub 2008/11/27. doi: 10.1073/pnas.0810199105. PubMed PMID: 19033189; PubMed Central PMCID: PMCPMC2596212.

26. Eberhardy SR, Farnham PJ. c-Myc mediates activation of the cad promoter via a post-RNA polymerase II recruitment mechanism. The Journal of biological chemistry. 2001;276(51):48562-71. Epub 2001/10/24. doi: 10.1074/jbc.M109014200. PubMed PMID: 11673469.
27. Gao P, Tchernyshyov I, Chang T-C, Lee Y-S, Kita K, Ochi T, et al. c-Myc suppression of miR-23a/b enhances mitochondrial glutaminase expression and glutamine metabolism. Nature. 2009;458(7239):762-5. doi: http://www.nature.com/nature/journal/v458/n7239/suppinfo/nature07823_S1.html.
28. Mannava S, Grachtchouk V, Wheeler LJ, Im M, Zhuang D, Slavina EG, et al. Direct role of nucleotide metabolism in C-MYC-dependent proliferation of melanoma cells. Cell cycle. 2008;7(15):2392-400. Epub 2008/08/05. doi: 10.4161/cc.6390. PubMed PMID: 18677108; PubMed Central PMCID: PMCPMC3744895.
29. Son J, Lyssiotis CA, Ying H, Wang X, Hua S, Ligorio M, et al. Glutamine supports pancreatic cancer growth through a KRAS-regulated metabolic pathway. Nature. 2013;496(7443):101-5. Epub 2013/03/29. doi: 10.1038/nature12040. PubMed PMID: 23535601; PubMed Central PMCID: PMCPMC3656466.
30. Kim JW, Tchernyshyov I, Semenza GL, Dang CV. HIF-1-mediated expression of pyruvate dehydrogenase kinase: a metabolic switch required for cellular adaptation to hypoxia. Cell metabolism. 2006;3(3):177-85. Epub 2006/03/07. doi: 10.1016/j.cmet.2006.02.002. PubMed PMID: 16517405.
31. Papandreou I, Cairns RA, Fontana L, Lim AL, Denko NC. HIF-1 mediates adaptation to hypoxia by actively downregulating mitochondrial oxygen consumption. Cell metabolism. 2006;3(3):187-97. Epub 2006/03/07. doi: 10.1016/j.cmet.2006.01.012. PubMed PMID: 16517406.
32. Metallo CM, Gameiro PA, Bell EL, Mattaini KR, Yang J, Hiller K, et al. Reductive glutamine metabolism by IDH1 mediates lipogenesis under hypoxia. Nature. 2011;481:380. doi: 10.1038/nature10602 https://www.nature.com/articles/nature10602#supplementary-information.
33. Mullen AR, Wheaton WW, Jin ES, Chen P-H, Sullivan LB, Cheng T, et al. Reductive carboxylation supports growth in tumour cells with defective mitochondria. Nature. 2011;481:385. doi: 10.1038/nature10642 https://www.nature.com/articles/nature10642#supplementary-information.
34. Kamphorst JJ, Nofal M, Commisso C, Hackett SR, Lu W, Grabocka E, et al. Human pancreatic cancer tumors are nutrient poor and tumor cells actively scavenge extracellular protein. Cancer research. 2015;75(3):544-53. Epub 2015/02/04. doi: 10.1158/0008-5472.can-14-2211. PubMed PMID: 25644265; PubMed Central PMCID: PMCPMC4316379.
35. Pan M, Reid MA, Lowman XH, Kulkarni RP, Tran TQ, Liu X, et al. Regional glutamine deficiency in tumours promotes dedifferentiation through inhibition of histone demethylation. Nat Cell Biol. 2016. Epub 2016/09/13. doi: 10.1038/ncb3410. PubMed PMID: 27617932.
36. Denkert C, Budczies J, Weichert W, Wohlgemuth G, Scholz M, Kind T, et al. Metabolite profiling of human colon carcinoma – deregulation of TCA cycle and amino acid turnover. Molecular Cancer. 2008;7:72-. doi: 10.1186/1476-4598-7-72. PubMed PMID: PMC2569965.
37. Roberts E, Frankel S. Free amino acids in normal and neoplastic tissues of mice as studied by paper chromatography. Cancer research. 1949;9(11):645-8, 3 pl. Epub 1949/11/01. PubMed PMID: 15392817.
38. Reid MA, Wang WI, Rosales KR, Welliver MX, Pan M, Kong M. The B55alpha subunit of PP2A drives a p53-dependent metabolic adaptation to glutamine deprivation. Molecular cell. 2013;50(2):200-11. Epub 2013/03/19. doi: 10.1016/j.molcel.2013.02.008. PubMed PMID: 23499005.
39. Tran TQ, Lowman XH, Reid MA, Mendez-Dorantes C, Pan M, Yang Y, et al. Tumor-associated mutant p53 promotes cancer cell survival upon glutamine deprivation through p21 induction. Oncogene. 2016. Epub 2016/10/11. doi: 10.1038/onc.2016.360. PubMed PMID: 27721412.
40. Lowman XH, Hanse EA, Yang Y, Ishak Gabra MB, Tran TQ, Li H, et al. p53 Promotes Cancer Cell Adaptation to Glutamine Deprivation by Upregulating Slc7a3 to Increase Arginine Uptake. Cell reports. 2019;26(11):3051-60.e4. doi: 10.1016/j.celrep.2019.02.037.
41. Yang Y, Ishak Gabra MB, Hanse EA, Lowman XH, Tran TQ, Li H, et al. MiR-135 suppresses glycolysis and promotes pancreatic cancer cell adaptation to metabolic stress by targeting phosphofructokinase-1. Nature communications. 2019;10(1):809. doi: 10.1038/s41467-019-08759-0.
42. Reid MA, Lowman XH, Pan M, Tran TQ, Warmoes MO, Ishak Gabra MB, et al. IKKbeta promotes metabolic adaptation to glutamine deprivation via phosphorylation and inhibition of PFKFB3. Genes & development. 2016;30(16):1837-51. Epub 2016/09/03. doi: 10.1101/gad.287235.116. PubMed PMID: 27585591; PubMed Central PMCID: PMCPMC5024682.
43. Zhang J, Fan J, Venneti S, Cross JR, Takagi T, Bhinder B, et al. Asparagine plays a critical role in regulating cellular adaptation to glutamine depletion. Molecular cell. 2014;56(2):205-18. Epub 2014/09/23. doi: 10.1016/j.molcel.2014.08.018. PubMed PMID: 25242145; PubMed Central PMCID: PMCPMC4224619.

44. Commisso C, Davidson SM, Soydaner-Azeloglu RG, Parker SJ, Kamphorst JJ, Hackett S, et al. Macropinocytosis of protein is an amino acid supply route in Ras-transformed cells. Nature. 2013;497(7451):633-7. Epub 2013/05/15. doi: 10.1038/nature12138. PubMed PMID: 23665962; PubMed Central PMCID: PMCPMC3810415.
45. Tajiri H, Uruno T, Shirai T, Takaya D, Matsunaga S, Setoyama D, et al. Targeting Ras-Driven Cancer Cell Survival and Invasion through Selective Inhibition of DOCK1. Cell reports. 2017;19(5):969-80. Epub 2017/05/04. doi: 10.1016/j.celrep.2017.04.016. PubMed PMID: 28467910.
46. Gao X, Reid MA, Kong M, Locasale JW. Metabolic interactions with cancer epigenetics. Molecular aspects of medicine. 2016. Epub 2016/09/14. doi: 10.1016/j.mam.2016.09.001. PubMed PMID: 27620316.
47. Suvà ML, Riggi N, Bernstein BE. Epigenetic Reprogramming in Cancer. Science. 2013;339(6127):1567-70. doi: 10.1126/science.1230184.
48. Fardi M, Solali S, Farshdousti Hagh M. Epigenetic mechanisms as a new approach in cancer treatment: An updated review. Genes & diseases. 2018;5(4):304-11. Epub 2018/12/29. doi: 10.1016/j.gendis.2018.06.003. PubMed PMID: 30591931; PubMed Central PMCID: PMCPMC6303480.
49. Greer EL, Shi Y. Histone methylation: a dynamic mark in health, disease and inheritance. Nature reviews Genetics. 2012;13(5):343-57. Epub 2012/04/05. doi: 10.1038/nrg3173. PubMed PMID: 22473383; PubMed Central PMCID: PMCPMC4073795.
50. Mosammaparast N, Shi Y. Reversal of histone methylation: biochemical and molecular mechanisms of histone demethylases. Annual review of biochemistry. 2010;79:155-79. Epub 2010/04/09. doi: 10.1146/annurev.biochem.78.070907.103946. PubMed PMID: 20373914.
51. Fong CY, Morison J, Dawson MA. Epigenetics in the hematologic malignancies. Haematologica. 2014;99(12):1772-83. Epub 2014/12/05. doi: 10.3324/haematol.2013.092007. PubMed PMID: 25472952; PubMed Central PMCID: PMCPMC4258753.
52. Morin RD, Mendez-Lago M, Mungall AJ, Goya R, Mungall KL, Corbett RD, et al. Frequent mutation of histone-modifying genes in non-Hodgkin lymphoma. Nature. 2011;476(7360):298-303. Epub 2011/07/29. doi: 10.1038/nature10351. PubMed PMID: 21796119; PubMed Central PMCID: PMCPMC3210554.
53. Nikoloski G, Langemeijer SM, Kuiper RP, Knops R, Massop M, Tonnissen ER, et al. Somatic mutations of the histone methyltransferase gene EZH2 in myelodysplastic syndromes. Nature genetics. 2010;42(8):665-7. Epub 2010/07/06. doi: 10.1038/ng.620. PubMed PMID: 20601954.
54. Locasale JW. Serine, glycine and one-carbon units: cancer metabolism in full circle. Nature reviews Cancer. 2013;13(8):572-83. Epub 2013/07/05. doi: 10.1038/nrc3557. PubMed PMID: 23822983; PubMed Central PMCID: PMCPMC3806315.
55. Kooistra SM, Helin K. Molecular mechanisms and potential functions of histone demethylases. Nature reviews Molecular cell biology. 2012;13(5):297-311. Epub 2012/04/05. doi: 10.1038/nrm3327. PubMed PMID: 22473470.
56. Mentch Samantha J, Mehrmohamadi M, Huang L, Liu X, Gupta D, Mattocks D, et al. Histone Methylation Dynamics and Gene Regulation Occur through the Sensing of One-Carbon Metabolism. Cell metabolism. 2015;22(5):861-73. doi: 10.1016/j.cmet.2015.08.024.
57. McDonald OG, Li X, Saunders T, Tryggvadottir R, Mentch SJ, Warmoes MO, et al. Epigenomic reprogramming during pancreatic cancer progression links anabolic glucose metabolism to distant metastasis. Nature genetics. 2017;49(3):367-76. Epub 2017/01/17. doi: 10.1038/ng.3753. PubMed PMID: 28092686; PubMed Central PMCID: PMCPMC5695682.
58. Klose RJ, Zhang Y. Regulation of histone methylation by demethylimination and demethylation. Nature reviews Molecular cell biology. 2007;8(4):307-18. Epub 2007/03/08. doi: 10.1038/nrm2143. PubMed PMID: 17342184.
59. Roesch A, Mueller AM, Stempfl T, Moehle C, Landthaler M, Vogt T. RBP2-H1/JARID1B is a transcriptional regulator with a tumor suppressive potential in melanoma cells. International journal of cancer. 2008;122(5):1047-57. Epub 2007/11/02. doi: 10.1002/ijc.23211. PubMed PMID: 17973255.
60. Lu C, Ward PS, Kapoor GS, Rohle D, Turcan S, Abdel-Wahab O, et al. IDH mutation impairs histone demethylation and results in a block to cell differentiation. Nature. 2012;483(7390):474-8. Epub 2012/02/22. doi: 10.1038/nature10860. PubMed PMID: 22343901; PubMed Central PMCID: PMCPMC3478770.
61. Li L, Li W. Epithelial–mesenchymal transition in human cancer: Comprehensive reprogramming of metabolism, epigenetics, and differentiation. Pharmacology & Therapeutics. 2015;150:33-46. doi: https://doi.org/10.1016/j.pharmthera.2015.01.004.
62. Lu C, Thompson Craig B. Metabolic Regulation of Epigenetics. Cell metabolism. 2012;16(1):9-17. doi: http://dx.doi.org/10.1016/j.cmet.2012.06.001.

63. Shen H, Laird Peter W. Interplay between the Cancer Genome and Epigenome. Cell. 2013;153(1):38-55. doi: https://doi.org/10.1016/j.cell.2013.03.008.
64. Grandy RA, Whitfield TW, Wu H, Fitzgerald MP, VanOudenhove JJ, Zaidi SK, et al. Genome-Wide Studies Reveal that H3K4me3 Modification in Bivalent Genes Is Dynamically Regulated during the Pluripotent Cell Cycle and Stabilized upon Differentiation. Molecular and cellular biology. 2016;36(4):615-27. doi: 10.1128/mcb.00877-15.
65. Prickaerts P, Adriaens ME, Beucken Tvd, Koch E, Dubois L, Dahlmans VEH, et al. Hypoxia increases genome-wide bivalent epigenetic marking by specific gain of H3K27me3. Epigenetics & Chromatin. 2016;9:46. doi: 10.1186/s13072-016-0086-0. PubMed PMID: PMC5080723.
66. Shen X, Liu Y, Hsu Y-J, Fujiwara Y, Kim J, Mao X, et al. EZH1 Mediates Methylation on Histone H3 Lysine 27 and Complements EZH2 in Maintaining Stem Cell Identity and Executing Pluripotency. Molecular cell. 2008;32(4):491-502. doi: https://doi.org/10.1016/j.molcel.2008.10.016.
67. Spangle Jennifer M, Dreijerink Koen M, Groner Anna C, Cheng H, Ohlson Carolynn E, Reyes J, et al. PI3K/AKT Signaling Regulates H3K4 Methylation in Breast Cancer. Cell reports. 2016;15(12):2692-704. doi: http://dx.doi.org/10.1016/j.celrep.2016.05.046.
68. Carey BW, Finley LW, Cross JR, Allis CD, Thompson CB. Intracellular alpha-ketoglutarate maintains the pluripotency of embryonic stem cells. Nature. 2015;518(7539):413-6. Epub 2014/12/10. doi: 10.1038/nature13981. PubMed PMID: 25487152; PubMed Central PMCID: PMCPMC4336218.
69. Cheng T, Sudderth J, Yang C, Mullen AR, Jin ES, Mates JM, et al. Pyruvate carboxylase is required for glutamine-independent growth of tumor cells. Proceedings of the National Academy of Sciences of the United States of America. 2011;108(21):8674-9. Epub 2011/05/11. doi: 10.1073/pnas.1016627108. PubMed PMID: 21555572; PubMed Central PMCID: PMCPMC3102381.
70. Marin-Valencia I, Yang C, Mashimo T, Cho S, Baek H, Yang X-L, et al. Analysis of Tumor Metabolism Reveals Mitochondrial Glucose Oxidation in Genetically Diverse Human Glioblastomas in the Mouse Brain In Vivo. Cell metabolism. 2012;15(6):827-37. doi: https://doi.org/10.1016/j.cmet.2012.05.001.
71. Vande Voorde J, Ackermann T, Pfetzer N, Sumpton D, Mackay G, Kalna G, et al. Improving the metabolic fidelity of cancer models with a physiological cell culture medium. Science advances. 2019;5(1):eaau7314. doi: 10.1126/sciadv.aau7314.
72. Kung HN, Marks JR, Chi JT. Glutamine synthetase is a genetic determinant of cell type-specific glutamine independence in breast epithelia. PLoS Genet. 2011;7(8):e1002229. Epub 2011/08/20. doi: 10.1371/journal.pgen.1002229. PubMed PMID: 21852960; PubMed Central PMCID: PMCPMC3154963.
73. Pavlova NN, Hui S, Ghergurovich JM, Fan J, Intlekofer AM, White RM, et al. As Extracellular Glutamine Levels Decline, Asparagine Becomes an Essential Amino Acid. Cell metabolism. 2018;27(2):428-38 e5. Epub 2018/01/18. doi: 10.1016/j.cmet.2017.12.006. PubMed PMID: 29337136; PubMed Central PMCID: PMCPMC5803449.
74. Tajan M, Hock AK, Blagih J, Robertson NA, Labuschagne CF, Kruiswijk F, et al. A Role for p53 in the Adaptation to Glutamine Starvation through the Expression of SLC1A3. Cell metabolism. 2018;28(5):721-36 e6. doi: 10.1016/j.cmet.2018.07.005. PubMed PMID: 30122553; PubMed Central PMCID: PMC6224545.
75. Klose RJ, Kallin EM, Zhang Y. JmjC-domain-containing proteins and histone demethylation. Nature Reviews Genetics. 2006;7(9):715-27. doi: 10.1038/nrg1945.
76. Davidson SM, Papagiannakopoulos T, Olenchock BA, Heyman JE, Keibler MA, Luengo A, et al. Environment Impacts the Metabolic Dependencies of Ras-Driven Non-Small Cell Lung Cancer. Cell metabolism. 2016;23(3):517-28. Epub 2016/02/09. doi: 10.1016/j.cmet.2016.01.007. PubMed PMID: 26853747; PubMed Central PMCID: PMCPMC4785096.
77. Sellers K, Fox MP, Bousamra M, II, Slone SP, Higashi RM, Miller DM, et al. Pyruvate carboxylase is critical for non–small-cell lung cancer proliferation. The Journal of clinical investigation. 2015;125(2):687-98. doi: 10.1172/JCI72873.
78. Fahr MJ, Kornbluth J, Blossom S, Schaeffer R, Klimberg VS. Harry M. Vars Research Award. Glutamine enhances immunoregulation of tumor growth. JPEN Journal of parenteral and enteral nutrition. 1994;18(6):471-6. Epub 1994/11/01. doi: 10.1177/0148607194018006471. PubMed PMID: 7602720.
79. Klimberg VS, Souba WW, Salloum RM, Plumley DA, Cohen FS, Dolson DJ, et al. Glutamine-enriched diets support muscle glutamine metabolism without stimulating tumor growth. Journal of Surgical Research. 1990;48(4):319-23. doi: https://doi.org/10.1016/0022-4804(90)90066-B.
80. Kuhn KS, Muscaritoli M, Wischmeyer P, Stehle P. Glutamine as indispensable nutrient in oncology: experimental and clinical evidence. European journal of nutrition. 2010;49(4):197-210. Epub 2009/11/26. doi: 10.1007/s00394-009-0082-2. PubMed PMID: 19936817.

81. Søndergaard JN, Nazarian R, Wang Q, Guo D, Hsueh T, Mok S, et al. Differential sensitivity of melanoma cell lines with BRAFV600Emutation to the specific Raf inhibitor PLX4032. Journal of Translational Medicine. 2010;8(1):39. doi: 10.1186/1479-5876-8-39.
82. Hernandez-Davies JE, Tran TQ, Reid MA, Rosales KR, Lowman XH, Pan M, et al. Vemurafenib resistance reprograms melanoma cells towards glutamine dependence. Journal of Translational Medicine. 2015;13(1):210. doi: 10.1186/s12967-015-0581-2.
83. Dankort D, Curley DP, Cartlidge RA, Nelson B, Karnezis AN, Damsky WE, Jr., et al. Braf(V600E) cooperates with Pten loss to induce metastatic melanoma. Nature genetics. 2009;41(5):544-52. doi: 10.1038/ng.356. PubMed PMID: 19282848; PubMed Central PMCID: PMC2705918.
84. Ho VW, Leung K, Hsu A, Luk B, Lai J, Shen SY, et al. A Low Carbohydrate, High Protein Diet Slows Tumor Growth and Prevents Cancer Initiation. Cancer research. 2011;71(13):4484-93. doi: 10.1158/0008-5472.can-10-3973.
85. Gray-Schopfer V, Wellbrock C, Marais R. Melanoma biology and new targeted therapy. Nature. 2007;445:851. doi: 10.1038/nature05661.
86. Hugo W, Zaretsky JM, Sun L, Song C, Moreno BH, Hu-Lieskovan S, et al. Genomic and Transcriptomic Features of Response to Anti-PD-1 Therapy in Metastatic Melanoma. Cell. 2016;165(1):35-44. doi: 10.1016/j.cell.2016.02.065. PubMed PMID: 26997480; PubMed Central PMCID: PMC4808437.
87. Weinstein D, Leininger J, Hamby C, Safai B. Diagnostic and Prognostic Biomarkers in Melanoma. The Journal of Clinical and Aesthetic Dermatology. 2014;7(6):13-24. PubMed PMID: PMC4086529.
88. Fischer GM, Vashisht Gopal YN, McQuade JL, Peng W, DeBerardinis RJ, Davies MA. Metabolic strategies of melanoma cells: Mechanisms, interactions with the tumor microenvironment, and therapeutic implications. Pigment Cell & Melanoma Research. 2018;31(1):11-30. doi: doi:10.1111/pcmr.12661.
89. Lyssiotis CA, Kimmelman AC. Metabolic Interactions in the Tumor Microenvironment. Trends in Cell Biology. 2017;27(11):863-75. doi: 10.1016/j.tcb.2017.06.003.
90. Liu P-S, Wang H, Li X, Chao T, Teav T, Christen S, et al. [alpha]-ketoglutarate orchestrates macrophage activation through metabolic and epigenetic reprogramming. Nature immunology. 2017;18(9):985-94. doi: 10.1038/ni.3796
http://www.nature.com/ni/journal/v18/n9/abs/ni.3796.html#supplementary-information.
91. Sciacovelli M, Gonçalves E, Johnson TI, Zecchini VR, da Costa ASH, Gaude E, et al. Fumarate is an epigenetic modifier that elicits epithelial-to-mesenchymal transition. Nature. 2016;537:544. doi: 10.1038/nature19353
https://www.nature.com/articles/nature19353#supplementary-information.
92. Tran TQ, Lowman XH, Kong M. Molecular Pathways: Metabolic Control of Histone Methylation and Gene Expression in Cancer. Clinical cancer research : an official journal of the American Association for Cancer Research. 2017;23(15):4004-9. Epub 2017/04/14. doi: 10.1158/1078-0432.ccr-16-2506. PubMed PMID: 28404599; PubMed Central PMCID: PMCPMC5553983.
93. Cantor JR, Abu-Remaileh M, Kanarek N, Freinkman E, Gao X, Louissaint A, et al. Physiologic Medium Rewires Cellular Metabolism and Reveals Uric Acid as an Endogenous Inhibitor of UMP Synthase. Cell. 2017;169(2):258-72.e17. doi: https://doi.org/10.1016/j.cell.2017.03.023.
94. Sayegh J, Cao J, Zou MR, Morales A, Blair LP, Norcia M, et al. Identification of small molecule inhibitors of Jumonji AT-rich interactive domain 1B (JARID1B) histone demethylase by a sensitive high throughput screen. The Journal of biological chemistry. 2013;288(13):9408-17. Epub 02/13. doi: 10.1074/jbc.M112.419861. PubMed PMID: 23408432.
95. Wang L, Chang J, Varghese D, Dellinger M, Kumar S, Best AM, et al. A small molecule modulates Jumonji histone demethylase activity and selectively inhibits cancer growth. Nature communications. 2013;4:2035. Epub 2013/06/26. doi: 10.1038/ncomms3035. PubMed PMID: 23792809; PubMed Central PMCID: PMCPMC3724450.
96. Kwong LN, Costello JC, Liu H, Jiang S, Helms TL, Langsdorf AE, et al. Oncogenic NRAS signaling differentially regulates survival and proliferation in melanoma. Nature medicine. 2012;18(10):1503-10. doi: 10.1038/nm.2941.
97. Metzner T, Bedeir A, Held G, Peter-Vörösmarty B, Ghassemi S, Heinzle C, et al. Fibroblast growth factor receptors as therapeutic targets in human melanoma: synergism with BRAF inhibition. J Invest Dermatol. 2011;131(10):2087-95. Epub 07/14. doi: 10.1038/jid.2011.177. PubMed PMID: 21753785.
98. Joseph EW, Pratilas CA, Poulikakos PI, Tadi M, Wang W, Taylor BS, et al. The RAF inhibitor PLX4032 inhibits ERK signaling and tumor cell proliferation in a V600E BRAF-selective manner. Proceedings of the National Academy of Sciences. 2010;107(33):14903-8. doi: 10.1073/pnas.1008990107.

99. Melis GC, ter Wengel N, Boelens PG, van Leeuwen PA. Glutamine: recent developments in research on the clinical significance of glutamine. Current Opinion in Clinical Nutrition & Metabolic Care. 2004;7(1):59-70. PubMed PMID: 00075197-200401000-00011.
100. Maddocks ODK, Athineos D, Cheung EC, Lee P, Zhang T, van den Broek NJF, et al. Modulating the therapeutic response of tumours to dietary serine and glycine starvation. Nature. 2017;544(7650):372-6. Epub 2017/04/21. doi: 10.1038/nature22056. PubMed PMID: 28425994.
101. Martuscello RT, Vedam-Mai V, McCarthy DJ, Schmoll ME, Jundi MA, Louviere CD, et al. A Supplemented High-Fat Low-Carbohydrate Diet for the Treatment of Glioblastoma. Clinical Cancer Research. 2016;22(10):2482-95. doi: 10.1158/1078-0432.ccr-15-0916.
102. Xia S, Lin R, Jin L, Zhao L, Kang HB, Pan Y, et al. Prevention of Dietary-Fat-Fueled Ketogenesis Attenuates BRAF V600E Tumor Growth. Cell metabolism. 2017;25(2):358-73. doi: 10.1016/j.cmet.2016.12.010. PubMed PMID: 28089569; PubMed Central PMCID: PMC5299059.
103. Kanarek N, Keys HR, Cantor JR, Lewis CA, Chan SH, Kunchok T, et al. Histidine catabolism is a major determinant of methotrexate sensitivity. Nature. 2018;559(7715):632-6. doi: 10.1038/s41586-018-0316-7.
104. Hopkins BD, Pauli C, Du X, Wang DG, Li X, Wu D, et al. Suppression of insulin feedback enhances the efficacy of PI3K inhibitors. Nature. 2018;560(7719):499-503. doi: 10.1038/s41586-018-0343-4.
105. Hensley Christopher T, Faubert B, Yuan Q, Lev-Cohain N, Jin E, Kim J, et al. Metabolic Heterogeneity in Human Lung Tumors. Cell. 2016;164(4):681-94. doi: http://dx.doi.org/10.1016/j.cell.2015.12.034.
106. Eales KL, Hollinshead KER, Tennant DA. Hypoxia and metabolic adaptation of cancer cells. Oncogenesis. 2016;5:e190. doi: 10.1038/oncsis.2015.50.
107. Yoo CB, Jones PA. Epigenetic therapy of cancer: past, present and future. Nature Reviews Drug Discovery. 2006;5:37. doi: 10.1038/nrd1930.
108. Li S, Shen L, Chen KN. Association between H3K4 methylation and cancer prognosis: A meta-analysis. Thoracic cancer. 2018;9(7):794-9. Epub 2018/05/09. doi: 10.1111/1759-7714.12647. PubMed PMID: 29737623; PubMed Central PMCID: PMCPMC6026618.
109. Lewis R, Li YD, Hoffman L, Hashizume R, Gravohac G, Rice G, et al. Global Reduction of H3K4me3 Improves Chemotherapeutic Efficacy for Pediatric Ependymomas. Neoplasia. 2019;21(6):505-15. doi: https://doi.org/10.1016/j.neo.2019.03.012.
110. Vatrinet R, Leone G, De Luise M, Girolimetti G, Vidone M, Gasparre G, et al. The α-ketoglutarate dehydrogenase complex in cancer metabolic plasticity. Cancer & metabolism. 2017;5(1):3. doi: 10.1186/s40170-017-0165-0.
111. Nazarian R, Shi H, Wang Q, Kong X, Koya RC, Lee H, et al. Melanomas acquire resistance to B-RAF(V600E) inhibition by RTK or N-RAS upregulation. Nature. 2010;468:973. doi: 10.1038/nature09626 https://www.nature.com/articles/nature09626#supplementary-information.
112. Carugo A, Genovese G, Seth S, Nezi L, Rose Johnathon L, Bossi D, et al. In Vivo Functional Platform Targeting Patient-Derived Xenografts Identifies WDR5-Myc Association as a Critical Determinant of Pancreatic Cancer. Cell reports. 2016;16(1):133-47. doi: http://dx.doi.org/10.1016/j.celrep.2016.05.063.
113. Liu X, Sadhukhan S, Sun S, Wagner GR, Hirschey MD, Qi L, et al. High-Resolution Metabolomics with Acyl-CoA Profiling Reveals Widespread Remodeling in Response to Diet. Molecular & cellular proteomics : MCP. 2015;14(6):1489-500. Epub 2015/03/22. doi: 10.1074/mcp.M114.044859. PubMed PMID: 25795660; PubMed Central PMCID: PMCPMC4458715.

Acknowledgments

We thank members of the Kong laboratory for helpful comments on the manuscript. This work was supported by National Institutes of Health (NIH)/R01CA183989 to MK, Chao Family Comprehensive Cancer Center Pilot Award, Cancer Center Support Grant P30-CA062203 (to University of California, Irvine), and the American Cancer Society Research Scholar (RSG-16-085-01-TBE). The research reported in this publication was also supported by the National Cancer Institute of the National Institutes of Health under Award Number T32CA009054. The content is solely the responsibility of the authors and does not necessarily represent the official views of the National Institutes of Health.

Author contributions

M.B.G performed most of the experiments, analyzed the data, prepared figures, and wrote the manuscript. Y.Y. assisted in xenograft and PDX animal experiments. H.L. performed bioinformatic analysis for RNA-seq and ChIP-seq samples. P.S. and D.E.S. assisted with the ChIP-seq experiment. E.A.H., and X.H.L. helped with IHC and metabolomics analysis. T.Q.T. assisted with viability testing *in vitro* and hypoxia system. L.Z assisted with the statistical analysis. L.D and X.X. provided IHC scoring analysis. D.A.F assisted in the experimental design and manuscript writing. M.K. conceived and designed experiments and contributed manuscript writing.

Competing interests

The authors declare no competing interests.

Supplementary Information

Dietary glutamine supplementation suppresses epigenetically-activated oncogenic pathways to inhibit melanoma tumour growth

Ishak Gabra et al.

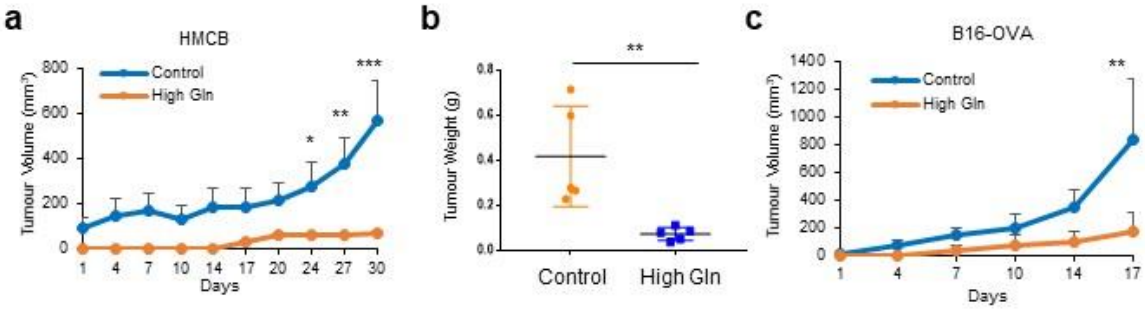

Supplementary Figure 1. a. Nude mice with subcutaneous injection of HMCB cells received control or high glutamine (High Gln) diet one-week post injection. Tumours were measured twice weekly (Control, n=5; High Gln, n=5). **b.** HMCB xenograft tumour weights post-mortem. **c.** B16 cells were injected subcutaneously in C57BL/6 mice and randomly placed on control or high glutamine (High Gln) diet post injection. Tumours were measured twice weekly (Control, n=6; High Gln, n=6).

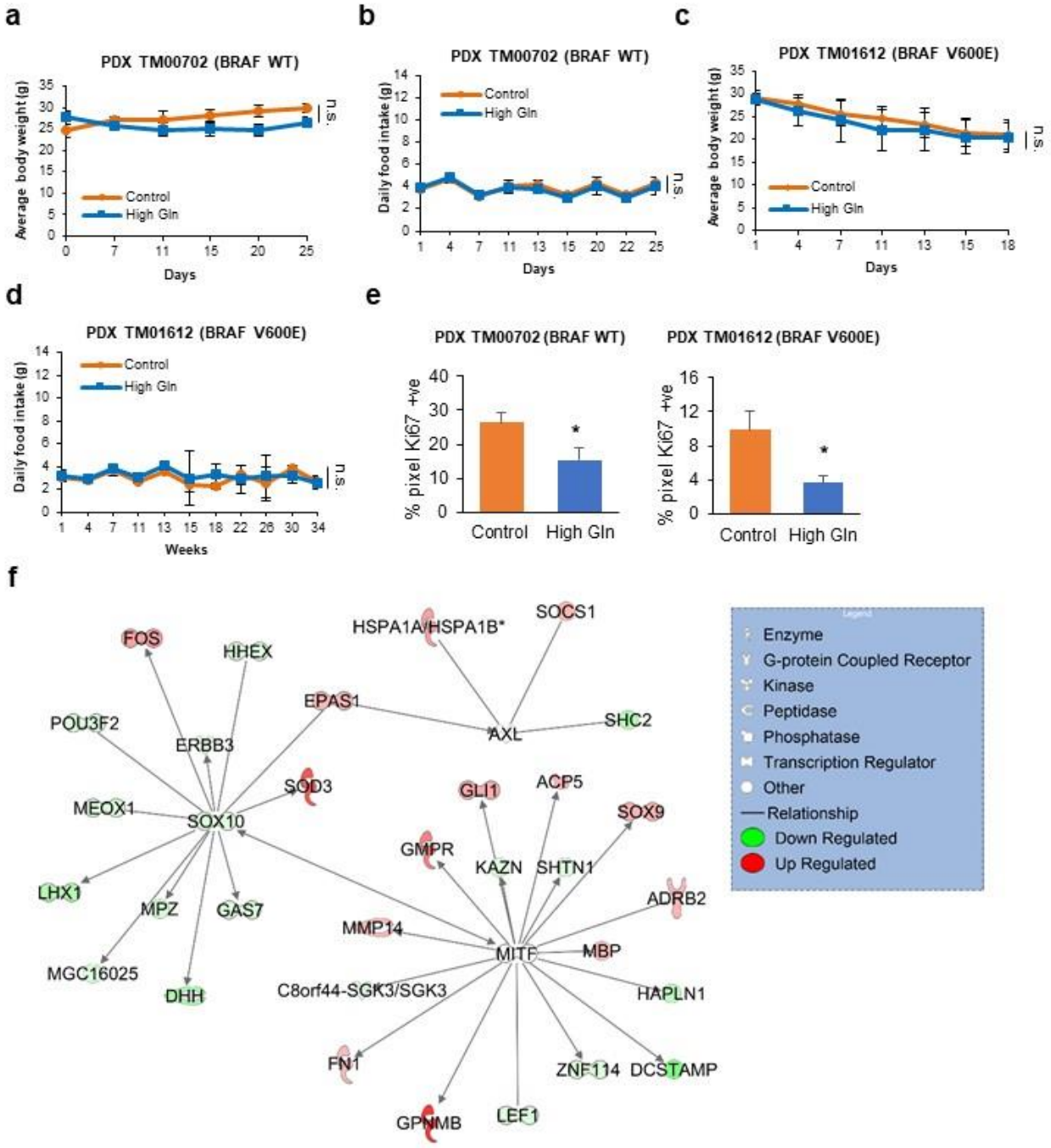
a
PDX TM00702 (BRAF WT)
Average body weight (g)
Days
Control
High Gln
n.s.
b
PDX TM00702 (BRAF WT)
Daily food intake (g)
Days
Control
High Gln
n.s.
c
PDX TM01612 (BRAF V600E)
Average body weight (g)
Days
Control
High Gln
n.s.
d
PDX TM01612 (BRAF V600E)
Daily food intake (g)
Weeks
Control
High Gln
n.s.
e
PDX TM00702 (BRAF WT)
% pixel Ki67 +ve
Control
High Gln
PDX TM01612 (BRAF V600E)
% pixel Ki67 +ve
Control
High Gln
f
FOS
HHEX
HSPA1A/HSPA1B*
SOCS1
EPAS1
POU3F2
AXL
SHC2
ERBB3
SOD3
GLI1
ACP5
MEOX1
SOX10
SOX9
GMPR
KAZN
SHTN1
LHX1
ADRB2
MPZ
GAS7
MMP14
MITF
MBP
MGC16025
DHH
C8orf44-SGK3/SGK3
HAPLN1
FN1
ZNF114
DCSTAMP
GPNMB
LEF1
Enzyme
G-protein Coupled Receptor
Kinase
Peptidase
Phosphatase
Transcription Regulator
Other
Relationship
Down Regulated
Up Regulated

Supplementary Figure 2. a, b. Body weight (**a**) and food intake (**b**) of NSG mice with PDX TM00702 tumours (Control, n=10; High Gln, n=9). **c, d**. Body weight (**c**) and food intake (**d**) of NSG mice with PDX TM01612 tumours (Control, n=8; High Gln, n=8). **e**. Ki67 microscope images of PDX TM00702 and PDX TM01612 tumours were quantified using Image Pro Plus software. % total area of pixels selected by threshold for the Ki67 stain was calculated using Image Pro's Count/Size tool. **f.** Downstream signalling network of SOX10, AXL and MITF. established using Ingenuity Pathway Analysis (IPA)'s Grow tool with Ingenuity Knowledge Base. 31 downstream genes of these three seed genes are significantly changed between control and high glutamine diet groups. Data represent means. Error bars are s.d. *P* value calculated by t-test (unpaired, two-tailed). **p*<0.05, n.s. not significant..

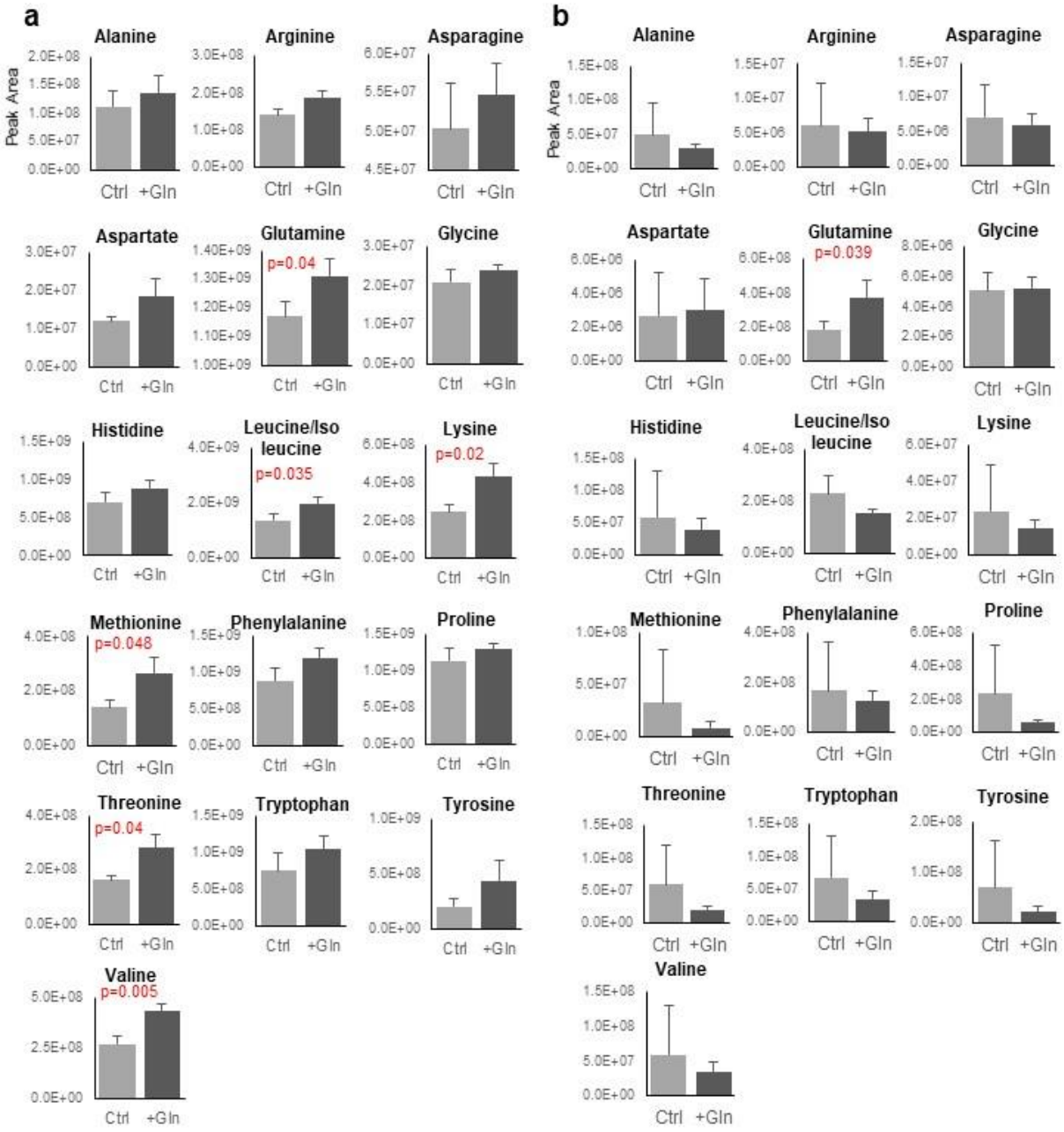

Supplementary Figure 3. NSG mice subcutaneously engrafted with PDX_TM00702 (**a**) or nude mice with M229 xenograft tumours (**b**) were placed on control (Ctrl) or glutamine supplemented (+Gln) diet and blood was collected with cardiac puncture at the end of the study. Serum was analyzed by LC-MS for relative levels of metabolites (presented as peak area on Y-axis). Error bars are s.d. *P* value calculated by t-test (unpaired, two-tailed). Only *P* value < 0.05 are indicated.

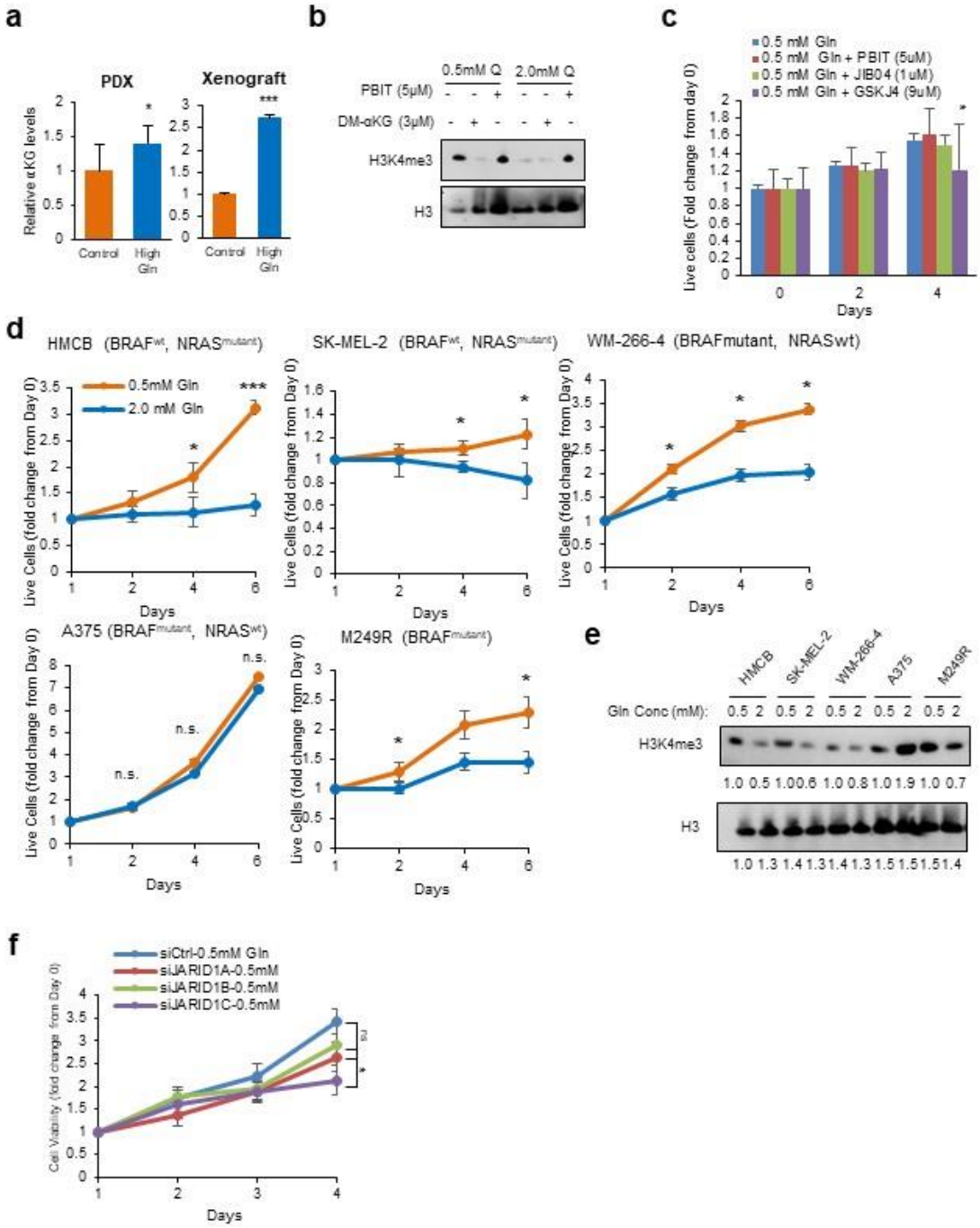
a
PDX
Xenograft
Relative αKG levels
Control
High Gln
b
0.5mM Q
2.0mM Q
PBIT (5μM)
DM-αKG (3μM)
H3K4me3
H3
c
0.5 mM Gln
0.5 mM Gln + PBIT (5uM)
0.5 mM Gln + JIB04 (1uM)
0.5 mM Gln + GSKJ4 (9uM)
Live cells (Fold change from day 0)
Days
d
HMCB (BRAFwt, NRASmutant)
SK-MEL-2 (BRAFwt, NRASmutant)
WM-266-4 (BRAFmutant, NRASwt)
0.5mM Gln
2.0 mM Gln
Live Cells (fold change from Day 0)
Days
A375 (BRAFmutant, NRASwt)
M249R (BRAFmutant)
n.s.
e
HMCB
SK-MEL-2
WM-266-4
A375
M249R
Gln Conc (mM):
0.5 2 0.5 2 0.5 2 0.5 2 0.5 2
H3K4me3
1.0 0.5 1.0 0.6 1.0 0.8 1.0 1.9 1.0 0.7
H3
1.0 1.3 1.4 1.3 1.4 1.3 1.5 1.5 1.5 1.4
f
siCtrl-0.5mM Gln
siJARID1A-0.5mM
siJARID1B-0.5mM
siJARID1C-0.5mM
Cell Viability (fold change from Day 0)
Days

Supplementary Figure 4. a. α-ketoglutarate levels were measured in PDX TM00702 and M229 xenograft tumours using EIA kit. (n=3, biological replicates) **b.** M229 cells culture in 6 cm dish. After 24 hours, medium was changed to either medium containing 0.5mM or 2.0mM glutamine with DMSO, PBIT (H3K4me3 demethylase inhibitor), or dimethyl-αKG. Medium was changed daily for 4 days. Cell lysate was used for histone extraction and immunoblotting with the indicated antibodies. **c.** M229 cells cultured overnight in medium containing 0.5mM glutamine under 1% hypoxia. Medium was changed after 24 hours to 0.5mM glutamine medium with DMSO, PBIT (5μM), JIB04 (1μM) or GSKJ4 (9μM), with medium changed daily. Cell viability was assessed by CellTiter Glo assay. (n=3, independent cell cultures). **d.** HMCB, SK-MEL-2, WM-266-4, A375, and M249R cells were seeded in medium with 0.5mM glutamine overnight. Medium was changed daily and cultured under 0.5mM or 2.0mM glutamine and live cells were counted at indicated time points (n=3, independent cell cultures). **g.** HMCB, SK-MEL-2, WM-266-4, A375, and M249R cells were seeded in 6cm dish as in **d-f**. Medium was changed daily for 4 days, and cell lysate was used for histone extraction and immunoblotting with the indicated antibodies. **f.** M229 cells were transfected with siRNA against control, JARID1A, JARID1B or JARID1C and seeded in medium with 0.5mM glutamine overnight. Medium was changed daily and cultured under 0.5mM glutamine. Live cell number was assessed using Trypan blue exclusion (n=3, independent cell cultures). Data represents means. Error bars are s.d. *P* value calculated by t-test (unpaired, two-tailed). $*p<0.05$, $***p<0.001$, n.s. not significant.

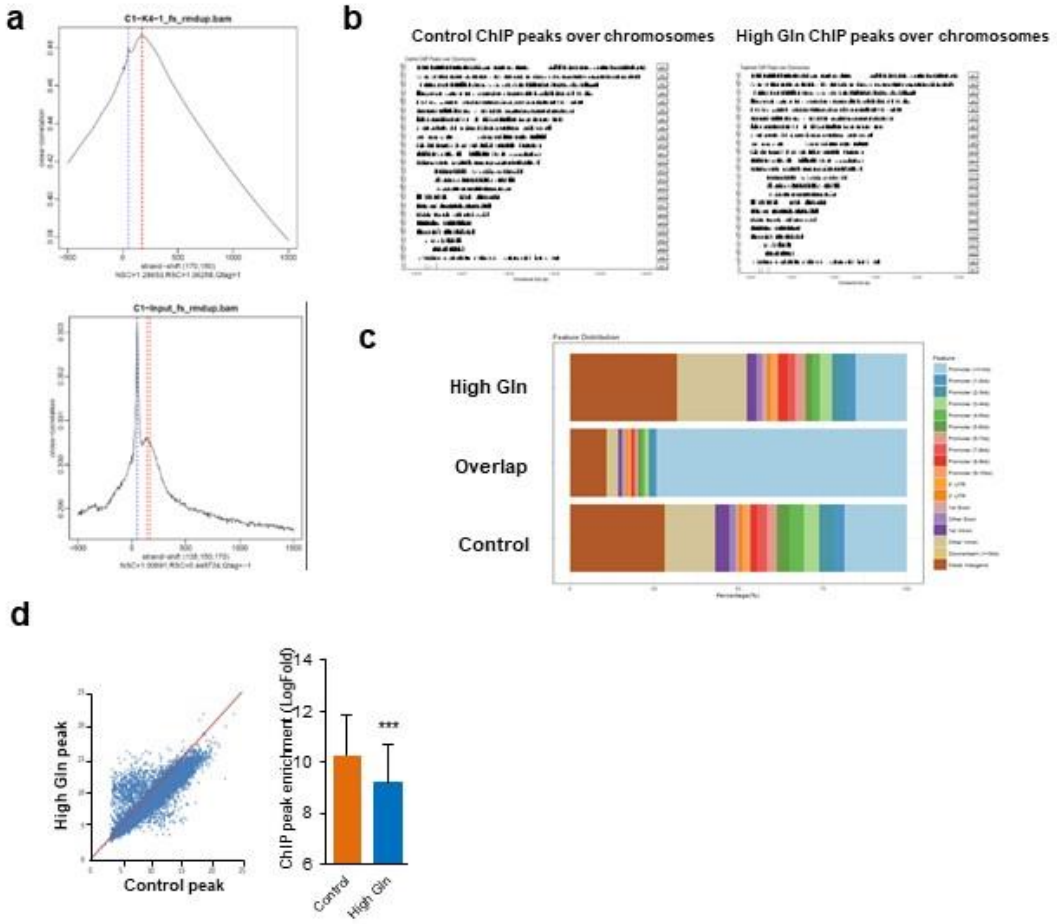

Supplementary Figure 5. a. Cross-correlation of ChIP-seq reads in sample versus sample input. One control sample and control sample input are shown as an example. **b.** ChIP-seq peaks distribution of chromosomes from control and glutamine supplemented (High Gln) samples. **c.** ChIP peaks annotation and closet genomic feature distribution in High Gln and control samples. **d.** PDX_TM00702 tumours were used for ChIP-sequencing analysis using H3K4me3 antibody. ChIP peaks of associated genes (LogFC between ChIP and Input) in control and High Gln tumour samples are represented as an average in each group (n=3, biological replicates per group performed in technical duplicates).

Figure 6a

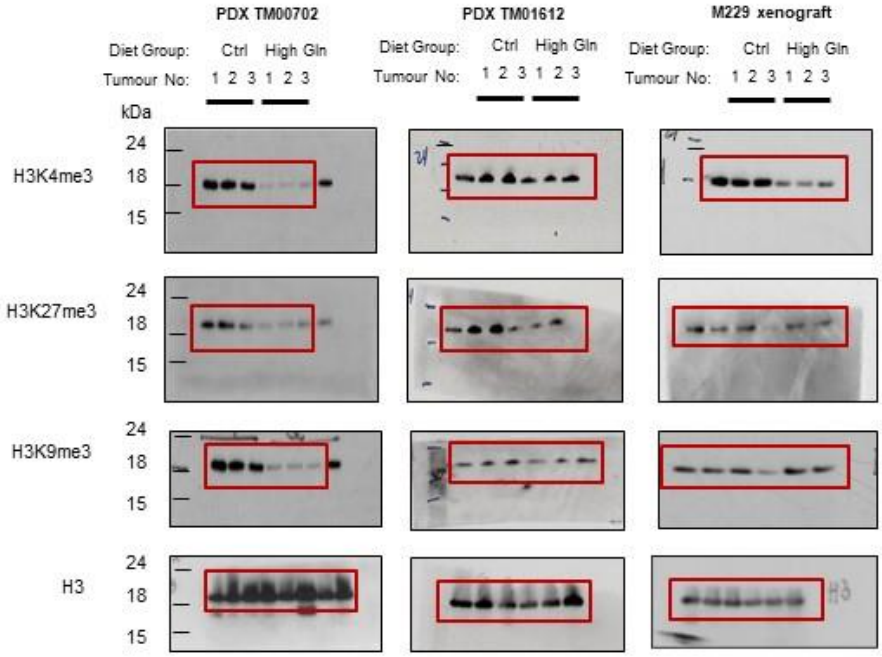

Figure 6d

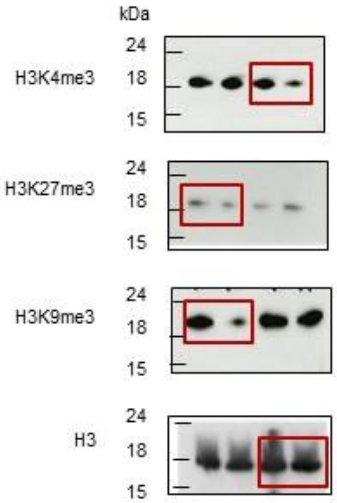

Figure 6i

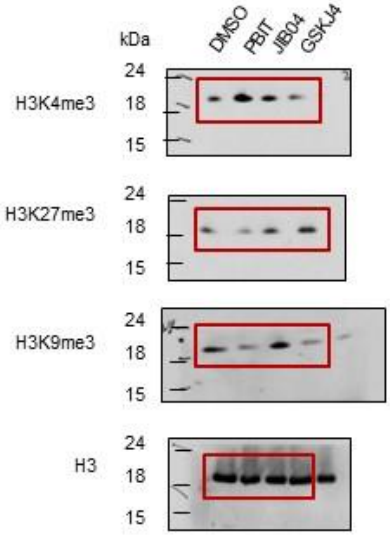

Figure 6l

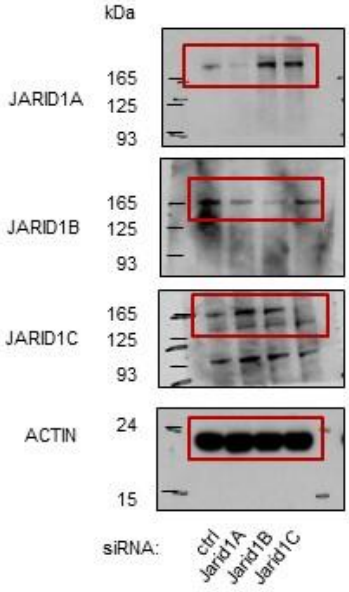

Figure 6m

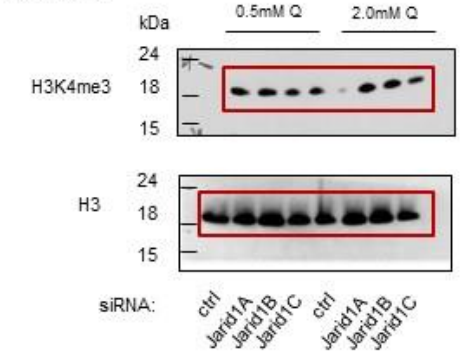

Supplemental Figures

Supplementary Figure 4b

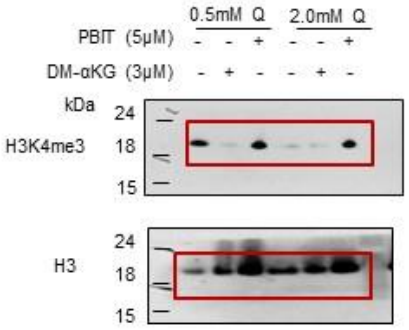

Supplementary Figure 4e

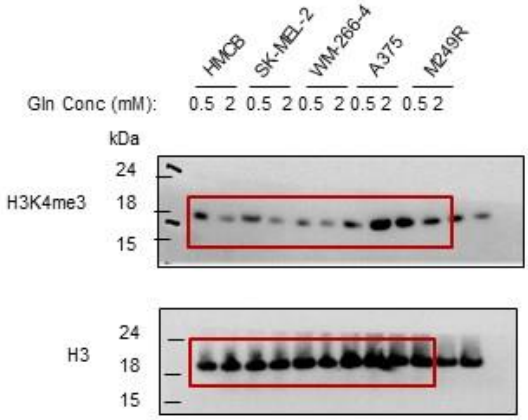

Supplementary Data 1: Diets formulated for the study of glutamine supplementation in vivo, Related to Figure 1 and 2

Diets were formulated by Research Diets, Inc

OpenStandard Diet with 15 kcal% Fat with Crystalline Amino Acids

	Control (A11112201)	High glutamine	Amino Acids
Ingredient	gm	gm	gm
L-Cystine	4.2	4.2	8.9
L-Isoleucine	7.6	7.6	16.1
L-Leucine	15.8	15.8	33.5
L-Lysine	13.2	13.2	28.0
L-Methionine	5.1	5.1	10.8
L-Phenyalanine	8.4	8.4	17.8
L-Threonine	7.2	7.2	15.2
L-Tryptophan	2.1	2.1	4.4
L-Valine	9.3	9.3	19.7
L-Histadine	4.6	4.6	9.7
L-Alanine	5.1	5.1	10.8
L-Arginine	6.0	6.0	12.7
L-Aspartic Acid	12.1	12.1	25.6
L-Glutamine	0.0	200.0	0.0
L-Glutamine Acid	38.2	38.2	80.9
Glycine	3.0	3.0	6.4
L-Proline	17.8	17.8	37.7
L-Serine	10.0	10.0	21.2
L-Tyrosine	9.2	9.2	19.5
Total Amino Acids	178.9	378.9	378.9
Corn Starch	381.0	181.0	181.0
Maltodextrin 10	110.0	110.0	110.0
Dextrose	150.0	150.0	150.0
Cellulose, BW200	75.0	75.0	75.0
Inulin	25.0	25.0	25.0
Soybean Oil	70.0	70.0	70.0
Mineral Mix	10.0	10.0	10.0
DiCalcium Phophate	13.0	13.0	13.0
Calcium Carbonate	5.5	5.5	5.5
Potassium Citrate, 1 H	16.5	16.5	16.5
Vitamin Mix	10.0	10.0	10.0
Choline Bitartrate	2.0	2.0	2.0
Total	1046.95	1046.95	1046.95
kcal%			
Protein	18.0	38.0	38.0
Carbohydrate	66.0	46.0	46.0
Fat	16.0	16.0	16.0
Total	100.0	100.0	100.0

Supplementary Data 2: Differentially expressed genes in PDX_TM00702 tumours from control (Ctrl) or glutamine supplementation (High Gln), related to Figure 4

Gene Symbol	p-value	FDR (qvalue)	Mean(Ctrl)	Mean(High Gln)	MeanRatio(Gln vs. Ctrl)	FoldChange(Gln vs. Ctrl)
GFRA3	1.83E-05	0.0222501	0.232438	0.0579125	0.249152	-4.01361
DNAJA4	2.14E-05	0.0222501	2.10343	3.2138	1.52788	1.52788
MGST1	2.60E-05	0.0222501	12.1545	18.7064	1.53904	1.53904
TSPEAR-AS1	2.65E-05	0.0222501	0.423138	0.0440838	0.104183	-9.59851
MEOX1	2.68E-05	0.0222501	4.93024	2.24846	0.456055	-2.19272
HAPLN4	3.15E-05	0.0222501	0.925551	0.285074	0.308005	-3.2467
RNF208	3.19E-05	0.0222501	10.1796	6.20207	0.609264	-1.64133
DIRC3-AS1	3.26E-05	0.0222501	1.27178	0.706899	0.555835	-1.7991
RPARP-AS1	3.26E-05	0.0222501	2.67323	1.61523	0.604225	-1.65501
LOC102724604	4.56E-05	0.0251528	1.15169	0.128994	0.112004	-8.92827
FABP7	5.56E-05	0.0251528	5.15805	2.2111	0.428671	-2.33279
CDCA7L	7.36E-05	0.0251528	2.08318	0.345495	0.16585	-6.02956
FZD8	8.29E-05	0.0252582	0.539436	0.0719989	0.133471	-7.49228
WFDC2	9.19E-05	0.0253185	1.43632	0.510584	0.355481	-2.81309
LOC100129291	9.43E-05	0.0253185	2.25968	0.230171	0.10186	-9.81738
TNFSF10	0.000102025	0.0255573	1.23308	0.624405	0.50638	-1.9748
LOC100507351	0.000114815	0.0269636	0.500387	0.155014	0.309789	-3.22801
SERPINA1	0.000128712	0.0272266	1.06268	0.265636	0.249967	-4.00052
IMMP2L	0.000134808	0.0272266	2.58641	1.7236	0.666408	-1.50058
LOC102723345	0.00015543	0.0272266	0.902285	1.81932	2.01634	2.01634
SCARF1	0.000156653	0.0272266	1.05323	0.301144	0.285926	-3.49741
MSR1	0.000170014	0.0272266	1.00496	0.191848	0.190902	-5.2383
ADAMTS8	0.000171322	0.0272266	1.52372	0.737504	0.484016	-2.06605
CCL26	0.000183389	0.0272266	0.279423	1.30464	4.66903	4.66903
MALL	0.000188646	0.0272266	6.20114	15.3702	2.4786	2.4786
ALDH2	0.000194055	0.0272266	0.718501	0.178253	0.24809	-4.0308
HILS1	0.000197228	0.0272266	5.27192	2.87013	0.544419	-1.83682
COL6A3	0.000197659	0.0272266	6.97772	1.62454	0.232818	-4.29519
OCA2	0.000202319	0.0272266	0.197742	0.0273016	0.138067	-7.24286
BRINP2	0.000202886	0.0272266	7.08021	3.8654	0.545944	-1.83169
ZNF788	0.000228839	0.0277151	0.684683	1.46153	2.13461	2.13461
MDGA2	0.000253838	0.0285205	0.302796	0.820061	2.7083	2.7083
FAM69B	0.000254275	0.0285205	1.66555	0.733684	0.440506	-2.27012
NRROS	0.000283509	0.0287223	0.506628	1.1785	2.32617	2.32617
TRIM7	0.000299984	0.0287223	0.37351	0.692231	1.85331	1.85331
CADM1	0.000323025	0.0292011	6.69487	4.02185	0.600736	-1.66463
LOC728392	0.000342459	0.0296588	2.27416	1.22107	0.536935	-1.86242
TPPP3	0.000365463	0.0296588	5.32832	12.1142	2.27355	2.27355
VAX1	0.000366166	0.0296588	1.61499	0.88706	0.549268	-1.8206
TIE1	0.000386174	0.0296588	1.14768	0.345847	0.301345	-3.31845
APCDD1L	0.000388848	0.0296588	1.836	2.81114	1.53113	1.53113
LIMCH1	0.000410579	0.0296588	1.68601	0.627412	0.372128	-2.68725
VAT1L	0.000412134	0.0296588	22.6993	6.92008	0.304858	-3.28021
XAGE5	0.000422201	0.0296588	0.446117	0.0310193	0.0695318	-14.3819
IRF5	0.000423221	0.0296588	1.29829	0.695151	0.535436	-1.86764
WNT9A	0.000424357	0.0296588	0.3993	1.10404	2.76493	2.76493
FAM167B	0.000433675	0.0296588	4.5479	7.03707	1.54732	1.54732
MCAM	0.000446979	0.0296588	188.946	118.693	0.628185	-1.59189
TRPM8	0.000447707	0.0296588	0.841966	0.288283	0.342392	-2.92063
MATN2	0.000454103	0.0296588	9.69607	3.86321	0.39843	-2.50985
KIF25-AS1	0.000454903	0.0296588	0.958831	0.313476	0.326935	-3.05871
FAM198B	0.000455045	0.0296588	3.93352	1.4541	0.369669	-2.70512
SERPINA5	0.000461753	0.0296588	6.489	2.50929	0.3867	-2.58599
DUSP4	0.000467335	0.0297629	8.05588	17.0956	2.12212	2.12212
HAPLN1	0.00048279	0.029924	0.37356	0.0913876	0.24464	-4.08764
DLK2	0.000485792	0.029924	1.49332	0.936398	0.627058	-1.59475
LINC02154	0.000494206	0.0300855	8.207	22.8223	2.78084	2.78084
TBXAS1	0.000497898	0.0300855	1.50323	0.809226	0.538323	-1.85762
ZNF114	0.00050376	0.0300855	1.42422	0.893528	0.627379	-1.59393
ANKH	0.000521466	0.0300855	4.65825	7.65233	1.64275	1.64275
TUBB4A	0.000524738	0.0300855	1.7753	0.547603	0.308456	-3.24195
CDH15	0.000528448	0.0300855	1.89162	0.378794	0.200248	-4.9938
DNAH9	0.000546652	0.0304303	1.22015	0.606321	0.496925	-2.01238
ADAM23	0.000557465	0.0305055	0.634006	0.2076	0.327441	-3.05398
PRTFDC1	0.000566777	0.0305055	5.60677	3.61288	0.644377	-1.55189
AIF1L	0.00057464	0.0305055	6.93979	4.26918	0.615173	-1.62556
FGFBP2	0.00061581	0.0310404	1.13714	0.519968	0.457259	-2.18694
PNMT	0.000617319	0.0310404	0.442682	0.266822	0.602739	-1.65909
RBM47	0.000624565	0.0310404	0.874303	0.444532	0.508442	-1.96679
AKR1C2	0.000638161	0.0310404	0.318699	0.971329	3.04779	3.04779
LINC01160	0.000644574	0.0310404	0.441638	0.231043	0.52315	-1.9115
NMNAT2	0.000644876	0.0310404	0.54901	1.02808	1.87261	1.87261
DHH	0.000647204	0.0310404	0.292899	0.0537176	0.1834	-5.45256
LOC105369486	0.000685025	0.0312223	1.36941	0.507239	0.370406	-2.69974
ARHGAP27	0.000693152	0.0312223	0.793738	0.422813	0.532685	-1.87728
FAM213A	0.000695637	0.0312223	9.76596	6.43716	0.659142	-1.51712
LOC101928069	0.000722634	0.0312223	0.59963	1.04407	1.74119	1.74119
FEV	0.000772711	0.0321301	1.69136	0.840984	0.497224	-2.01117
KLHL4	0.000777521	0.0321301	0.926132	0.381927	0.41239	-2.42489
ZNF28	0.000780068	0.0321301	0.54515	0.317357	0.582145	-1.71778

ADORA3	0.000780111	0.0321301	0.673659	0.350898	0.520884	-1.91981
SLC5A8	0.00078471	0.0321301	0.370779	0.195853	0.528222	-1.89314
FGFR4	0.000786775	0.0321301	5.17423	3.28106	0.634116	-1.577
NRXN3	0.000787274	0.0321301	2.75038	1.31074	0.476567	-2.09834
ANPEP	0.000802716	0.0324323	261.84	398.703	1.5227	1.5227
COL11A1	0.000835623	0.0325332	69.3796	44.5703	0.642413	-1.55663
AGK	0.000845485	0.0325332	20.8231	11.3982	0.547383	-1.82688
MIR31HG	0.000845979	0.0325332	0.416106	0.923721	2.21992	2.21992
IL7R	0.000846597	0.0325332	2.59609	1.27801	0.492283	-2.03135
LOC729732	0.000859375	0.0325332	0.408092	0.251356	0.61593	-1.62356
IQCA1	0.000865011	0.0325332	2.35985	0.725319	0.307358	-3.25354
FAM46C	0.000873407	0.0326277	3.62014	2.20095	0.607974	-1.64481
NBL1	0.000877536	0.0326277	12.1037	19.1818	1.58479	1.58479
OLFML2A	0.000884711	0.0326277	12.2919	7.74854	0.630377	-1.58635
RUNX1T1	0.000885702	0.0326277	2.1034	1.22807	0.583853	-1.71276
DNAH2	0.000902895	0.0329381	0.459135	0.194236	0.423047	-2.36381
HOGA1	0.000934117	0.0335919	0.412985	0.124696	0.301937	-3.31194
MCF2L2	0.000962639	0.0339269	0.306824	0.583026	1.9002	1.9002
MYRF	0.000977487	0.0339269	5.67629	2.91321	0.513224	-1.94847
NEFH	0.00101499	0.0339269	3.30617	1.00413	0.303713	-3.29258
GNG11	0.00103098	0.0339269	9.31952	16.0022	1.71706	1.71706
RAB27B	0.00103629	0.0339269	0.680903	1.23424	1.81265	1.81265
LOC101927482	0.00104411	0.0339269	2.18645	1.38093	0.631587	-1.58331
METRN	0.00106018	0.0339269	6.0215	3.87788	0.644005	-1.55278
VASN	0.00106907	0.0339269	5.32453	9.20722	1.72921	1.72921
LRP1	0.00107567	0.0339269	9.3875	16.4138	1.74847	1.74847
IL10RA	0.00109368	0.0339269	0.549584	0.211863	0.385498	-2.59405
VWA1	0.00109534	0.0339269	3.30846	2.0568	0.62168	-1.60855
SLC38A3	0.00110211	0.0339269	1.09086	0.513737	0.470947	-2.12338
KCNC3	0.00111111	0.0339269	0.208095	0.0304268	0.146215	-6.83922
KCTD12	0.00112774	0.0339269	0.742643	1.15504	1.5553	1.5553
HAS3	0.00116035	0.0339269	5.7097	2.95529	0.517592	-1.93202
ADGRL3	0.00119375	0.0339269	0.489679	0.232567	0.474937	-2.10554
ABCB4	0.0011998	0.0339269	1.85941	0.974892	0.524301	-1.9073
LOC283683	0.00121604	0.0339269	4.652	2.7196	0.584607	-1.71055
ROR1	0.00121893	0.0339269	0.949029	1.63082	1.71841	1.71841
GPNMB	0.00124144	0.0342312	1.03638	4.86468	4.69393	4.69393
TPBG	0.00125819	0.0343679	13.0307	24.9925	1.91797	1.91797
ZNF385D	0.00126568	0.0343679	0.417924	0.727877	1.74165	1.74165
SOX10	0.00126824	0.0343679	114.211	70.372	0.616159	-1.62296
NOX4	0.00127727	0.0343679	0.242251	0.511915	2.11316	2.11316
ITGAX	0.00128958	0.0343679	2.49619	0.62352	0.249788	-4.00339
CTSB	0.00129034	0.0343679	202.853	337.8	1.66525	1.66525
LIMS2	0.0012988	0.0343679	1.53868	4.15654	2.70136	2.70136
TFF2	0.0013081	0.0344552	0.234571	0.0104641	0.0446094	-22.4168
LHX1	0.00131594	0.0344552	0.719119	0.149161	0.207422	-4.82109
CBSL	0.00133628	0.0344552	2.66398	4.16274	1.5626	1.5626
GATM	0.00133878	0.0344552	3.78535	2.02736	0.53558	-1.86714
PLEKHG1	0.00134706	0.03455	3.91687	2.13207	0.54433	-1.83712
GPR89B	0.00136802	0.0346859	3.37948	2.1987	0.650602	-1.53704
FAP	0.00139611	0.0350895	8.52899	13.366	1.56713	1.56713
TGFB3	0.00143989	0.035439	40.6014	23.1837	0.571008	-1.75129
TNK1	0.00144545	0.035439	0.466716	0.21052	0.451067	-2.21696
LINC01812	0.00146504	0.035439	0.105633	0.33871	3.20649	3.20649
TRIM2	0.00147625	0.035439	9.94892	6.03181	0.606278	-1.64941
MAGEE1	0.00152506	0.0359717	0.499972	0.0954426	0.190896	-5.23846
GPX3	0.00153173	0.0359717	9.69398	4.68282	0.483064	-2.07012
PCDH7	0.00157749	0.0360137	0.271994	0.811333	2.98291	2.98291
ABAT	0.00161978	0.0360137	0.414298	0.216427	0.522395	-1.91426
AKR1C3	0.00164369	0.0362238	9.87702	18.5702	1.88014	1.88014
ZNF560	0.0016538	0.0363401	0.18916	0.51419	2.71828	2.71828
LOC105369971	0.00168055	0.0365944	0.158518	0.0323033	0.203783	-4.90718
VEGFC	0.00169609	0.0365944	19.8132	32.6624	1.64852	1.64852
ITGA1	0.00169724	0.0365944	0.69278	1.29917	1.8753	1.8753
PRRX1	0.00173509	0.0368339	15.6152	34.5357	2.21167	2.21167
ENC1	0.00174288	0.0368547	17.9732	10.7981	0.600789	-1.66448
B4GALNT2	0.00176051	0.0368547	0.83006	0.203143	0.244733	-4.08608
C2orf70	0.00176829	0.0368547	0.215478	0.661343	3.06918	3.06918
TMEM178A	0.00176948	0.0368547	0.935283	0.321116	0.343335	-2.91261
HAS2	0.00177964	0.0368547	1.17258	2.02423	1.72632	1.72632
FAM43A	0.00178236	0.0368547	2.58917	5.02423	1.94048	1.94048
ARL14	0.00180115	0.037084	0.898449	0.230897	0.256995	-3.89112
F11R	0.00182332	0.0372372	6.54052	3.9204	0.599401	-1.66833
SLC35F1	0.00185067	0.0376437	15.3817	9.74987	0.633862	-1.57763
TNFSF9	0.00187077	0.0376913	1.52062	2.36661	1.55634	1.55634
BCAN	0.00196565	0.0384818	1.71368	0.95403	0.556714	-1.79625
TMIGD3	0.00200305	0.0386269	2.06658	1.09738	0.531011	-1.8832
MAGED4B	0.00200415	0.0386269	1.16321	0.106044	0.091165	-10.9691
GBGT1	0.00205577	0.0387681	0.112941	0.0166183	0.147142	-6.79617
CPQ	0.00206949	0.0387681	7.82607	11.7721	1.50421	1.50421
MAP3K5	0.00207964	0.0387681	0.832535	1.52295	1.8293	1.8293
TRAF1	0.00208105	0.0387681	21.4997	12.6002	0.586063	-1.7063
GJA1	0.00209858	0.0388158	15.226	22.9673	1.50842	1.50842

SHC2	0.00212003	0.0388158	1.19787	0.2468	0.206032	-4.85361
CYP7A1	0.00212285	0.0388158	0.206003	0.718524	3.48793	3.48793
ABI3	0.00212286	0.0388158	1.15975	0.390876	0.337036	-2.96705
GGT8P	0.00214256	0.0388921	0.389178	0.132063	0.339338	-2.94692
PGM5	0.00216817	0.0389189	0.943169	0.596365	0.632299	-1.58153
PGF	0.00218428	0.0389272	1.29972	2.48524	1.91213	1.91213
ETHE1	0.00220473	0.0389272	11.9732	18.6955	1.56145	1.56145
TTC28	0.00220898	0.0389272	5.09127	8.31281	1.63276	1.63276
MAGED4	0.00224431	0.0389272	1.15162	0.105432	0.0915512	-10.9229
HHEX	0.00226935	0.0389272	37.8594	23.1849	0.612395	-1.63293
TGIF1	0.00227365	0.0389272	9.61249	14.4541	1.50368	1.50368
TRIML2	0.00227951	0.0389272	0.316008	0.0755005	0.238919	-4.18551
RGS2	0.00229705	0.0389272	1.79505	4.73189	2.63607	2.63607
PRRX2	0.0023066	0.0389272	3.94793	7.69195	1.94835	1.94835
COL6A2	0.00231749	0.0389272	526.17	805.155	1.53022	1.53022
PARD6B	0.0023402	0.0389272	0.530151	0.283448	0.534655	-1.87037
TSPEAR-AS2	0.0023488	0.0389272	0.263659	0.0131995	0.0500629	-19.9749
ASIC2	0.00236222	0.0389272	0.183764	0.0279249	0.151961	-6.58064
RASL11B	0.00236504	0.0389272	2.04662	1.32658	0.648179	-1.54278
FZD6	0.00236697	0.0389272	0.454979	0.990428	2.17687	2.17687
OR2W3	0.00241925	0.0391825	1.7666	0.966038	0.546834	-1.82871
AHR	0.002432	0.0392864	8.71756	13.4878	1.5472	1.5472
ABCG2	0.002449	0.0392864	0.552577	0.238951	0.43243	-2.31252
AQP3	0.00248119	0.0392871	0.543425	0.342426	0.630125	-1.58699
COL6A1	0.00250789	0.0392871	952.637	1523.13	1.59885	1.59885
TUBB2B	0.00253207	0.0392871	104.321	63.0843	0.604716	-1.65367
MB21D2	0.00256726	0.0392871	14.867	8.45268	0.568552	-1.75886
NEDD9	0.00261039	0.0392871	3.94844	2.26806	0.57442	-1.74089
FAM180A	0.00261884	0.0392871	1.08519	3.25419	2.99872	2.99872
LOC729080	0.00261887	0.0392871	1.46898	0.608948	0.414538	-2.41232
NUDT11	0.00262437	0.0392871	0.230457	0.0414848	0.180011	-5.55521
LYL1	0.00263139	0.0393139	0.600369	0.368504	0.613796	-1.62921
COLEC12	0.00267159	0.0393872	10.1513	18.729	1.84498	1.84498
MMP15	0.00269059	0.0393872	16.9195	7.99696	0.472647	-2.11575
FAS	0.00270235	0.0393872	0.851528	1.54933	1.81947	1.81947
P4HA3	0.00271216	0.0393872	2.40669	5.42409	2.25375	2.25375
NTSR1	0.00272932	0.0393886	5.69343	12.9932	2.28214	2.28214
GATA2-AS1	0.00274196	0.0393886	0.747141	0.426617	0.571	-1.75131
LPAR2	0.00276444	0.0393886	4.11989	2.59174	0.629081	-1.58962
PRSS12	0.00277247	0.0393886	0.617138	1.47032	2.38248	2.38248
HOXB13	0.00278486	0.0393886	1.06934	0.0981145	0.0917528	-10.8988
CYP2S1	0.00283572	0.0395023	0.73991	0.322585	0.435978	-2.29369
PCDH9	0.00285451	0.0395023	0.310966	0.486903	1.56577	1.56577
BAALC	0.00287723	0.0395023	1.49701	3.17348	2.11988	2.11988
ZNF536	0.00290145	0.0395023	2.78857	1.59294	0.57124	-1.75058
NDNF	0.00291655	0.0395023	0.43063	0.902399	2.09553	2.09553
LMO7	0.00292141	0.0395023	0.79639	2.20068	2.76331	2.76331
ICOSLG	0.00300277	0.0395023	3.15156	5.92249	1.87923	1.87923
NIPA1	0.00300753	0.0395023	8.42292	5.22698	0.620566	-1.61143
PCDH1	0.0030195	0.0395023	35.906	20.4492	0.56952	-1.75586
MEGF10	0.00302941	0.0395023	0.820028	1.52787	1.86319	1.86319
CPXM1	0.0030325	0.0395023	8.91481	1.52655	0.171238	-5.83983
SNORD80	0.00303569	0.0395023	3.2736	6.40487	1.95652	1.95652
DSC3	0.00306341	0.0395023	5.11654	1.21683	0.237823	-4.2048
GGT1	0.00307752	0.0395023	3.21107	1.2929	0.402639	-2.48361
FBLN5	0.00309263	0.0395023	10.2336	17.4327	1.70348	1.70348
CASKIN1	0.00310979	0.0395023	0.557719	0.295494	0.529827	-1.88741
PPP1R13B	0.00311924	0.0395023	1.25331	0.802354	0.640189	-1.56204
BMP4	0.0031636	0.0395023	0.812425	2.4154	2.97308	2.97308
CRTAC1	0.00316506	0.0395023	0.201155	0.121864	0.605822	-1.65065
EPAS1	0.00318643	0.0395023	7.10675	11.5845	1.63006	1.63006
PDE3B	0.00318659	0.0395023	0.278093	0.52749	1.89681	1.89681
LINC01238	0.00320681	0.0395023	0.8297	0.543115	0.654592	-1.52767
ZNF804A	0.00322743	0.0395023	0.504756	1.00172	1.98456	1.98456
LINC01033	0.00322921	0.0395023	20.2427	9.1127	0.450173	-2.22137
EMC10	0.00323717	0.0395023	16.3533	9.45853	0.578388	-1.72894
C16orf45	0.00326469	0.0395023	7.55694	12.7942	1.69304	1.69304
PAK3	0.00326508	0.0395023	0.526927	0.341073	0.647287	-1.54491
CCR10	0.00328559	0.0395023	0.809772	0.357102	0.440991	-2.26762
ATF7IP2	0.00332206	0.0395023	1.47895	0.836579	0.565656	-1.76786
CADPS	0.00332539	0.0395023	0.301569	0.848512	2.81366	2.81366
AMIGO2	0.00333196	0.0395023	7.27144	4.58594	0.630677	-1.5856
RETREG1	0.00334161	0.0395023	2.90626	4.68337	1.61148	1.61148
CT45A7	0.00334785	0.0395023	6.36881	2.47091	0.387971	-2.57751
SHTN1	0.00334788	0.0395023	10.8869	7.05602	0.648121	-1.54292
CCDC184	0.00343029	0.0397608	0.899193	1.40812	1.56598	1.56598
SSX4B	0.00343846	0.0397608	1.10673	0.113651	0.10269	-9.73801
LINC00312	0.00344222	0.0397608	0.915601	0.58486	0.638772	-1.5655
HTRA1	0.00345652	0.0397608	5.11554	19.5129	3.81443	3.81443
LINC00052	0.00348344	0.0397608	1.54491	0.464284	0.300525	-3.32751
SSX4	0.00348943	0.0397608	1.73894	0.179979	0.103499	-9.66194
PROSER2	0.00349064	0.0397608	0.196788	0.0251767	0.127938	-7.81629
GRHL1	0.00349303	0.0397608	1.37063	0.764987	0.55813	-1.7917

FBXO27	0.00349726	0.0397608	2.62067	1.73794	0.663167	-1.50792
BMP7	0.00355692	0.039907	2.18818	5.32464	2.43337	2.43337
FAM78B	0.00355791	0.039907	1.10242	0.56718	0.514487	-1.94368
MATN4	0.00357809	0.0400735	6.91378	3.70683	0.536152	-1.86514
LOC101059915	0.00362315	0.0403377	1.68907	0.183638	0.108722	-9.19779
RAB11FIP4	0.00365332	0.0406135	1.10153	0.718007	0.65183	-1.53414
RCAN1	0.00367665	0.0406922	51.2354	31.6107	0.616969	-1.62083
ZNF586	0.00368672	0.0407026	2.24493	1.35708	0.604507	-1.65424
SLC25A27	0.00370535	0.0407026	1.86072	3.03175	1.62935	1.62935
QPCT	0.0037366	0.0407555	3.64515	7.09866	1.94742	1.94742
CPA6	0.00378595	0.0409203	0.483533	0.228996	0.473589	-2.11153
ITGB3	0.00379931	0.0409203	1.67206	0.737922	0.441325	-2.2659
CCL3	0.00383981	0.0410472	1.44848	0.637798	0.440321	-2.27107
PREX1	0.00384566	0.0410476	7.2496	4.24979	0.586211	-1.70587
LINC00314	0.00385077	0.0410476	2.70622	1.51399	0.559448	-1.78747
C1QTNF2	0.00390606	0.0413937	0.316687	0.717422	2.2654	2.2654
GBAT2	0.00391255	0.0413937	3.0257	1.67311	0.552966	-1.80843
B4GALNT1	0.00392301	0.0413937	1.35416	2.41184	1.78106	1.78106
FLRT3	0.00394905	0.0413937	6.73502	4.47039	0.663753	-1.50658
ANK1	0.00395485	0.0413937	1.13274	2.34753	2.07244	2.07244
SEMA3B	0.0039778	0.0414209	42.3516	26.5258	0.626322	-1.59662
SLC2A3	0.00400154	0.0414209	0.286914	0.0688674	0.240028	-4.16618
ITGA10	0.00405182	0.0415787	1.9903	3.04881	1.53183	1.53183
DOCK10	0.00405215	0.0415787	4.81674	7.66774	1.59189	1.59189
GPR161	0.00410624	0.0418703	0.369332	0.612444	1.65824	1.65824
FOXF1	0.00420977	0.0422947	1.65153	0.806805	0.488519	-2.047
PAGE2B	0.00424734	0.0423112	10.3161	2.34072	0.226898	-4.40726
TIAM2	0.00424923	0.0423112	1.20769	0.738057	0.611133	-1.63631
ASPHD2	0.00426576	0.0423112	12.8771	21.8587	1.69749	1.69749
NGEF	0.00427697	0.0423112	4.39532	6.89943	1.56972	1.56972
GPR17	0.00429042	0.0423112	0.17092	0.472635	2.76525	2.76525
PDZRN3	0.00430229	0.0423112	0.764606	1.54135	2.01588	2.01588
UNC5B	0.00433011	0.0423112	2.05177	4.52119	2.20356	2.20356
TMX2-CTNND1	0.00434697	0.0423112	1.47616	0.919311	0.622772	-1.60573
PDE4D	0.00435274	0.0423112	0.622139	1.03863	1.66946	1.66946
CA12	0.00436098	0.0423112	7.99862	13.0314	1.62921	1.62921
SMOC1	0.00437917	0.0423112	0.626449	1.55324	2.47943	2.47943
FAR2P1	0.00439036	0.0423112	8.93383	5.33018	0.596629	-1.67608
SMIM3	0.00441391	0.0423112	3.3071	7.75732	2.34566	2.34566
MMP14	0.00442349	0.0423112	139.181	222.216	1.5966	1.5966
DUSP9	0.00442559	0.0423112	0.777484	0.37411	0.48118	-2.07822
ISM1	0.00446916	0.0423328	0.80402	1.24973	1.55435	1.55435
ZFP42	0.00447402	0.0423328	0.412399	0.0986915	0.239311	-4.17867
CLDN3	0.00457269	0.0427942	3.61942	2.04172	0.564103	-1.77273
TP63	0.00459579	0.0428503	0.617099	0.962864	1.56031	1.56031
SYT7	0.00462905	0.0430004	1.5239	3.09812	2.03302	2.03302
NUDT7	0.00468783	0.0430638	1.25208	0.519981	0.415293	-2.40794
ALG11	0.00472307	0.0430751	0.720248	0.449256	0.623752	-1.6032
ARHGAP40	0.00473664	0.0431346	0.611104	0.362955	0.593933	-1.68369
KCNH3	0.00475256	0.0431346	0.362333	0.696542	1.92238	1.92238
CSTB	0.00484771	0.0432314	50.8861	76.8369	1.50998	1.50998
CXADRP3	0.0048502	0.0432314	1.54845	2.9983	1.93632	1.93632
ELFN1	0.00491221	0.0432314	2.19524	4.56553	2.07974	2.07974
NTN4	0.00492179	0.0432314	0.604535	2.07714	3.43593	3.43593
FOXE1	0.00500795	0.0432463	1.2767	0.730566	0.572232	-1.74754
ZNF816	0.00501098	0.0432463	0.372069	0.0469367	0.126151	-7.92704
NQO1	0.00501666	0.0432463	33.8836	55.7725	1.64601	1.64601
PCDHA3	0.00507571	0.0433823	0.601087	0.971529	1.61629	1.61629
LOC105371703	0.00508003	0.0433823	1.56851	0.121478	0.077448	-12.9119
KRTAP5-1	0.00509367	0.0434222	0.892632	0.318397	0.356695	-2.80352
NKX2-5	0.00512908	0.0434559	0.781458	0.113824	0.145656	-6.86549
GALNT13	0.00515389	0.0434799	1.08187	1.79138	1.65583	1.65583
CDA	0.00517627	0.0434799	14.791	2.04049	0.137954	-7.24878
B4GALNT4	0.00521113	0.0434799	6.7038	4.07482	0.607838	-1.64518
NMRAL2P	0.00521677	0.0434799	1.54727	2.46248	1.59151	1.59151
NEO1	0.00521895	0.0434799	0.715088	0.307512	0.430034	-2.3254
PCDHA6	0.00522727	0.0434799	0.217532	0.443985	2.04101	2.04101
ERBB3	0.00523032	0.0434799	17.0528	9.33248	0.54727	-1.82725
ARHGAP24	0.00523743	0.0434803	0.213135	0.528913	2.48159	2.48159
CCNE1	0.00524772	0.0434803	4.32121	2.85333	0.660309	-1.51444
LINC00649	0.00530522	0.0435866	0.383036	0.597717	1.56047	1.56047
ARHGAP26	0.00531078	0.0435866	4.71595	3.06781	0.650519	-1.53723
GMPR	0.00543668	0.0442651	0.962697	2.79749	2.90589	2.90589
COCH	0.00547165	0.0443854	1.06512	0.343975	0.322945	-3.0965
CPZ	0.00549077	0.0444646	0.714913	1.21318	1.69697	1.69697
DOCK4	0.00551021	0.0445261	0.965673	1.63637	1.69454	1.69454
OLFM1	0.0055342	0.0446269	1.00809	0.357919	0.355047	-2.81653
LOC101926963	0.00553921	0.0446269	3.74884	2.46195	0.656722	-1.52271
OCLN	0.00558163	0.0447662	2.32983	1.45049	0.622574	-1.60624
CCDC78	0.00560762	0.0448789	3.30982	2.146	0.648374	-1.54232
OPN3	0.00564017	0.0449479	3.08323	4.95179	1.60604	1.60604
DOCK11	0.00564841	0.0449659	1.10244	1.89267	1.7168	1.7168
SLC19A3	0.00569826	0.0451237	0.478019	0.216515	0.452942	-2.20779

CBX5	0.00576103	0.0451922	15.3813	10.1534	0.660111	-1.5149
ADGRD1-AS1	0.00576969	0.045213	2.17269	1.39754	0.643228	-1.55466
DPYSL4	0.00583617	0.0454496	1.88742	0.822931	0.436009	-2.29353
TMEM92-AS1	0.00586191	0.0455848	1.0987	1.88119	1.71219	1.71219
DBH-AS1	0.00597865	0.0457763	1.09837	0.689627	0.627866	-1.5927
RASGRP1	0.0060364	0.0459367	1.16239	0.573799	0.493637	-2.02578
APBA2	0.00614317	0.0459367	0.563915	0.127821	0.226668	-4.41175
NOTCH3	0.0061807	0.0459505	7.73792	12.9609	1.67499	1.67499
ANKLE1	0.00623888	0.0461082	2.38059	1.37419	0.577247	-1.73236
CPT1A	0.00624271	0.0461082	6.04321	10.0699	1.66632	1.66632
C1QTNF1	0.00630913	0.0461082	4.55293	10.3292	2.26869	2.26869
RRAD	0.00631694	0.0461082	0.562543	0.929102	1.65161	1.65161
DPYSL3	0.00632988	0.0461082	59.6363	99.2302	1.66392	1.66392
LINC01603	0.00633183	0.0461082	0.751689	0.305273	0.406117	-2.46235
IGF2BP1	0.00637917	0.0461845	15.1716	8.73611	0.57582	-1.73665
IL31RA	0.00643811	0.0462989	1.15733	0.76399	0.660133	-1.51485
CCBE1	0.00645258	0.0463254	0.925475	2.35315	2.54264	2.54264
EBF4	0.00648842	0.046356	0.931813	0.347396	0.372817	-2.68228
ACSS1	0.00649735	0.046356	7.63265	5.04444	0.660904	-1.51308
RGS9	0.00651852	0.046356	0.683574	0.340378	0.497938	-2.00828
POTEC	0.00659338	0.046356	0.557662	1.19606	2.14478	2.14478
DSC2	0.00665667	0.0464015	2.05183	0.475261	0.231628	-4.31727
VCAN	0.00675119	0.0464291	2.33815	5.4816	2.34442	2.34442
LINC00857	0.0067689	0.0464291	2.75554	1.7754	0.6443	-1.55207
ARHGAP45	0.0067713	0.0464291	0.975415	0.592693	0.607632	-1.64573
HPCAL1	0.00680303	0.04647	34.0659	51.2167	1.50346	1.50346
KCNIP4	0.00681891	0.04647	2.00641	1.226	0.611042	-1.63655
LINC01341	0.00682517	0.04647	1.77117	1.01557	0.573388	-1.74402
FHDC1	0.00683697	0.04647	3.20463	1.13849	0.355262	-2.81482
CCDC3	0.00689957	0.04647	0.654937	0.260097	0.397133	-2.51805
EDNRA	0.00692357	0.04647	1.59526	5.67501	3.55741	3.55741
PLS3-AS1	0.00692797	0.04647	0.296665	0.476377	1.60577	1.60577
DEF6	0.0069367	0.04647	0.344121	0.0727181	0.211316	-4.73225
LOC101928674	0.00694605	0.04647	1.00617	0.558982	0.555556	-1.8
SSX2	0.00697388	0.04647	5.93502	2.62665	0.442567	-2.25954
AOC2	0.00698295	0.04647	0.741793	0.469589	0.633046	-1.57966
SSX2B	0.00699532	0.04647	6.14933	2.72118	0.442516	-2.2598
DLX4	0.00699715	0.04647	1.82366	0.995304	0.545773	-1.83226
PLCG2	0.00700139	0.04647	0.316392	0.146726	0.463746	-2.15635
OTOGL	0.00707598	0.0466255	3.59899	2.2126	0.614783	-1.62659
MMP7	0.00717251	0.0469003	0.267581	0.0507528	0.189673	-5.27224
SBK1	0.00717411	0.0469003	0.393323	0.200039	0.508587	-1.96623
LINC00528	0.00723012	0.0469584	0.620545	0.307792	0.496002	-2.01612
GAS7	0.0072356	0.0469584	15.8041	9.74872	0.616849	-1.62114
FDCSP	0.0072359	0.0469584	16.2329	4.68738	0.288758	-3.4631
BMP8B	0.00728582	0.0470386	2.36946	1.36585	0.576438	-1.73479
KRBA1	0.00739952	0.0472124	4.51157	2.48575	0.550972	-1.81497
CNTN1	0.00741298	0.0472507	2.27243	1.16017	0.510543	-1.9587
GPR19	0.00750709	0.0476284	2.34261	1.53392	0.654789	-1.52721
CASZ1	0.00752786	0.0476284	1.05387	0.649614	0.61641	-1.6223
AIM2	0.00758218	0.0476992	2.49012	1.23218	0.494826	-2.02091
RASD1	0.00761031	0.0477303	0.291414	0.460165	1.57908	1.57908
PIK3AP1	0.00761526	0.0477303	0.450732	0.217648	0.482877	-2.07092
LIN7A	0.00764585	0.0478191	0.275606	0.471212	1.70973	1.70973
RALY-AS1	0.00766963	0.0478191	1.55339	1.01342	0.65239	-1.53282
PDGFRA	0.00768839	0.0478297	2.0683	4.14938	2.00618	2.00618
FLJ20021	0.00774785	0.0479311	2.08418	3.35364	1.6091	1.6091
TSPAN9	0.00775171	0.0479311	14.579	22.7478	1.56031	1.56031
ADGRA2	0.00779534	0.0479953	3.87484	5.98944	1.54573	1.54573
PTHLH	0.00786488	0.0480525	0.531029	0.936255	1.76309	1.76309
EGFL7	0.00809122	0.0491159	0.44186	0.237522	0.537549	-1.86029
PCOTH	0.00813405	0.0491228	0.716518	1.13703	1.58688	1.58688
CNIH3	0.00816628	0.0491228	2.18826	4.01203	1.83344	1.83344
TM4SF19	0.00821637	0.0492785	3.51957	6.03009	1.7133	1.7133
SCG2	0.0082573	0.0493658	75.4103	148.287	1.96641	1.96641
CHN2	0.00829353	0.0493658	0.469655	0.781376	1.66372	1.66372
COL16A1	0.00829661	0.0493658	19.3498	10.7756	0.556885	-1.7957
CYGB	0.00835638	0.0494641	1.5078	0.775516	0.514336	-1.94425
ADAMTSL3	0.00839555	0.0495394	0.507693	0.221455	0.436199	-2.29253
DPT	0.00849936	0.0499786	11.146	25.0996	2.2519	2.2519
TNFRSF6B	0.00854684	0.050062	8.10116	3.6878	0.455219	-2.19674
SOX2-OT	0.00859207	0.0500926	1.76945	1.01131	0.571541	-1.74966
TINAGL1	0.00861118	0.0501397	2.88952	1.21611	0.420869	-2.37604
CGN	0.00863307	0.0502148	0.655815	0.376232	0.573686	-1.74311
UPK1A	0.0087899	0.0505951	0.343812	0.157052	0.456796	-2.18916
LARGE2	0.00888468	0.0505951	1.71959	0.921721	0.536013	-1.86562
ENPP2	0.00889369	0.0505951	0.891687	1.68871	1.89384	1.89384
RTL5	0.00891351	0.0506055	0.898284	1.38709	1.54415	1.54415
PRKCZ	0.00891573	0.0506055	3.9709	2.5792	0.649525	-1.53959
PMAIP1	0.00902606	0.050678	5.22714	7.84959	1.5017	1.5017
CPLX1	0.00906306	0.0506911	0.743868	0.34897	0.469128	-2.13161
PGM2L1	0.00906745	0.0506911	2.57329	4.34727	1.68938	1.68938
TRIM58	0.00910232	0.0506911	5.18738	2.52846	0.487426	-2.0516

TMEM145	0.00915261	0.0506986	1.06743	0.686535	0.643167	-1.55481
TSPAN15	0.00917901	0.0506986	5.82326	3.73588	0.641544	-1.55874
SERPINA3	0.00921529	0.0506986	19.2942	6.33578	0.328377	-3.04528
EFCAB13	0.00922172	0.0506986	0.500884	0.295719	0.590393	-1.69379
MAGEB1	0.00922222	0.0506986	4.3778	0.3496	0.0798574	-12.5223
FN1	0.00923377	0.0507124	128.915	196.458	1.52393	1.52393
IL1R1	0.00926697	0.0507124	2.76475	4.19578	1.5176	1.5176
MSI1	0.0092702	0.0507124	1.60616	0.445951	0.277651	-3.60165
EEF1A2	0.009293	0.0507905	194.664	120.168	0.61731	-1.61993
SHOX2	0.00940693	0.0511157	0.927853	1.80551	1.9459	1.9459
MBP	0.00951214	0.0513754	0.931448	1.4794	1.58828	1.58828
CARNS1	0.00952991	0.0513754	0.403007	0.226041	0.560886	-1.78289
PLAC9	0.00957203	0.0514417	0.505029	1.56618	3.10117	3.10117
CLDN4	0.00962063	0.0514584	49.3694	28.7786	0.582925	-1.71549
LINC02109	0.00963342	0.0514808	0.430369	0.261185	0.606886	-1.64776
TMEM158	0.00975774	0.0516041	33.3457	57.6247	1.7281	1.7281
ADGRB1	0.00977748	0.0516358	1.35692	3.18603	2.34798	2.34798
LOC105370697	0.00982811	0.0516894	0.357872	0.188872	0.527763	-1.89479
ASRGL1	0.00982889	0.0516894	0.716298	0.457837	0.639171	-1.56453
ID1	0.0099839	0.0519717	5.19567	10.1594	1.95535	1.95535
COL9A2	0.0100005	0.0519717	27.98	16.6548	0.59524	-1.67999
PNMA8A	0.0100015	0.0519717	1.25981	0.527125	0.418417	-2.38996
FUCA1	0.0100109	0.0519717	3.41541	2.22966	0.652822	-1.53181
MYH14	0.0101093	0.0521423	1.21441	0.17962	0.147908	-6.76096
MBL1P	0.0101308	0.0522056	0.601139	0.357967	0.595482	-1.67931
PRDX2	0.0101603	0.0522056	2.00819	0.593884	0.295731	-3.38145
FBXL21	0.0102597	0.0523654	1.61681	0.876552	0.54215	-1.84451
KRTAP2-3	0.010271	0.0523654	1.0283	0.354778	0.345015	-2.89842
SPANXA1	0.0103131	0.0524063	1.02863	2.5764	2.5047	2.5047
SPANXA2	0.0103131	0.0524063	1.02863	2.5764	2.5047	2.5047
SAP25	0.0103561	0.0525178	1.48359	0.899805	0.606504	-1.64879
RASSF7	0.0104929	0.0528513	0.854728	0.502763	0.588213	-1.70006
DDX25	0.0105026	0.0528647	0.212921	0.115651	0.543165	-1.84106
CCDC160	0.010543	0.0529617	1.53288	0.874895	0.570753	-1.75207
PKD1L2	0.0106144	0.0531781	1.6382	0.586839	0.358222	-2.79156
LINC01234	0.0106534	0.053338	0.271252	0.152209	0.561136	-1.7821
LINC01770	0.0107428	0.0535598	0.946774	0.498565	0.526594	-1.899
IL2RG	0.0107476	0.0535598	0.959996	0.14288	0.148834	-6.71888
ZNF257	0.0107628	0.0536	0.732875	0.377976	0.515744	-1.93895
MGC16025	0.0107738	0.0536179	0.845702	0.391383	0.462791	-2.1608
LRRC56	0.0107974	0.0536179	0.479211	0.319313	0.66633	-1.50076
SSX3	0.01083	0.0536337	5.77874	1.13835	0.196989	-5.07644
CLDN7	0.010879	0.0537167	0.435728	0.181779	0.417184	-2.39702
FOXO1	0.0109224	0.0538072	0.410062	0.63184	1.54084	1.54084
WFDC10B	0.0109584	0.053811	1.49902	0.661729	0.441442	-2.2653
DUSP8	0.0109746	0.0538343	2.66904	1.57929	0.591708	-1.69002
ABCA6	0.0110652	0.0538828	0.349511	0.648649	1.85587	1.85587
OPLAH	0.0111185	0.0538828	0.403459	0.224764	0.557092	-1.79504
TRIM6	0.0111246	0.0538828	3.42734	2.23594	0.652382	-1.53285
PAGE2	0.0113842	0.054473	19.6006	5.34655	0.272775	-3.66602
PDGFRL	0.0114057	0.0544907	0.916232	2.51402	2.74387	2.74387
CABP7	0.0114624	0.0545535	1.15303	0.631528	0.547711	-1.82578
CSDC2	0.0116258	0.0548152	0.784126	0.217632	0.277547	-3.60299
SNED1	0.0116619	0.0548909	3.92735	7.76703	1.97768	1.97768
VSIG10L	0.0117031	0.0548909	0.236551	0.0834933	0.352961	-2.83317
NPPA	0.0117778	0.0549687	0.651793	0.375669	0.576362	-1.73502
LINC00888	0.0117847	0.0549687	1.62862	2.68259	1.64715	1.64715
CRISPLD2	0.0118263	0.0549687	10.1818	5.02211	0.493246	-2.02739
TNFRSF11B	0.0118728	0.0549687	1.32911	2.03819	1.5335	1.5335
TPCN1	0.0118808	0.0549687	4.6838	7.18467	1.53394	1.53394
LOC100288181	0.0119071	0.0549687	0.5947	0.372894	0.627028	-1.59483
INPP5F	0.0119163	0.0549687	14.6093	9.55142	0.653791	-1.52954
DSP	0.0119169	0.0549687	2.11019	1.04084	0.493246	-2.02739
PIANP	0.0120472	0.0552378	3.52156	5.42696	1.54107	1.54107
DCHS1	0.0120699	0.0552744	1.19843	2.23535	1.86524	1.86524
GAPLINC	0.0121184	0.055429	0.538343	1.48751	2.76313	2.76313
EYA2	0.0124909	0.0565802	0.224923	0.109719	0.487806	-2.05
LAMA5	0.0125028	0.0565802	14.4268	23.1941	1.60771	1.60771
AATK	0.0125114	0.0565802	4.12698	1.85489	0.449454	-2.22492
LINC01914	0.0126175	0.0566763	0.471571	0.218652	0.463668	-2.15672
PHF24	0.0126216	0.0566763	0.276398	0.157968	0.571526	-1.7497
PLEKHA7	0.0126662	0.0567612	0.960336	0.355247	0.369919	-2.70329
SCO2	0.0126738	0.0567612	0.953041	1.77074	1.85798	1.85798
PLA2R1	0.0126985	0.0567612	0.988767	1.68737	1.70654	1.70654
GLI1	0.0127269	0.0567612	0.326831	0.623193	1.90678	1.90678
MYOSLID	0.0128937	0.0570017	1.05848	0.422409	0.399071	-2.50582
ARL15	0.012944	0.0570858	6.54816	4.2163	0.643891	-1.55306
COL24A1	0.0129722	0.0571431	0.984599	1.68495	1.71131	1.71131
VSNL1	0.0130703	0.0573609	0.431583	0.843253	1.95386	1.95386
QRFPR	0.0130898	0.0573609	0.297903	0.624146	2.09513	2.09513
UCN2	0.0131273	0.0573609	32.8992	18.4121	0.559653	-1.78682
KLF2	0.0132129	0.0573821	8.49632	13.3146	1.56711	1.56711
EGR1	0.013222	0.0573821	22.9403	38.692	1.68664	1.68664

MPP4		0.0133592	0.0575696	11.9409	7.28512	0.610098	-1.63908
GAL3ST4		0.0134019	0.0575734	0.521393	1.11303	2.13473	2.13473
LUZP4		0.0135434	0.0579245	5.67894	8.93865	1.574	1.574
	12-Sep	0.0136202	0.0579825	0.569702	0.339138	0.595289	-1.67986
HSPB3		0.0136616	0.0579825	0.50925	0.195722	0.384334	-2.6019
KAZN		0.0136681	0.0579825	0.830044	0.511734	0.616514	-1.62202
PTPRN		0.0136792	0.0579825	15.3825	10.2322	0.665184	-1.50334
MYOM3		0.0137903	0.0580131	0.954682	0.387027	0.405399	-2.46671
EGF		0.013809	0.0580131	0.367187	0.169744	0.462283	-2.16318
BCL2L11		0.0138243	0.0580131	1.62339	2.88685	1.77829	1.77829
SLC7A5		0.0138379	0.0580131	22.5522	14.9437	0.662627	-1.50914
KLHL23		0.0138722	0.0580131	1.42922	0.45385	0.31755	-3.14911
PTPN6		0.0139402	0.0581035	1.25201	0.803493	0.64176	-1.55822
TNFRSF9		0.0139491	0.0581084	2.36255	0.676564	0.28637	-3.49199
SERTAD4		0.0139577	0.058112	5.0983	8.00749	1.57062	1.57062
JCAD		0.013997	0.0582111	0.907318	1.9016	2.09585	2.09585
PTGS2		0.0141655	0.0585589	1.22757	3.02706	2.4659	2.4659
NOS2		0.0141945	0.0585589	0.244412	0.547331	2.23938	2.23938
LIMD1		0.014281	0.058742	6.35702	9.60764	1.51134	1.51134
HMGN2P46		0.0144075	0.0589719	0.542153	0.330864	0.610277	-1.6386
MIR4737		0.0145718	0.0592482	3.29084	1.57326	0.478071	-2.09174
PLAU		0.014697	0.0594976	12.0227	24.1359	2.00753	2.00753
PLEKHS1		0.0147559	0.0595545	4.24357	2.74984	0.648001	-1.54321
AOC3		0.0148888	0.0597151	0.522586	0.275746	0.527656	-1.89517
SOX9		0.0148943	0.0597151	8.80674	15.1238	1.7173	1.7173
MGAT5B		0.0149184	0.0597151	10.09	6.62354	0.656447	-1.52335
C1S		0.0149945	0.0597846	5.59279	9.00886	1.6108	1.6108
ZNF765		0.0149988	0.0597846	0.378418	0.222402	0.587714	-1.70151
LINC00882		0.0150209	0.0597846	0.382524	0.695202	1.81741	1.81741
GDF1		0.0150541	0.0597947	0.540561	0.326134	0.603325	-1.65748
LOC105616981		0.0151648	0.060044	2.22262	0.598752	0.26939	-3.71209
CACNA2D1		0.0151921	0.0600773	0.731039	1.16974	1.60011	1.60011
SRPK3		0.0153403	0.0602274	1.1024	0.659505	0.598242	-1.67156
BMPER		0.0153557	0.0602274	0.22723	0.419976	1.84824	1.84824
POU3F2		0.0153713	0.0602274	1.6344	0.936815	0.573187	-1.74463
UBE2Q1-AS1		0.0153825	0.0602274	0.127534	0.307656	2.41234	2.41234
ULBP1		0.0154793	0.0602274	0.452703	0.254381	0.561915	-1.77963
EMP1		0.0155037	0.0602274	81.4022	124.527	1.52977	1.52977
C8orf46		0.0155131	0.0602274	6.59185	3.34691	0.507734	-1.96953
TLN2		0.0156687	0.0606648	9.4161	5.78134	0.613985	-1.62871
DNASE1L2		0.0158955	0.0610547	1.57508	1.0215	0.648539	-1.54193
FAR2P2		0.0159523	0.061166	2.05962	0.920885	0.447114	-2.23657
PLEKHN1		0.0160678	0.0611891	1.10261	0.550926	0.499655	-2.00138
GUCY1B3		0.0162429	0.0614629	1.48907	2.43122	1.63271	1.63271
SDR42E1		0.0162804	0.0615429	1.42409	0.807356	0.566927	-1.7639
RAP1GAP		0.0163274	0.0616377	2.68894	1.68417	0.626334	-1.59659
LOC100630923		0.0163995	0.0617686	3.87586	2.36317	0.609717	-1.64011
ATP8B1		0.0164284	0.0617915	0.56668	1.00945	1.78135	1.78135
WNK4		0.0166241	0.0619079	2.7896	1.74745	0.626417	-1.59638
SLC17A7		0.0167129	0.0620468	0.394591	0.612365	1.5519	1.5519
FAM26F		0.0167192	0.0620468	0.565191	0.931319	1.6478	1.6478
ASS1		0.0170334	0.0626414	7.39452	19.4723	2.63333	2.63333
MIAT		0.017144	0.0628162	2.45687	4.64417	1.89028	1.89028
TRIM17		0.0171522	0.0628162	0.383361	0.174962	0.45639	-2.19111
SOCS1		0.0172469	0.0629506	2.2136	3.57002	1.61276	1.61276
FABP3		0.0172568	0.0629506	1.43957	2.43648	1.6925	1.6925
DCSTAMP		0.0173002	0.0630204	1.59625	0.196543	0.123127	-8.12167
PAPSS2		0.0173531	0.0630606	3.32177	5.08192	1.52989	1.52989
PDE4B		0.017379	0.0630886	0.406218	0.91827	2.26053	2.26053
LYPD1		0.0175137	0.0632749	9.69602	5.3976	0.556682	-1.79636
ZNF563		0.0175604	0.0632749	0.401901	0.641512	1.59619	1.59619
MMP11		0.0176491	0.0633639	1.49766	2.29561	1.53279	1.53279
LRRC61		0.0177041	0.0634222	0.792312	0.121602	0.153478	-6.51561
DKK1		0.0177162	0.0634289	64.4815	42.3666	0.657035	-1.52199
RASIP1		0.0177879	0.0635947	0.164485	0.103962	0.632048	-1.58216
LY6K		0.017824	0.063633	4.84565	2.61189	0.539018	-1.85523
SNORA91		0.0178655	0.0636851	0.0782412	0.518231	6.62351	6.62351
SHC4		0.017948	0.0637425	10.4026	6.20259	0.596254	-1.67714
WFDC3		0.0183221	0.0644599	0.910395	0.57183	0.628111	-1.59207
KIAA1217		0.0183387	0.0644599	1.76505	1.10928	0.628469	-1.59117
NLGN3		0.018353	0.06448	2.85496	1.79119	0.627395	-1.59389
PLLP		0.0186132	0.064768	0.590924	0.329664	0.557879	-1.7925
KIF5C		0.0186332	0.064768	4.15391	2.44319	0.588167	-1.7002
TNFRSF21		0.0187123	0.0648331	16.6394	27.9691	1.68089	1.68089
MAGEB2		0.0187936	0.0649949	25.344	15.7277	0.620568	-1.61143
LINC01355		0.0188532	0.0650651	1.40459	0.803425	0.572	-1.74825
ENPP5		0.0189556	0.0652494	0.619917	1.06836	1.72339	1.72339
DNM3		0.0191178	0.0654174	0.673606	0.423869	0.629254	-1.58918
ATP1A3		0.0191567	0.0654375	0.548073	0.275806	0.503228	-1.98717
LINC01468		0.019407	0.0659411	3.96141	1.83423	0.463023	-2.15972
FLRT1		0.0194712	0.0660614	0.673126	0.390863	0.580669	-1.72215
MYO7B		0.0195174	0.066154	11.3837	19.1253	1.68006	1.68006
APBA1		0.0195804	0.0662195	0.348924	0.55142	1.58035	1.58035

IL17RD	0.0198254	0.0664828	0.478344	0.758345	1.58535	1.58535
ROPN1B	0.0198723	0.066558	1.86973	1.04788	0.560442	-1.78431
STON1	0.0198896	0.066558	0.494103	0.844967	1.7101	1.7101
CFH	0.0199568	0.0666261	0.305381	0.872276	2.85635	2.85635
ESPN	0.0199901	0.066678	0.982739	0.405903	0.413032	-2.42112
TTC29	0.0202072	0.0669859	0.327805	0.616071	1.87938	1.87938
EREG	0.0203929	0.0671022	0.483606	1.54387	3.19241	3.19241
RAB3B	0.0204727	0.0671022	0.342628	0.742903	2.16825	2.16825
GDPD5	0.020513	0.0671022	0.930684	0.569571	0.611992	-1.63401
SLC16A8	0.0205375	0.067104	0.386972	0.201845	0.521601	-1.91717
IQCD	0.0206211	0.0671146	0.835395	1.37703	1.64836	1.64836
LOC100287036	0.0206486	0.0671444	0.328696	0.164271	0.499766	-2.00094
OXCT2	0.0207025	0.0671759	1.57239	0.804679	0.511755	-1.95406
PIEZO2	0.0207132	0.0671816	0.146083	0.0479514	0.328248	-3.04647
KRT80	0.020731	0.0671956	17.9096	9.86366	0.550745	-1.81572
ERV3-1-ZNF117	0.0207455	0.0671993	0.51117	0.302513	0.591805	-1.68974
GABRE	0.0208088	0.0672884	0.827653	0.347792	0.420214	-2.37974
TMEM59L	0.0210186	0.0675768	0.224711	0.0835029	0.371601	-2.69106
NPR3	0.0211021	0.0675768	0.631323	0.272198	0.431156	-2.31935
GYPE	0.021112	0.0675768	0.274042	0.507688	1.85259	1.85259
LINC01192	0.0211219	0.0675768	0.607297	0.367845	0.605709	-1.65096
SDC2	0.0211226	0.0675768	3.47541	6.93259	1.99475	1.99475
SH3RF2	0.02129	0.067823	6.13662	3.34055	0.544363	-1.83701
CLU	0.0213967	0.0679105	28.4652	43.8864	1.54176	1.54176
FIBCD1	0.0214533	0.0679105	1.23001	3.13408	2.548	2.548
ADAMTS14	0.0214824	0.0679105	3.23473	8.06891	2.49446	2.49446
NDN	0.0215702	0.068003	0.624903	0.0560653	0.0897184	-11.146
GACAT2	0.0216153	0.0680239	1.81182	2.74819	1.51681	1.51681
NDUFA4L2	0.0216973	0.0680239	3.6704	7.45248	2.03043	2.03043
ADRB2	0.0217801	0.068058	0.314362	0.521073	1.65756	1.65756
LINC01719	0.0219315	0.0680773	1.44278	0.799604	0.554211	-1.80437
COX6B2	0.0219445	0.0680896	0.667249	0.312318	0.468069	-2.13644
C1QTNF5	0.0220286	0.0681283	2.66742	4.65206	1.74403	1.74403
LINC00511	0.0220295	0.0681283	1.07265	0.634711	0.591723	-1.68998
FLJ42393	0.0222417	0.0685307	0.502884	0.282875	0.562504	-1.77777
F2RL1	0.022449	0.0687842	8.95943	18.2731	2.03954	2.03954
FNDC10	0.0227569	0.0692563	0.193707	0.0781515	0.403452	-2.47861
SOD3	0.0227754	0.0692563	4.05595	15.7361	3.87975	3.87975
ITPR1-AS1	0.0229333	0.0693539	0.36774	0.59061	1.60605	1.60605
DMKN	0.0229646	0.0693539	1.54432	0.194963	0.126246	-7.92107
PCDH18	0.0229725	0.0693539	0.67167	1.24946	1.86023	1.86023
PPP2R2C	0.0229787	0.0693539	3.72592	1.58636	0.425763	-2.34872
PTPRR	0.0230432	0.0694103	0.739321	0.474582	0.641916	-1.55784
SAYSD1	0.0231584	0.0695863	0.459909	0.258139	0.561281	-1.78164
MMP25	0.0234422	0.0699488	1.62191	0.984155	0.606789	-1.64802
AKR1C1	0.0234943	0.0700096	2.06387	5.94768	2.88181	2.88181
LMNTD2	0.0235351	0.0700183	0.588753	0.341578	0.580173	-1.72362
LOC101927204	0.0240807	0.0707856	0.317195	0.476681	1.5028	1.5028
NXPH4	0.0241667	0.0708318	7.74869	13.8726	1.79031	1.79031
ADTRP	0.0242791	0.0709404	0.479785	0.193198	0.402675	-2.48339
NDP	0.0245497	0.0713146	0.643493	0.202051	0.313991	-3.18481
CD200	0.0247071	0.0716058	1.62157	0.987337	0.608877	-1.64237
CATSPER2	0.0247539	0.0716357	0.35507	0.600764	1.69196	1.69196
EGLN3	0.0247868	0.0716434	1.22252	2.19536	1.79577	1.79577
DIO2	0.0248605	0.0717736	1.96595	0.77976	0.396633	-2.52123
SNORA11	0.025108	0.0720384	0.356952	0.0524858	0.147039	-6.80092
SPATA31C2	0.0254774	0.0726243	0.538627	0.35665	0.662147	-1.51024
LIMS3	0.0257427	0.0728924	0.818884	0.519415	0.634297	-1.57655
LIMS4	0.0257427	0.0728924	0.818884	0.519415	0.634297	-1.57655
MIR193BHG	0.0258058	0.0729293	1.72607	2.78557	1.61382	1.61382
TMPRSS5	0.0258531	0.0729293	0.753251	0.306409	0.406781	-2.45832
SNORD45C	0.0258825	0.0729293	0.43264	0.0892072	0.206193	-4.84984
NR4A2	0.0259957	0.073065	1.85457	3.73323	2.01299	2.01299
LOC105374338	0.0259981	0.073065	0.631589	1.05914	1.67695	1.67695
GNRH2	0.0260491	0.0730717	0.966524	0.244295	0.252756	-3.95639
GPR35	0.0263083	0.0732774	0.518525	0.272304	0.525151	-1.90421
SCNN1B	0.0263397	0.0732774	0.258463	0.102282	0.395731	-2.52697
LINC02057	0.0263467	0.0732774	0.24403	0.451024	1.84823	1.84823
GCHFR	0.0267775	0.0738469	0.684561	1.73636	2.53646	2.53646
LOC642361	0.0268483	0.0739465	2.70864	1.69077	0.624212	-1.60202
LOC100132249	0.026997	0.0740988	0.466815	0.287625	0.616144	-1.623
SIK1	0.0271179	0.0742138	3.45097	5.1979	1.50621	1.50621
BAGE4	0.0271991	0.0743217	0.47164	0.310538	0.658422	-1.51878
BAGE5	0.0272011	0.0743217	0.485265	0.31951	0.658425	-1.51878
IL1RL1	0.0272177	0.0743245	0.0690069	0.308791	4.47479	4.47479
HSPA1A	0.0274742	0.0746051	2.32208	4.9823	2.14562	2.14562
MIR1254-1	0.0275879	0.0747379	0.34991	0.0708829	0.202574	-4.93646
SULF2	0.0276505	0.0748266	45.6763	70.592	1.54548	1.54548
HHIP-AS1	0.0276653	0.0748397	1.16348	1.96389	1.68795	1.68795
PTGES3L-AARSD1	0.0278246	0.0750815	0.441755	0.233804	0.529261	-1.88943
SCUBE3	0.02796	0.075281	0.557706	0.30789	0.552065	-1.81138
LOC100507600	0.0281159	0.0754526	0.465841	0.266158	0.571349	-1.75024
CHST2	0.0282042	0.0755093	4.70936	7.28774	1.5475	1.5475

NPIPB15	0.0282332	0.07556	0.36488	0.160222	0.439109	-2.27734
ISLR2	0.0283387	0.0757075	0.336158	0.767616	2.2835	2.2835
MT1A	0.0284048	0.0758033	3.82108	1.83865	0.481185	-2.0782
LINC01320	0.0286131	0.0759814	0.628422	0.152663	0.24293	-4.11641
IL20RB	0.0286376	0.0760196	1.14346	2.64809	2.31586	2.31586
RORA	0.02891	0.0763188	0.365958	0.561474	1.53426	1.53426
SZT2-AS1	0.0289128	0.0763188	1.19145	0.588617	0.494033	-2.02416
LOC100507156	0.0289359	0.076353	0.807719	0.529156	0.655123	-1.52643
MIR4489	0.0291207	0.0765616	0.112898	0.564926	5.00388	5.00388
HLF	0.029137	0.0765616	0.488199	0.215883	0.442203	-2.2614
SECTM1	0.0295223	0.0770348	0.742651	0.431488	0.581011	-1.72114
HAS2-AS1	0.0296806	0.0772333	0.208959	0.386335	1.84886	1.84886
PNMA2	0.0297884	0.0774334	0.941051	0.410799	0.436532	-2.29078
GALNT16	0.0298803	0.0775064	0.419945	0.812817	1.93553	1.93553
NTNG2	0.0300291	0.0775953	1.54867	1.023	0.660569	-1.51385
FCRLA	0.030082	0.0775953	0.273458	0.0982866	0.359422	-2.78225
PECAM1	0.0301174	0.0775953	0.524007	0.879435	1.67829	1.67829
GJC2	0.0301256	0.0775953	0.649629	0.427801	0.658531	-1.51853
APOL3	0.0301714	0.0776395	1.16188	1.87044	1.60983	1.60983
TRIM22	0.0302446	0.0776812	0.323058	0.501556	1.55253	1.55253
MIR221	0.0304258	0.0779311	1.93749	3.4438	1.77745	1.77745
NPTX2	0.0304663	0.0779551	16.712	32.378	1.93741	1.93741
OR7E14P	0.0306204	0.0780571	0.611828	0.253539	0.414396	-2.41315
HHIP	0.0312417	0.0788926	0.891898	1.40443	1.57466	1.57466
LOC389831	0.0313796	0.0790539	1.69165	0.938347	0.554695	-1.80279
TEKT2	0.0314065	0.0790645	0.466474	0.823346	1.76504	1.76504
NFATC2	0.031468	0.0791704	0.605017	0.372362	0.615457	-1.62481
OCM	0.0315701	0.0792827	0.137376	0.355838	2.59026	2.59026
C11orf96	0.0316197	0.0793154	1.25289	2.60406	2.07844	2.07844
LOC105371184	0.0316486	0.0793154	0.481079	0.225142	0.467994	-2.13678
CPM	0.0317106	0.0793557	1.29374	0.663044	0.5125	-1.95122
CBLN1	0.031963	0.0795844	0.421912	0.247811	0.587353	-1.70255
GLT8D2	0.0321183	0.0797014	2.68114	4.86626	1.815	1.815
SFN	0.0323165	0.0797078	16.685	5.37168	0.321946	-3.10611
ADAMTS9	0.0325381	0.0799359	0.864164	0.510496	0.590739	-1.6928
LOC101928143	0.0332981	0.0809077	2.19891	0.855934	0.389254	-2.56902
C1orf54	0.0333105	0.0809077	0.305881	0.739916	2.41896	2.41896
ALDH1A2	0.0335533	0.0811335	0.203231	0.425628	2.0943	2.0943
CLDN1	0.0337251	0.0813103	0.705203	1.1461	1.62521	1.62521
ZNF204P	0.0340167	0.0816146	0.585148	0.378254	0.646425	-1.54697
TLR9	0.034039	0.0816219	0.24725	0.132863	0.537361	-1.86095
PDGFRB	0.0340571	0.0816269	6.79894	13.3347	1.9613	1.9613
GPR4	0.0340795	0.0816269	0.767117	0.445874	0.581233	-1.72048
MIR4517	0.0342312	0.0818217	0.687062	1.95966	2.85224	2.85224
ZNF702P	0.0342663	0.0818665	0.294174	0.0414526	0.140912	-7.09662
FRG1JP	0.0342767	0.0818665	1.27805	1.96403	1.53675	1.53675
SPIRE2	0.0342826	0.0818665	0.525602	0.345287	0.656937	-1.52222
SLAMF9	0.0344112	0.0819912	0.742463	0.327487	0.441082	-2.26715
LAMA4	0.0344508	0.0820099	8.33615	13.1609	1.57877	1.57877
P2RX5	0.0345623	0.0821392	1.19586	1.8275	1.52819	1.52819
LOC107984974	0.0350494	0.0826108	28.081	7.05998	0.251415	-3.97749
ZNF608	0.0357973	0.0833744	0.638431	0.32877	0.514965	-1.94188
CGB3	0.0361718	0.0839244	0.798305	0.286034	0.358302	-2.79094
NUPR1	0.0368484	0.0847008	1.24983	2.90333	2.32298	2.32298
HAGLROS	0.0368784	0.0847008	0.158698	0.388315	2.44688	2.44688
SPDYE6	0.0373986	0.0852702	0.988372	0.550665	0.557144	-1.79487
FOS	0.0374335	0.085273	2.93513	6.2872	2.14205	2.14205
RFX3-AS1	0.0374914	0.085346	0.430326	0.283654	0.659161	-1.51708
EDIL3	0.0375416	0.0854017	7.32146	12.3999	1.69364	1.69364
DOCK3	0.0378662	0.0858415	0.39773	0.191451	0.481358	-2.07746
FSTL5	0.0381161	0.0861416	0.489627	0.277747	0.567263	-1.76285
LINC00200	0.0382901	0.0862168	0.305134	0.0426693	0.139838	-7.15114
UBE2Q2L	0.0391401	0.0872554	0.572056	1.06946	1.8695	1.8695
STC1	0.0391638	0.0872772	17.6596	30.543	1.72954	1.72954
HSPA1L	0.0400189	0.08822	0.911863	1.58102	1.73384	1.73384
ESPNP	0.0402546	0.088513	0.462228	0.217532	0.470617	-2.12487
NLRP10	0.0407938	0.0889627	1.04225	0.278465	0.267176	-3.74285
ZNF223	0.0408876	0.0891014	0.202411	0.119235	0.589075	-1.69758
GAMT	0.0412137	0.0895134	0.51731	0.22448	0.433938	-2.30448
HSPA1B	0.0414803	0.0897565	2.66864	4.99921	1.87332	1.87332
LEF1	0.0417687	0.0900952	0.289259	0.16439	0.568313	-1.75959
IL11	0.0429996	0.0914898	16.1629	10.5984	0.655721	-1.52504
FMR1NB	0.0431017	0.0916286	0.338699	0.00681504	0.0201212	-49.6987
AJUBA	0.0431983	0.0916807	7.8406	5.19546	0.662635	-1.50913
INSR	0.0436558	0.0920423	0.885275	0.555113	0.627052	-1.59476
HGC6.3	0.0440603	0.0925414	0.480892	0.203386	0.422934	-2.36443
CALB2	0.0442511	0.0926831	70.0011	39.273	0.561034	-1.78242
SBK2	0.0443769	0.0927398	4.04183	1.23214	0.304846	-3.28035
ID3	0.0445399	0.0928996	8.46687	15.9677	1.8859	1.8859
PCSK1	0.0445776	0.0929009	1.34729	3.22252	2.39185	2.39185
URAHP	0.0449075	0.0932974	0.501877	0.325892	0.649347	-1.54001
NRG1	0.0453734	0.0935733	0.179795	0.0369843	0.205702	-4.86139
IL23A	0.0456763	0.0936225	0.4079	0.228181	0.559405	-1.78761

PRR15	0.045773	0.0936225	0.249379	0.447345	1.79384	1.79384
LINC02263	0.0459316	0.0937398	0.449275	0.259798	0.578261	-1.72932
MPZ	0.0459858	0.0937556	9.61725	3.21639	0.33444	-2.99007
SNORD29	0.0460665	0.0938438	7.98859	5.1383	0.643205	-1.55472
WISP1	0.046189	0.0939336	1.95287	4.009	2.05288	2.05288
TACSTD2	0.0469999	0.0947541	0.21978	0.109682	0.499051	-2.0038
ACPP	0.0471987	0.0950424	9.36394	4.37556	0.467278	-2.14006
NR0B1	0.0475139	0.0953959	2.46895	1.56582	0.634205	-1.57678
TPM3P9	0.0475899	0.0954975	0.409737	0.129682	0.316501	-3.15955
SGK3	0.0479706	0.0960051	0.568757	0.349846	0.615107	-1.62573
LIMD1-AS1	0.0480565	0.0960725	3.29437	5.31492	1.61334	1.61334
ZNF790-AS1	0.048729	0.0969548	0.204282	0.465853	2.28044	2.28044
OLFML2B	0.0492189	0.0975165	1.70671	2.95933	1.73393	1.73393
PHF21B	0.0495284	0.0976682	0.732828	0.346855	0.47331	-2.11278
TMTC1	0.0495684	0.0976682	0.796885	1.26718	1.59017	1.59017
ACP5	0.0496681	0.0977877	0.469382	0.796801	1.69755	1.69755

REACTOME pathway enrichment for downregulated genes by glutamine supplmenetation, related to Figure 4

Pathway	log p-value	p-value	# genes in list	genes in list
Extracellular matrix organization	4.33	4.72E-05	294 (294)	F11R;TGFB3;MMP15;ITGAX;MMP7;ITGB3;COL6A3;MATN4;BCAN;COL11A1;ADAMTS8;COL16A1;HAPLN1
ECM proteoglycans	4.26	5.54E-05	57 (57)	TGFB3;ITGAX;ITGB3;MATN4;BCAN;HAPLN1
TGF-beta receptor signaling in EMT	3.09	0.000816	16 (16)	F11R;CGN;PRKCZ
Cell-cell junction organization	3.05	0.000886	63 (64)	F11R;CADM1;PARD6B;CDH15;CLDN3
MAPK family signaling cascades	2.70	0.002	236 (237)	PAK3;ITGB3;RASGRP1;ERBB3;IGF2BP1;GFRA3;FGFR4;DUSP9;SHC2
Tight junction interactions	2.28	0.00524	30 (31)	F11R;PARD6B;CLDN3
Rho GTPase cycle	2.19	0.00642	140 (144)	ARHGAP45;PREX1;ARHGAP26;TIAM2;ARHGAP27;ARHGAP40
RAF/MAP kinase cascade	2.05	0.00882	196 (197)	ITGB3;RASGRP1;ERBB3;GFRA3;FGFR4;DUSP9;SHC2
MAPK1/MAPK3 signaling	1.99	0.0103	202 (203)	ITGB3;RASGRP1;ERBB3;GFRA3;FGFR4;DUSP9;SHC2
FGFR4 mutant receptor activation	1.92	0.0119	1 (1)	FGFR4
Cell-Cell communication	1.81	0.0155	123 (124)	F11R;CADM1;PARD6B;CDH15;CLDN3
VEGFA-VEGFR2 Pathway	1.63	0.0237	92 (92)	ITGB3;PAK3;PRKCZ;SHC2
Signaling by VEGF	1.51	0.031	100 (100)	ITGB3;PAK3;PRKCZ;SHC2
Integrin signaling	1.39	0.0404	27 (27)	ITGB3;RASGRP1
Signaling by TGF-beta Receptor Complex	1.35	0.0451	67 (67)	F11R;CGN;PRKCZ

REACTOME pathway enrichment for upregulated genes by glutamine supplmenetation, related to Figure 4

Pathway	log p-value	p-value	# genes in list	genes in list
Extracellular matrix organization	7.51	3.07E-08	294 (294)	MMP14;CTSB;VCAN;P4HA3;BMP4;COL6A1;COL6A2;NTN4;BMP7;ITGA10;FBLN5;HTRA1;ITGA1;FN1
CHL1 interactions	4.50	3.18E-05	9 (9)	ITGA1;ITGA10;ANK1
Synthesis of bile acids and bile salts via 27-hy	3.78	0.000167	15 (15)	AKR1C3;CYP7A1;AKR1C2
Axon guidance	2.89	0.00128	357 (358)	ITGA10;COL6A1;COL6A2;NTN4;DPYSL3;UNC5B;ITGA1;ANK1;NGEF
TP53 Regulates Transcription of Death Recept	2.47	0.0034	12 (12)	TP63;FAS
Signaling by PDGF	2.13	0.00738	54 (54)	PDGFRA;COL6A1;COL6A2
Apoptosis	1.95	0.0113	118 (118)	UNC5B;TP63;FAS;PMAIP1
Programmed Cell Death	1.91	0.0123	121 (121)	UNC5B;TP63;FAS;PMAIP1
Integrin cell surface interactions	1.88	0.0133	67 (67)	ITGA1;ITGA10;FN1
Collagen biosynthesis and modifying enzymes	1.86	0.0139	68 (68)	P4HA3;COL6A1;COL6A2

Supplementary Data 3: KEGG global gene-metabolic network, related to Figure 5

Pathway	Total Cmpd	Hits	Raw p	log pvalue	FDR	Impact
Pyrimidine metabolism	47	12	1.65E-06	13.318	0.000132	0.3356
Purine metabolism	38	11	0.000636	7.3602	0.025442	0.22282
Cysteine and methionine metabolism	27	8	0.001131	6.7851	0.030146	0.44391
Amino sugar and nucleotide sugar metabolism	48	10	0.001693	6.381	0.031692	0.27581
Aminoacyl-tRNA biosynthesis	32	9	0.001981	6.2243	0.031692	0
Glutathione metabolism	41	6	0.002873	5.8525	0.03761	0.23743
Nitrogen metabolism	88	6	0.003291	5.7166	0.03761	0

CHAPTER 4: Conclusion and future direction

The work presented in this dissertation demonstrates a previously unidentified role for IKKβ in phosphorylating p53 upon glutamine depletion to promote cancer cell survival by driving the upregulation of pro-survival genes. These results delineate a new IKKβ-p53 signaling axis that is critical to cancer cell adaptation to metabolic stress. Additionally, it explores the therapeutic potential for using glutamine supplementation in reprogramming cancer epigenetics and inhibiting tumor growth. The availability of circulating glutamine increases cellular pools of αKG, thereby, promoting the activity of histone demethylases and leading to a state of histone hypomethylation. Specifically, H3K4me3, a mark for active promoters, is significantly reduced in tumors from mice receiving glutamine supplementation and directly leads to the down-regulation of key melanoma oncogenes. This chapter aims to highlight future experiments based on these results.

Metabolic adaptations via IKKβ-p53 signaling axis

The results shown in Chapter 2 suggest that cancer cells can adapt to the low glutamine levels in their microenvironment and modulate the activity of p53 to promote its survival and progression. Accumulating evidence now indicate a more complex role for p53 in cancer cells. In contrast to its role in inducing apoptosis in response to DNA damage or oncogene activation, p53 can promote cancer survival during metabolic stress (Figure 1) (1). For instance, p53 activation during serine deprivation modulates the serine synthesis pathway and suppresses aerobic glycolysis to support survival in cancer cells (2). Similarly, wild type and mutant p53 activation upon glutamine deprivation promote survival in various cancer types by mediating metabolic

adaptions as well as expression of downstream genes that support survival under this metabolic stress (3-5).

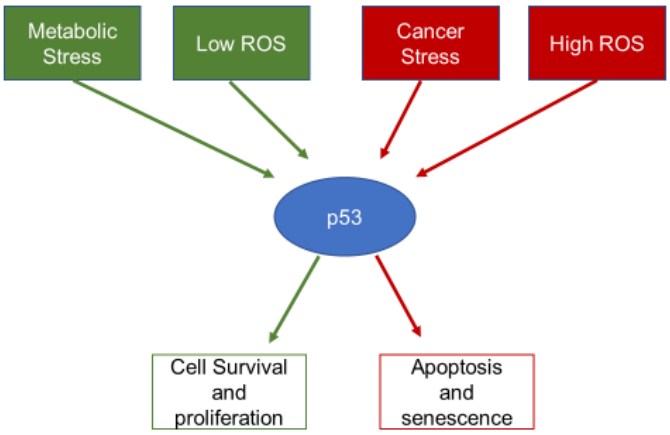

Figure 1: Cellular signals regulate p53 functions in cancer. p53 can promote cell survival in cancer under metabolic stress signals including transient oxidative stress and nutrient starvation. p53 can also induce cell death under cancer associated signals including high levels of ROS, DNA damage and oncogene activation.

In chapter 2, we demonstrated that glutamine deprivation induces the phosphorylation of IKKβ, which can directly interact with p53 and phosphorylates it on Ser392. We showed that activated p53 can in turn upregulate p21 and Gadd45, previously shown to be expressed in response to glutamine deprivation, and rescue cells by inducing growth arrest (4). Recently, p53 has also been shown to modulate glycolysis in response to glutamine depletion in pancreatic cancer (5). Given this data, it is possible that p53 activation promotes survival in cancer cells under glutamine deprivation by inducing cell arrest to allow time for necessary metabolic adaptions. This hypothesis is supported by our preliminary observation that p53-downstream genes involved in metabolic regulation are also induced in an IKKβ dependent manner (Figure 2). Tp53-inducible glycolysis and apoptosis regulator (TIGAR), phosphoglycerate dehydrogenase (PHGDH) and glutaminase 2 (GLS2), all identified as p53 inducible genes, play a role in modulating cancer metabolism to support survival and proliferation (6-8). Thus, it would be interesting to perform a time course study in order to observe whether there is a sequence in the

activation of p53-downstream genes and their effect on cell proliferation upon glutamine deprivation at different time points. Additionally, glucose tracing experiment can help in understanding the changes in glycolysis mediated by TIGAR and PHGDH in response to low glutamine levels and whether knockdown of IKKβ or p53 affect the ability of cancer cells to survive under this metabolic stress.

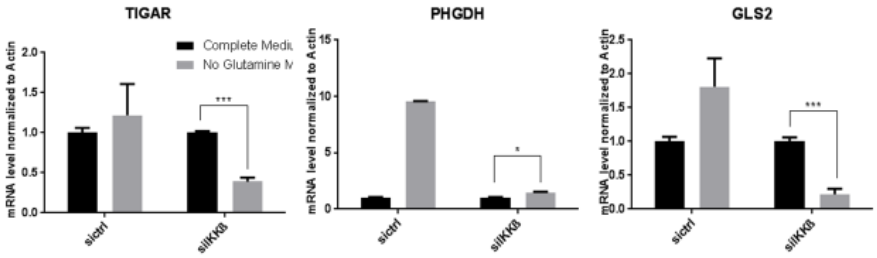

Figure 2: Upregulation of p53-inducible genes upon glutamine deprivation. HT1080 cells transiently transfected with siRNA against scramble control or IKKβ were cultured in complete or glutamine free media overnight. mRNA was extracted, and expression of p53-target genes was determined using qPCR. Data represents means + s.d. of triplicates from three independent experiments (*p<0.05, ***p<0.001 using Student's *t*-test).

Moreover, the connection between IKKβ and the phosphorylation of p53 on Ser392 and Ser15 under different metabolic stress remains unclear. Several studies indicated the activation of p53 via phosphorylation on Ser15 under glutamine, serine, glucose, and arginine (2-4, 9). We wondered if IKKβ affected p53 activation upon withdrawal of serine and arginine. Our preliminary results indicate a link between loss of IKKβ and p53 phosphorylation at Ser15 upon glutamine and serine deprivation (Figure 3). However, arginine withdrawal stimulated p53 phosphorylation in control and IKKβ knockdown cells. Thus, it is interesting to further investigate whether the IKKβ-p53 signaling axis mediates survival upon serine deprivation through the expression of p53-downstream genes, similar to glutamine-deprived conditions. More importantly, it would be interesting to delineate why arginine deprivation does not depend on IKKβ and identify other kinases mediating this effect by performing immuno-precipitation

experiments of p53 from cells deprived of arginine and screen for interacting kinases by protein mass spectrometry.

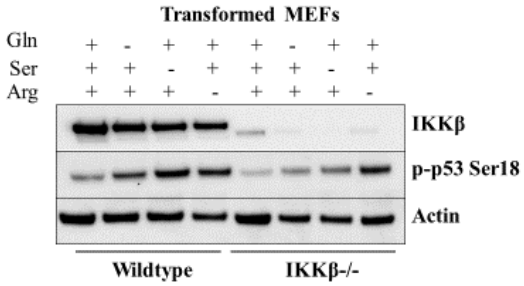

Figure 3: Activation of p53 under metabolic stress. Western blot analysis of wild type (WT), or Ikkβ$^{-/-}$ MEFs cultured in complete, glutamine (Gln) free, serine (Ser) free, and arginine (Arg) free medium overnight and cell lysate was used for immunoblotting using the antibodies indicated.

Finally, it remains to be known whether cancer cells will be able to resist the effect of glutamine depletion and exhibit resistance to glutaminase inhibitors, currently used in patients, due to the activation of IKKβ and p53 signaling pathways or other parallel pathways. Thus, as a continuation of the work presented in this thesis dissertation, it will be interesting to test the efficacy of targeting IKKβ activation of p53 and glutamine metabolism as a dual strategy in the treatment of various cancer types and combating potential resistance to glutamine targeted treatments.

Glutamine supplementation in cancer therapy

Tumors experience differential levels of glutamine, as well as oxygen, which have been previously shown to promote an epigenetic state that favors the expression of several dedifferentiation genes and promote resistance to targeted therapies in melanoma tumors. The data presented in Chapter 3 explores the use of glutamine supplementation in cancer therapy,

however, there are a number of biological questions that deserve further study based on these results. For example, under hypoxic conditions, how do cells allocate glutamine in numerous pathways. Several studies indicated a profound difference in glutamine utilization in normoxia versus hypoxia (10-12). It is apparent that more work is needed to elucidate the exact mechanism of how glutamine is utilized under more physiological or tumor-like conditions. This work in melanoma tumors supports previously published observations showing that glutamine does not directly replenish the TCA intermediate under hypoxic conditions. In order to further test this hypothesis, glutamine tracing can be used in cells cultured under hypoxia and either low or high levels of glutamine. Mass spectrometry analysis can then be used to show how glutamine-derived carbon is being utilized in these cells (13). Delineating how glutamine is metabolized would also support the use of glutamine supplementation in other solid tumors based on their metabolic profile.

Another fundamental question regarding the use of glutamine supplementation is understanding how glutamine can effectively reach the core regions of solid tumors. Indeed, the complexity of the *in vivo* microenvironment in solid tumors poses multiple biological barriers for the delivery of molecular agents (14). In Chapter 3, we demonstrated that glutamine supplementation in diet

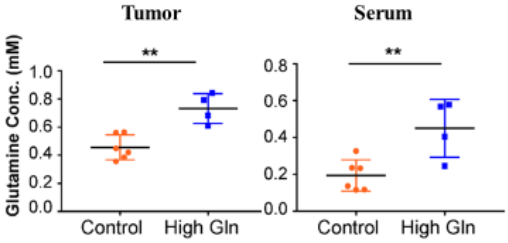

Figure 4: Glutamine supplementation increases glutamine in tumors and serum. Glutamine concentration from M229 tumors and nude mice serum measured by EIA kit (n=6 for Control and n=4 for High Gln biological replicates).

effectively increased the concentration of glutamine in serum and tumors (Figure 4). Thus, it is reasonable to believe that metabolites with low molecular weight would be able to reach the tumor through diffusion as well as membrane transporters expressed on the different cells present in the tumor microenvironment. To test this hypothesis, glutamine infusion experiment can be conducted, where ^{13}C-labelled glutamine is administered through the tail vein of tumor-bearing mice over a period of one hour (13). Tumor tissues are then collected for cell sorting to separate the different cell populations, which can be analyzed by mass spectrometry analysis to trace the accumulation of ^{13}C-labeled glutamine in these cell population and reconstruct a potential molecular map of glutamine delivery *in vivo*.

The results in Chapter 3 also indicate that glutamine supplementation can cooperate with BRAF targeted therapy to inhibit tumor growth. More importantly, the use of glutamine supplementation re-sensitized resistant melanoma to BRAF inhibition. We hypothesized that glutamine-induced hypomethylation of H3K4 led to the downregulation of oncogenes, which directly impacted the RAS pathway (Figure 5a) further increasing the efficacy of targeted

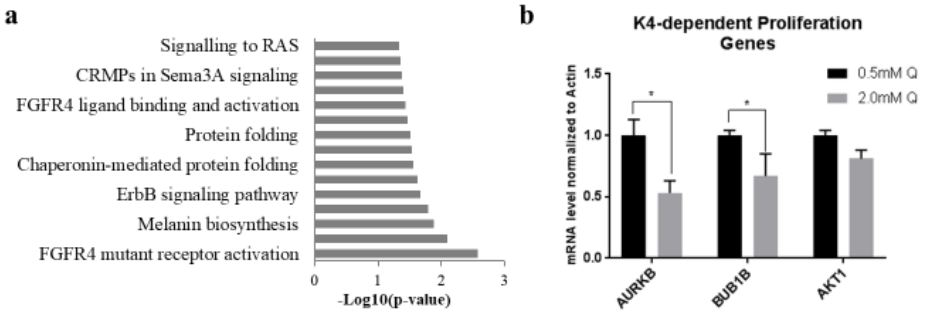

Figure 5: Glutamine supplementation downregulates genes in an H3K4me3 dependent manner. a. Pathway analysis of 51 common genes between RNA-seq and ChIP-seq high glutamine supplemented tumors compared to control ($p<0.05$). b. M229 cells cultured under hypoxia and either 0.5 or 2.0mM glutamine (Q) medium for 4 days with medium changed daily. Cells were collected for qPCR analysis (n=3, independent cell cultures). Data represent means. Error bars are s.d. P value calculated by *t*-test (unpaired, two-tailed). *$p<0.05$

therapy. The success of using BRAF inhibitor in combination with glutamine supplementation suggest that BRAF was not completely suppressed by dietary glutamine and it is also possible that glutamine can be mediating its effect through other pathways. Thus, identification of the mechanism of how glutamine supplementation inhibits tumor growth can help identify other targets. Since we noted a decreased in Ki67 in melanoma tumors from mice receiving glutamine supplementation, we used M229 cells to investigate changes in K4-dependent genes involved in proliferation (15). We noted a decrease in proliferation genes that could cooperate with the effects of BRAF inhibitors and potentially other targeted therapies (Figure 5b). It would be necessary to study the changes in other K4-dependent genes that affect tumor growth and proliferation. Furthermore, we noted that the knockdown of JARID1A, JARID1B or JARID1C rescues melanoma cells cultured under high glutamine. Thus, it would be interesting to delineate whether all JARID1 demethylases act on the identified proliferation genes. This can be tested using ChIP analysis with JARID1 specific antibodies followed by qPCR to confirm whether these enzymes demethylate H3K4me3 at the promoter of these genes.

Another exciting direction for the use of glutamine supplementation to induce epigenetic reprogramming that inhibit tumor progression *in vivo* is to study its effect in combination with immune-therapy. T-cell activation and proliferation is highly dependent on aerobic glycolysis and glutamine metabolism. In fact, glutamine supplementation has been used clinically to boost immune response in hospitalized patients and expediate recovery (16, 17). This work also demonstrates that dietary glutamine was effective in the inhibition of the syngeneic B16 melanoma in mice with intact immune response (Figure 6). Thus, it would be interesting to study whether glutamine supplementation can synergize with immune therapy to enhance killing of cancer cells or reverse resistance via altered epigenetics. Future experiments with the anti-PD1

responsive syngeneic melanoma YUMM cells can be used to demonstrate whether glutamine supplemented diet can work synergistically with checkpoint inhibitors (18).

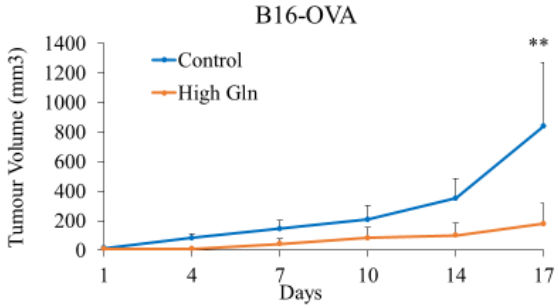

Figure 6: Glutamine supplementation inhibits B16 melanoma tumors growth. B16 cells were injected subcutaneously in C57BL/6 mice and randomly placed on control or high glutamine (High Gln) diet post injection. Tumours were measured twice weekly (Control, n=6; High Gln, n=6). Data represent means. Error bars are s.e.m. P value calculated by *t*-test (unpaired, two-tailed). **p<0.01

In conclusion, this dissertation provides an alternative mechanism to survive glutamine deprivation in cancer via the activation of wild type or mutant p53 and potentially leads to the rise of a resistant population to glutaminase targeted inhibition. More importantly, there is a need to understand glutamine metabolism and adaptive mechanism *in vivo*. This work challenges the current understanding of glutamine metabolism and demonstrate that glutamine supplementation is detrimental to melanoma tumors via epigenetic reprograming and can increase susceptibly to current cancer therapeutics.

References

1. Labuschagne CF, Zani F, Vousden KH. Control of metabolism by p53 - Cancer and beyond. Biochimica et biophysica acta Reviews on cancer. 2018;1870(1):32-42. Epub 2018/06/09. doi: 10.1016/j.bbcan.2018.06.001. PubMed PMID: 29883595; PubMed Central PMCID: PMCPMC6102416.
2. Maddocks OD, Berkers CR, Mason SM, Zheng L, Blyth K, Gottlieb E, et al. Serine starvation induces stress and p53-dependent metabolic remodelling in cancer cells. Nature. 2013;493(7433):542-6. Epub 2012/12/18. doi: 10.1038/nature11743. PubMed PMID: 23242140.
3. Lowman XH, Hanse EA, Yang Y, Ishak Gabra MB, Tran TQ, Li H, et al. p53 Promotes Cancer Cell Adaptation to Glutamine Deprivation by Upregulating Slc7a3 to Increase Arginine Uptake. Cell reports. 2019;26(11):3051-60.e4. doi: 10.1016/j.celrep.2019.02.037.
4. Tran TQ, Lowman XH, Reid MA, Mendez-Dorantes C, Pan M, Yang Y, et al. Tumor-associated mutant p53 promotes cancer cell survival upon glutamine deprivation through p21 induction. Oncogene. 2016. Epub 2016/10/11. doi: 10.1038/onc.2016.360. PubMed PMID: 27721412.
5. Yang Y, Ishak Gabra MB, Hanse EA, Lowman XH, Tran TQ, Li H, et al. MiR-135 suppresses glycolysis and promotes pancreatic cancer cell adaptation to metabolic stress by targeting phosphofructokinase-1. Nature Communications. 2019;10(1):809. doi: 10.1038/s41467-019-08759-0.
6. Bensaad K, Tsuruta A, Selak MA, Vidal MN, Nakano K, Bartrons R, et al. TIGAR, a p53-inducible regulator of glycolysis and apoptosis. Cell. 2006;126(1):107-20. Epub 2006/07/15. doi: 10.1016/j.cell.2006.05.036. PubMed PMID: 16839880.
7. Hu W, Zhang C, Wu R, Sun Y, Levine A, Feng Z. Glutaminase 2, a novel p53 target gene regulating energy metabolism and antioxidant function. Proceedings of the National Academy of Sciences. 2010;107(16):7455-60. doi: 10.1073/pnas.1001006107.
8. Mullarky E, Mattaini KR, Vander Heiden MG, Cantley LC, Locasale JW. PHGDH amplification and altered glucose metabolism in human melanoma. Pigment Cell & Melanoma Research. 2011;24(6):1112-5. doi: 10.1111/j.1755-148X.2011.00919.x.
9. Mauro C, Leow SC, Anso E, Rocha S, Thotakura AK, Tornatore L, et al. NF-kappaB controls energy homeostasis and metabolic adaptation by upregulating mitochondrial respiration. Nat Cell Biol. 2011;13(10):1272-9. Epub 2011/10/05. doi: 10.1038/ncb2324. PubMed PMID: 21968997; PubMed Central PMCID: PMCPMC3462316.
10. Nakazawa MS, Keith B, Simon MC. Oxygen availability and metabolic adaptations. Nat Rev Cancer. 2016;16(10):663-73. doi: 10.1038/nrc.2016.84.
11. Wise DR, Ward PS, Shay JE, Cross JR, Gruber JJ, Sachdeva UM, et al. Hypoxia promotes isocitrate dehydrogenase-dependent carboxylation of alpha-ketoglutarate to citrate to support cell growth and viability. Proc Natl Acad Sci U S A. 2011;108(49):19611-6. Epub 2011/11/23. doi: 10.1073/pnas.1117773108. PubMed PMID: 22106302; PubMed Central PMCID: PMCPMC3241793.
12. Xie H, Simon MC. Oxygen availability and metabolic reprogramming in cancer. J Biol Chem. 2017. Epub 2017/08/27. doi: 10.1074/jbc.R117.799973. PubMed PMID: 28842498.
13. Kang YP, Ward NP, DeNicola GM. Recent advances in cancer metabolism: a technological perspective. Experimental & molecular medicine. 2018;50(4):31. Epub 2018/04/17. doi: 10.1038/s12276-018-0027-z. PubMed PMID: 29657324; PubMed Central PMCID: PMCPMC5938018.
14. Lyssiotis CA, Kimmelman AC. Metabolic Interactions in the Tumor Microenvironment. Trends in Cell Biology. 2017;27(11):863-75. doi: 10.1016/j.tcb.2017.06.003.
15. Spangle JM, Dreijerink KM, Groner AC, Cheng H, Ohlson CE, Reyes J, et al. PI3K/AKT Signaling Regulates H3K4 Methylation in Breast Cancer. Cell reports. 2016;15(12):2692-704. Epub 2016/06/14. doi: 10.1016/j.celrep.2016.05.046. PubMed PMID: 27292631; PubMed Central PMCID: PMCPMC5094353.
16. Johnson MO, Wolf MM, Madden MZ, Andrejeva G, Sugiura A, Contreras DC, et al. Distinct Regulation of Th17 and Th1 Cell Differentiation by Glutaminase-Dependent Metabolism. Cell. 2018;175(7):1780-95 e19. Epub 2018/11/06. doi: 10.1016/j.cell.2018.10.001. PubMed PMID: 30392958; PubMed Central PMCID: PMCPMC6361668.
17. Labow BI, Souba WW. Glutamine. World Journal of Surgery. 2000;24(12):1503-13. doi: 10.1007/s002680010269.
18. Homet Moreno B, Zaretsky JM, Garcia-Diaz A, Tsoi J, Parisi G, Robert L, et al. Response to Programmed Cell Death-1 Blockade in a Murine Melanoma Syngeneic Model Requires Costimulation, CD4, and CD8 T Cells. Cancer Immunology Research. 2016;4(10):845-57. doi: 10.1158/2326-6066.cir-16-0060.